

POLITECNICO DI TORINO

Collegio di Ingegneria Chimica e dei Materiali

**Master of Science Course
in Materials Engineering**

Master of Science Thesis

**Realization and characterization of randomly
disordered fiber with tellurite glass**



Tutors

Prof. Davide Janner

Prof. Axel Schülzgen

Candidate

Alberto Rovera

July 2020

Index

Abstract in italian.....	1
1 Introduction	1
1.1 Historical review.....	1
1.2 Basic structure of an optical fiber.....	2
1.3 Main applications.....	5
1.4 Goals of the thesis	5
1.5 Structure of the thesis	7
2 Tellurite glasses.....	9
2.1 Introduction to tellurite glasses	9
2.2 Physical properties.....	12
2.3 TNGPZ glasses	14
2.4 Existing tellurite glass applications	15
3 Disordered fibers.....	17
3.1 Introduction to photonic crystals.....	17
3.2 Anderson localization	19
3.2.1 Transverse Anderson localization	23
3.3 Applications of disordered fibers	25
3.4 State of the art of disordered optical fibers	25
4 Optical fiber production	29
4.1 Common techniques.....	29
4.2 Chosen technique	36
4.3 Choice of the glass tube.....	38
4.4 Fiber preparation.....	44
4.5 Results.....	48
5 Characterization.....	51
5.1 Glass thermo-mechanical properties	51
5.1.1 DTA.....	51
5.1.2 Dilatometry	53
5.1.3 Viscosity	54
5.1.4 Hardness	57
5.2 Glass optical properties	59
5.2.1 Refractive index.....	59

5.2.2	FTIR Spectroscopy.....	60
5.3	Fiber properties	62
5.3.1	Cut-back method for total attenuation	62
5.1	Results.....	63
6	Conclusions.....	65
7	List of symbols and abbreviations.....	66
	Acknowledgements	79
	Ringraziamenti.....	80

Abstract in italian

Riassunto della Tesi di Laurea Magistrale

(Sessione luglio 2020)

" Realization and characterization of randomly disordered fiber with tellurite glass"

Candidato: Alberto Rovera

Relatore: Prof. Davide Janner

Prof. Axel Schülzgen

Introduzione ed obiettivi del lavoro

Il settore dei sensori in fibra ottica è in continuo sviluppo sia nell'ambito della ricerca che in quello di produzione industriale, con un mercato da 1732,91 M\$ nel 2019 e numerose applicazioni. Tra queste il trasporto di immagini ottiche sta ricevendo un interesse particolare con la richiesta di immagini sempre più nitide e iperspettrali, che cioè coprano finestre ottiche al di là del solo visibile.

Finora la richiesta veniva soddisfatta da fibre multicore, o MCOF, ma le immagini sfocate e a basso contrasto hanno fortemente limitato lo sviluppo. Inoltre, queste fibre sono prodotte in silice, che ha bassi costi, ottime caratteristiche termomeccaniche, basse perdite ottiche (possono arrivare sotto i 0.15 dB/km) ma anche una finestra di trasparenza limitata (Il range ottimale è 1310 – 1500 nm). L'incremento di interesse al di fuori delle telecomunicazioni in campi come quello medico e biologico richiede finestre spettrali di rilevamento che vanno oltre tale intervallo, in particolare nel vicino e medio infrarosso (near-IR e mid-IR).

Dal punto di vista dei materiali utilizzabili, i vetri a base tellurite sono di particolare interesse grazie alla possibilità di trasmettere fino a 7 μm con basse perdite intrinseche, indice di rifrazione elevato, ottima stabilità termica e chimica e senza problemi di tossicità come accade per i calcogenuri. Un confronto tra le proprietà di vari vetri per applicazioni ottiche è rappresentato in Tab. 1.

Tab. 1 *Confronto fra differenti vetri ottici.*

	Silica	Tellurite	Fluoride	Chalcogenide
Refractive index n at $1.55 \mu\text{m}$	1.46	2–2.2	~1.5	2.3–3
Nonlinear refractive index n_2 ($\times 10^{-20} \text{ m}^2/\text{W}$)	2.5	20–50	2–3	100–1000
Raman gain coefficient g_R at $1.064 \mu\text{m}$ ($\times 10^{-11} \text{ cm/W}$)	0.93	32	1.1 ± 0.3	280–720
Raman shift (cm^{-1})	440	650–750	550	250–350
λ_0 , zero-dispersion wavelength of material (μm)	~1.3	~2	~1.7	>5
IR longwave transmission limit	Up to $3 \mu\text{m}$	$6\text{--}7 \mu\text{m}$	$7\text{--}8 \mu\text{m}$	$12\text{--}16 \mu\text{m}$
Reported lowest loss dB/m (wavelength)	0.15×10^{-3} ($1.55 \mu\text{m}$)	0.0204 ($1.56 \mu\text{m}$)	0.45×10^{-3} ($2.35 \mu\text{m}$)	0.023 ($2.3 \mu\text{m}$)
Thermal stability for fiber drawing	Excellent	Good	Poor	Good
Viscosity around fiber- drawing temperature	Flat	Steep	Steep	Flat
Durability in environment	Excellent	Good	Poor, hygroscopic	Good
Toxicity	Safe	Safe	Relatively high	Relatively high

Da questa tabella si evince che i vetri a base tellurite mostrano il miglior compromesso, tra le varie proprietà, per le applicazioni nel mid-IR.

Dal punto di vista di design sono state realizzate recentemente fibre ottiche disordinate per imaging, sia a base tellurite con una struttura all-solid, ovvero con due vetri telluriti diversi che compongono il core, sia con struttura GARF (Glass-Air Random Fiber), cioè con un core composto da silice e una frazione d'aria. Queste fibre disordinate hanno dimostrato di poter trasmettere immagini ottiche con qualità maggiore delle fibre commerciali MCOF attraverso una fibra lunga un metro.

L'obiettivo del seguente lavoro di tesi è stato quello di realizzare e caratterizzare una fibra ottica disordinata GARF con core in vetro tellurite con composizione TeO_2 , Nb_2O_5 , GeO_2 , PbO and ZnF_2 (TNGPZ) e clad con vetro commerciale compatibile per migliorare le proprietà meccaniche. La ricerca è stata svolta presso la University of Central Florida in collaborazione con il Politecnico di Torino dove è stato prodotto il vetro TNGPZ, visibile in Fig.1.



Fig. 1 *Preforma in vetro a base tellurite prodotta dal Dipartimento di Scienza Applicata e Tecnologia (DISAT).*

Metodologie utilizzate

Il vetro TNGPZ è stato realizzato presso il Politecnico di Torino utilizzando la tradizionale tecnica di colata in stampo di ottone e successivo annealing, seguito da un raffreddamento graduale fino a temperatura ambiente. Tale processo è stato realizzato in una glove-box con tecnica dry melting, mentre la miscela delle polveri è stata realizzata in una dry-box con atmosfera d'azoto per ridurre la presenza di gruppi OH. I gruppi idrossilici sono la principale causa di perdite ottiche nei vetri a base tellurite, con picchi di assorbimento a 3.3 e 4.4 μm . Questa tecnica è stata scelta perché è difficile ottenere composti gassosi necessari per la tecnica CVD (Chemical Vapor Deposition), nonostante questa sia scelta solitamente per la maggiore qualità delle preforme ottenute.

La composizione è stata ottimizzata a partire dalla composizione standard dei TZN, 75 TeO₂-20 ZnO - 5 Na₂O. L'ossido di sodio (Na₂O) è stato eliminato per migliorare le proprietà meccaniche mentre l'ossido di zinco (ZnO) è stato sostituito con il fluoruro di zinco che ne migliora la stabilità termica e diminuisce la presenza dei gruppi ossidrilici come contaminanti.

Le fibre GARF sono fibre disordinate che sfruttano la localizzazione di Anderson. Questo fenomeno fisico, anche chiamato *localizzazione forte*, avviene quando è presente un alto grado di disordine nel sistema, sia questo un reticolo cristallino o la sezione trasversale del core di una fibra.

Quando è presente questa condizione il normale trasporto di onde (non solo quelle elettromagnetiche ma anche elettroni o onde acustiche) viene inibito. Fu scoperto da Anderson mentre analizzava come cambiasse la conducibilità di un metallo con il disordine del reticolo cristallino. Quando il disordine, dato dalle impurità nel reticolo, raggiunge una certa soglia, gli elettroni diventano completamente localizzati, una transizione metallo-isolante.

Oltre al disordine, anche le dimensioni determinano la localizzazione di Anderson; per dimensioni $d = 1,2$ (fili e lamine) gli stati sono tutti localizzati mentre per $d = 3$ è presente un *mobility edge*, l'energia per la quale tutti gli stati al di sotto sono localizzati, come mostrato in Fig. 2.

Mobility edge

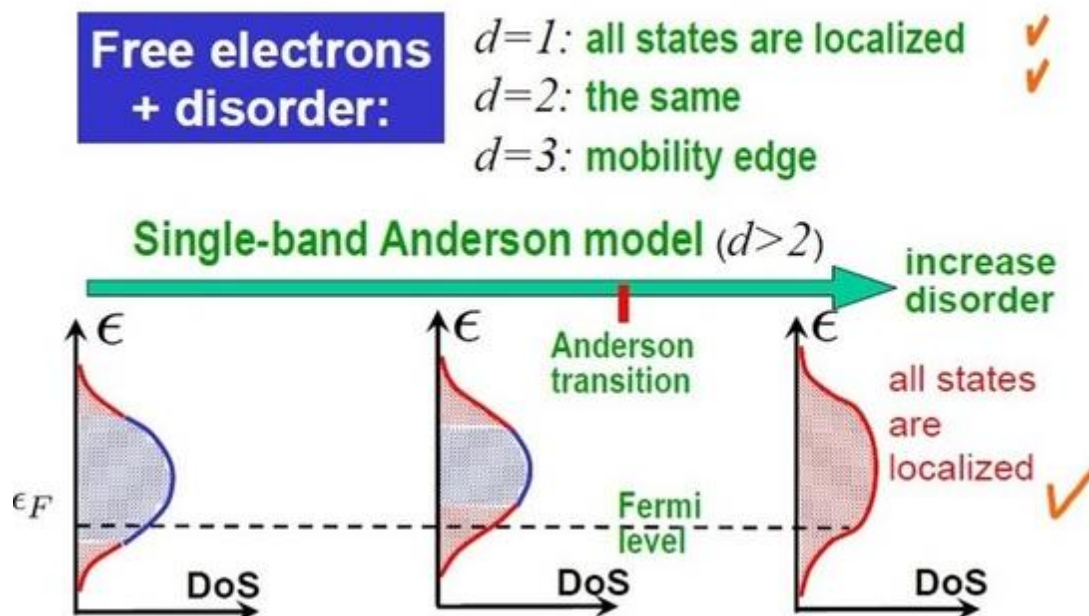


Fig. 2 Rapporto tra disordine e localizzazione.

Il disordine nelle fibre che sfruttano questo meccanismo è dato dalla differenza di indice di rifrazione con una struttura come quella proposta da De Raedt in Fig. 3.

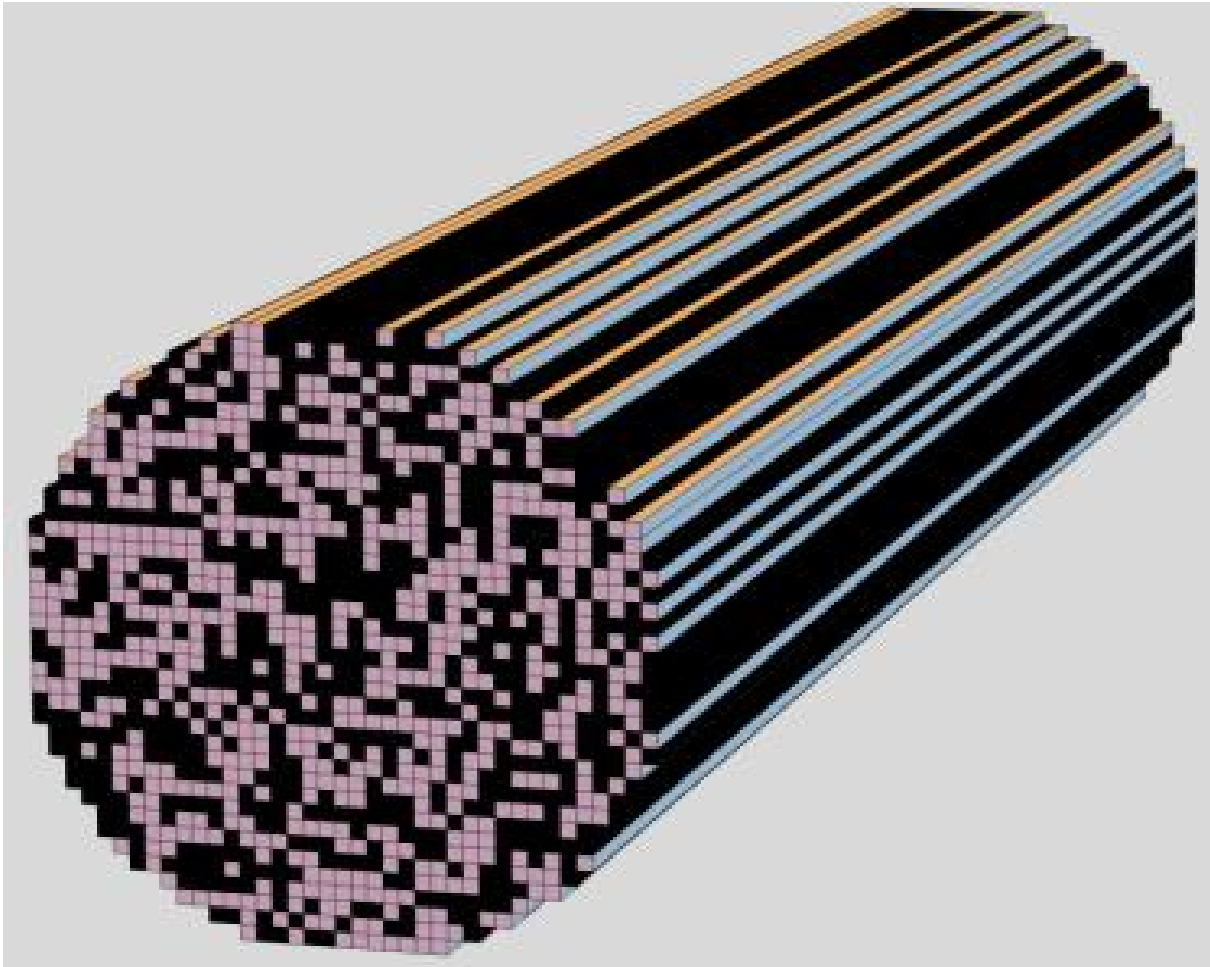


Fig. 3 Struttura proposta da De Raedt per localizzazione di Anderson in un sistema quasi-2D. Il colore differente dei pixel rappresenta i differenti indici di rifrazione n .

Questa differenza di n nelle fibre GARF è data dal materiale del core e l'aria, cosa che permette un maggiore valore di Δn . Negli scorsi anni sono state fabbricate fibre ottiche disordinate usando diversi materiali e forme osservando la localizzazione anche per piccoli valori di Δn pari a 0.095. Sono stati utilizzati polimeri (PMMA e PS) e vetri a base tellurite per fibre all-solid (fibre con il core compatto) e silice per fibre GARF.

Per ottimizzare il design e la produzione della fibra sono state effettuate delle prove di caratterizzazione sul vetro e, qualora non fosse stato possibile, una ricerca in letteratura per dedurre il possibile intervallo di valori.

L'analisi DTA dei vetri realizzati ha identificato i valori di temperatura di transizione vetrosa (T_g) e la temperatura di onset di cristallizzazione (T_x) con valori, rispettivamente, di 360,2 °C e 588°C come mostrato in Fig.4.

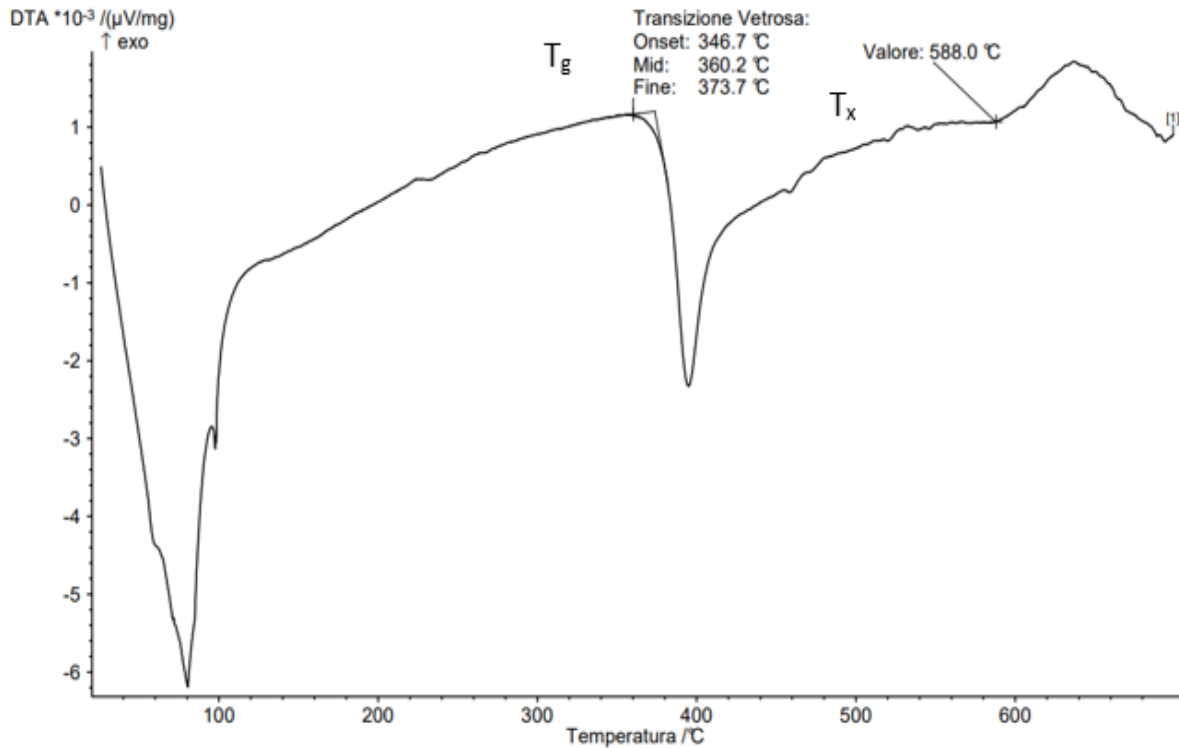


Fig. 4 Analisi DTA del vetro TNGPZ.

Per misurare il coefficiente di espansione termica (CTE o α) è stato usato un dilatometro orizzontale in allumina (NETZSCH, DIL 402 PC) con una rampa di riscaldamento di 5°C/min su un campione di 5 mm. Il valore di CTE misurato nel range 200-400 °C è di $13 \cdot 10^{-6} \text{ C}^{-1}$ con un margine di errore di $\pm 0.1 \text{ } ^\circ\text{C}^{-1}$.

L'indice di rifrazione è stato misurato a 5 differenti lunghezze d'onda (633, 855, 1061, 1312 e 1533 nm) attraverso un Metricon 2010 Prism coupler effettuando due misurazioni per ogni lunghezza d'onda, l'errore stimato è di ± 0.001 e ha un valore massimo per 633 nm di 2,1317 e un minimo per 1533 di 2,0683, il grafico della misurazione è mostrato in Fig. 5.

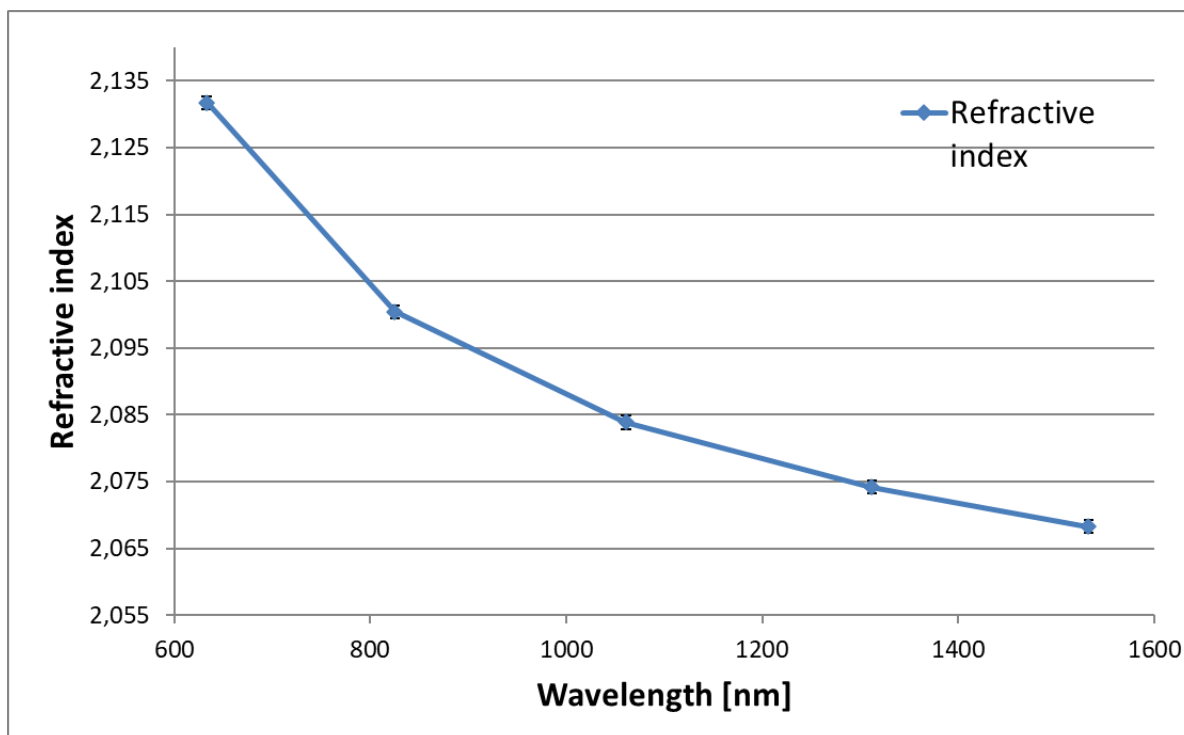


Fig. 5 Misurazione dell'indice di rifrazione del vetro TNGPZ.

Una spettroscopia FTIR (Fourier Transform Infrared) è stata effettuata per misurare lo spettro di assorbimento, per le lunghezze d'onda tra 2,5 e 5,5 μm che ha permesso di verificare il livello di gruppi OH presenti nel vetro e quindi di determinare la qualità dello stesso per la trasmissione nella regione dell'IR.

Per misurare l'attenuazione ottica totale della fibra è stato proposto il metodo cut-back per le lunghezze d'onda tra 2,5 e 6 μm .

Conclusione

Basandosi sulle caratterizzazioni eseguite, per poter ottenere una fibra GARF di qualità con minimi stress e un clad con vetro compatibile, la scelta del vetro commerciale è ricaduta sullo SCHOTT 8095 con una dimensione finale della fibra di 500 μm di diametro esterno e 150 μm di diametro del core.

Lo SCHOTT 8095 è un vetro cristallo (28% di PbO) con le seguenti proprietà:

Mean coefficient of linear thermal expansion $a(20-300\text{ }^{\circ}\text{C})$	$9.1 * 10^{-6}\text{ }^{\circ}\text{C}^{-1}$
Glass transition temperature T_g	$430\text{ }^{\circ}\text{C}$
Glass temperature at viscosity η in dPa*s	10^{13} (annealing point) $\rightarrow 435\text{ }^{\circ}\text{C}$ $10^{7.6}$ (softening point) $\rightarrow 630\text{ }^{\circ}\text{C}$ 10^4 (working point) $\rightarrow 982\text{ }^{\circ}\text{C}$
Young's modulus E	$60 * 10^3\text{ N} * \text{mm}^{-2}$
Poisson's ratio μ	0.22

Lo stress teorico calcolato risulta essere di compressione (desiderabile per una fibra ottica) ed inferiore a 30 Mpa utilizzando il modello di Khron e la sua equazione (Eq.1):

$$\sigma = \frac{(\alpha_1 - \alpha_2)(T - T_{g1})E}{(R^2/r^2)(1 - \mu)} + \frac{(\alpha_1^* - \alpha_2)(T_{g2} - T_{g1})}{((1 - R^2/r^2)/3K_1^*) - (1/(3K_2))}$$

Eq. 1 *Equazione di Khron per calcolare lo stress interno nelle fibre.*

Dove:

- 1 and 2 si riferiscono al core e al clad,rispettivamente;
- E è il modulo di Young;
- μ è il modulo di Poisson;
- R/r è il rapport tra il raggio del clad e il raggio del core;
- T è la temperatura ambiente;
- T_g è la temperatura di strain point ma viene assunta equivalente a quella di transizione vetrosa;
- a può essere differente, idealmente con il valore di a del cladding inferiore per assicurare sforzi di compressione sul core;
- * si riferisce ai valori subito sopra la T_g ;
- K^* è il modulo di bulk sopra la T_g che è tipicamente 0.5 volte il modulo di bulk al di sotto della T_g .

Dopo aver ottenuto la fibra di tellurite con diametro di circa 150 μm , questa deve essere tagliata in pezzi da 15 cm per poterli impilare nel tubo di 8095 e, successivamente, fondere i capillari di tellurite e il vetro del clad con una fornace Lindberg/Blue M così da evitare movimenti durante la filatura della fibra definitiva.

Questa geometria, mostrata in Fig. 6, è stata ideata per cercare di ottenere una frazione d'aria del 50%, ovvero il valore teorico per massimizzare il fenomeno fisico alla base del funzionamento delle fibre disordinate, la localizzazione di Anderson trasversale.

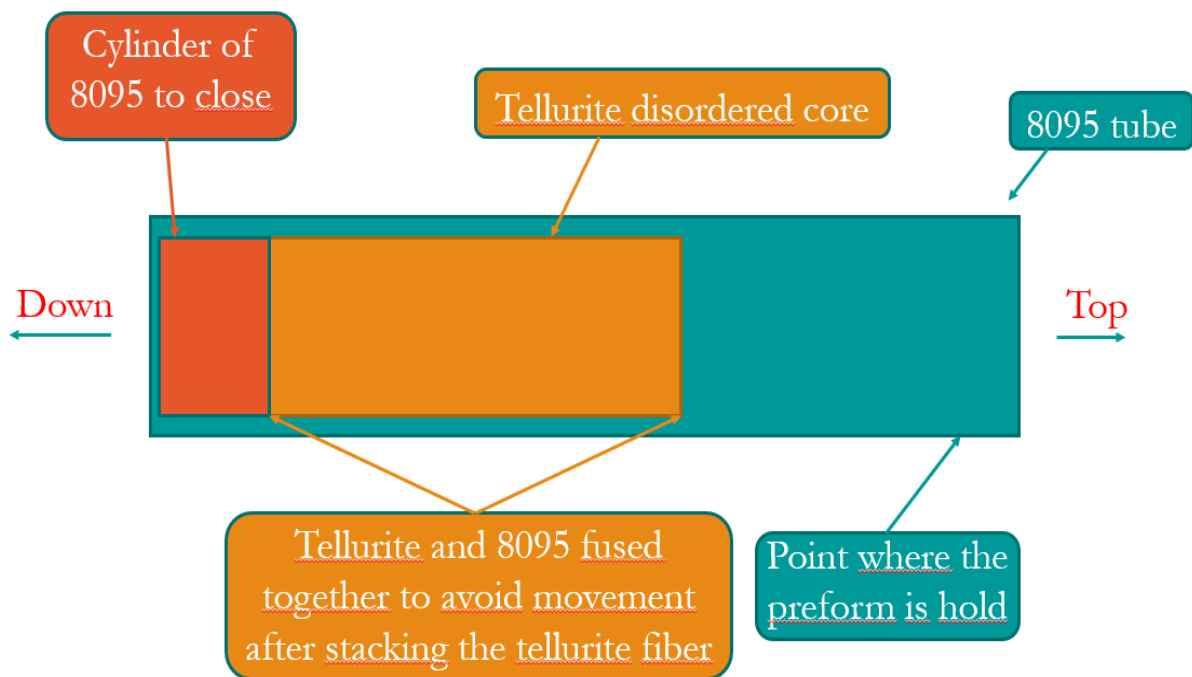


Fig. 6 *Illustrazione schematica del design della preforma.*

Con una ΔT di 227,8 il vetro mostra una elevata stabilità termica contro la devettrificazione.

In Fig.7 è possibile vedere un confronto tra le perdite di un vetro TZNL e il nostro TNGPZ

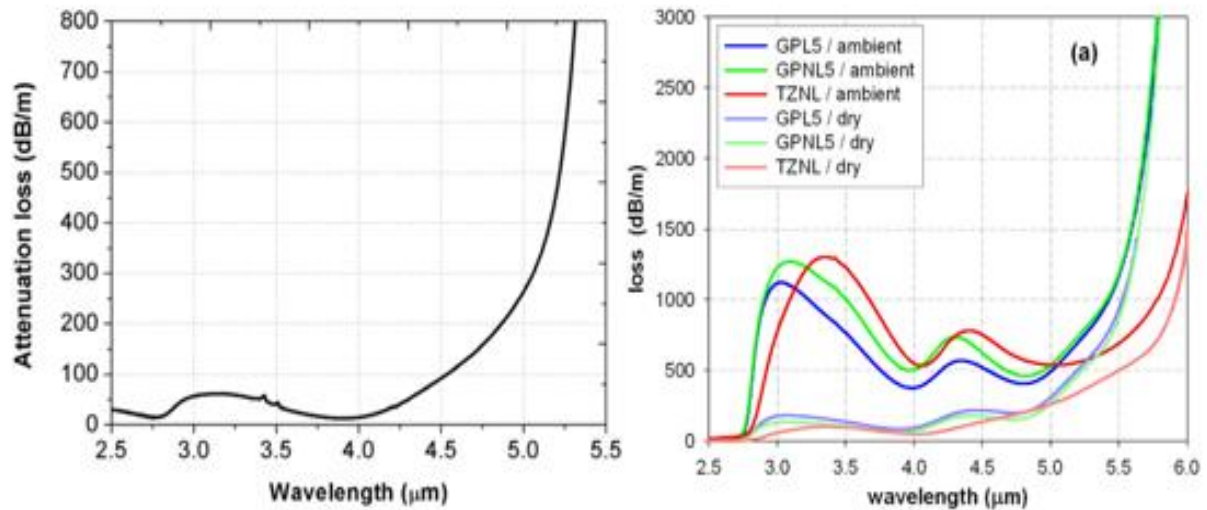


Fig. 7 Spettro di assorbimento vetro TNGPZ (a sinistra) e di differenti vetri TZNL e fosfati con tecnica di dry melting o senza (a destra).

L'assorbimento da parte di gruppi OH è ancora presente ma sensibilmente diminuito grazie agli accorgimenti. L'elevata differenza di indice di rifrazione (Δn), superiore a 1, dovrebbe risultare in una localizzazione di Anderson particolarmente accentuata, nonostante sia già presente anche per valori di 0.095.

I risultati ottenuti hanno mostrato le potenzialità di questo vetro per creare fibre ottiche GARF ed è stato creato un design della fibra che possa aumentare le possibilità di successo nella realizzazione della fibra e nella sua qualità. La fibra è in fase di filatura presso la University of Central Florida.

1 Introduction

1.1 Historical review

Light has been used to communicate for thousands of years, even before language. From the signal bonfires used on the Great Wall of China during the Ming Dynasty to the first optical telegraph built by Claude Chappe in France [1], visual communication has evolved continuously. The great limit of optical signals was that light travels in straight lines, but in 1870 John Tyndall in Boston gave proof of the possibility to guide the light. This was made filling a barrel with water as in Fig 1.1.

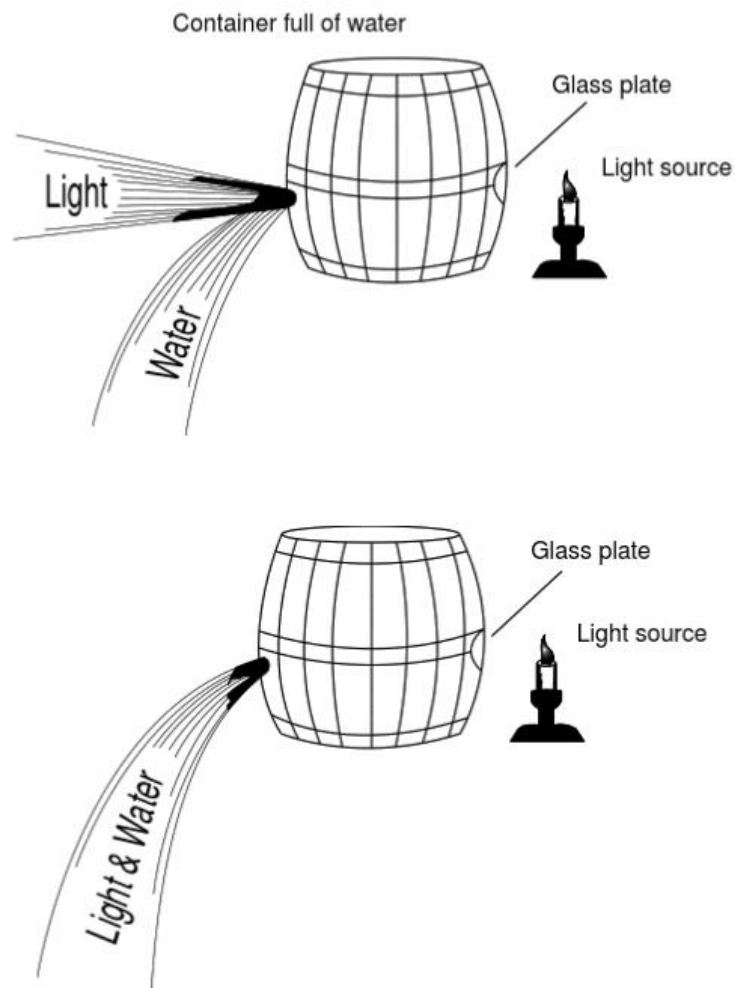


Fig 1.1 Tyndall's experiment [2].

The barrel had one glass window and, on the opposite side, a tap.

Putting a light outside the window and pulling out the tap will cause the water to gush out, and the light was thought to go out in a straight line; but the light followed the water, curving its path. This was the first way to guide the light [2].

Optical communication was left behind for a long time between the XIX and XX centuries, while electric technology became central for our society.

Electric telegraph, followed by the telephone, completely shadowed the older technology that had the great problem of not having a good light source aside the sun and so being too dependent from the weather. Even if Bell, after the construction of the telephone, tried with the photophone, a similar concept but using optical signals it was discarded for the prior motives.

The first optical fiber was fabricated in the early 1920s [3] but there wasn't still a light source.

With the breakthrough of the invention of the laser in the 1960s the study of the propagation of laser beams and the possibility to guide them inside ducts rekindle.

The first attempts were made with several lenses to refocus the beam continuously, another way was a gas-filled duct with a temperature gradient maintained which gave a refractive index profile that worked as a lens. This concept is similar to modern gradient index fibers. [4]

The first optical fiber with low losses for telecommunications was built in 1970, just 4 years after K.C. Kao predicted it theoretically. Made with fused silica it had only few tens of dB/km of loss. Combined with the laser it started a revolution in the world of telecommunications. [3]

1.2 Basic structure of an optical fiber

Optical fibers are materials shaped as thread with very small diameter.

Fig. 1.2 shows the most common structure for an optical fiber with a core where the light is guided, a cladding of a different glass with lower refractive index surrounding the core and a protective coating called jacket, typically made of polymers like acrylics or polyimide [5]. A variety of polymers can be used based on the environment where they will be used.

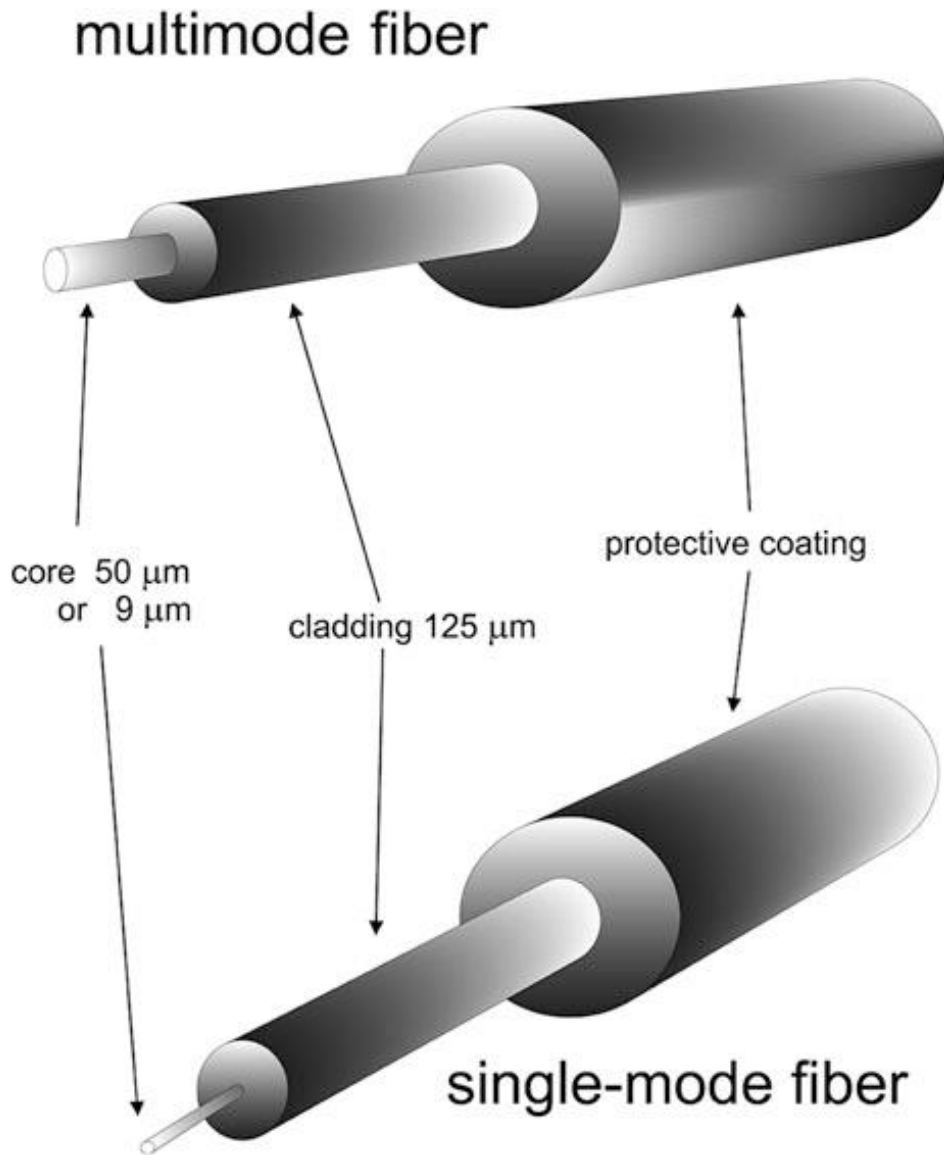


Fig. 1.2 Core-cladding structure for single-mode and multi-mode fiber with most common diameter [1].

Commonly, a commercial fiber has a diameter of 250 μm with 125 μm of cladding and a core that can vary depending on whether it is single-mode (smaller core) or multi-mode (larger).

Total internal reflection (TIR) is used to guide the light waves.

The physical principle is summarized by Snell's Law:

$$n_1 \sin(\theta_1) = n_2 \sin(\theta_2)$$

Eq. 1.1 Snell's Law

In Eq. 1.1 n_1 and n_2 are the indices of refraction of the different media, while θ_1 and θ_2 are the angles of incidence and refraction.

In Fig. 1.3 a schematic illustration of the TIR is reported.

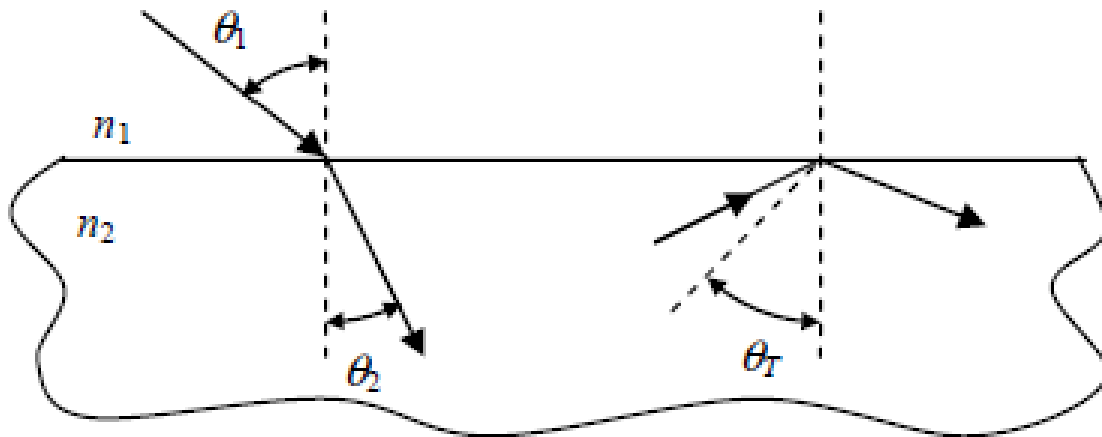


Fig 1.3 Total internal refraction scheme [6].

When the light wave enters from a medium with a higher index of refraction it bends toward the normal direction and bends away from it if it enters a medium with lower index. If the angle of incidence is higher than the critical angle θ_c , all the light is reflected back in the medium with the higher index of refraction. This situation is called TIR.

If light propagates inside the core of the optical fiber, parallel or with a small angle between the ray and the core-cladding interface, there will be TIR and the light will be trapped and guided inside the core without losing energy.

This is called “guided mode”, while a light that enters with a greater angle and loses a part of energy each refraction is called “leaky mode”.[6]

With a larger core, more optical modes are supported by the fiber.

A single-mode fiber is a fiber with a core so small that it can support only one mode. It is particularly interesting because its losses can be below 0.15 dB/km or, in other words, less than 4% of the light is lost after 1 km.

1.3 Main applications

There are many applications for fibers, aside from the telecommunications which is the most known and largest market. they are used also for flexible lighting, imaging, sensors, power transmission and they are found in various fields such as biomedical and military applications.

Some concrete examples are:

- road signs, where a bundle of fibers is used instead of light bulbs directly. In this way, only one bulb is used to illuminate the selected fiber to compose the number, letter, or image desired. This way there are never parts not visible caused by one broken light source. One light bulb is always ready to switch and substitute the broken one;
- endoscopes, again based on a bundle of fibers, where some of the fibers are used to illuminate the point to analyze and some acts like pixels to transmit a whole image thanks to a lens at their end that collects the information;
- connections between microphones and speakers, optic fibers can be made also of plastics like polymethylmethacrylate (PMMA) even if they have considerably higher losses. Even with these losses their applications in hi-fi systems and control circuitry (for short distances) are increasing [2].

1.4 Goals of the thesis

Fiber optics sensor applications span between oil well monitoring to homeland security and are becoming a major stimulant to the economy. The average annual growth rate of OFS (optical fiber sensors) was 63% between the period 2005-2010 [7] and a steady growth continued in the recent years thanks to the fast growing market of Asia pacific. A growth of the market from USD 1732.91 million in 2019 to USD 3850.83 million by 2025 is forecasted [8].

Even if silica glass fibers can achieve, with the right dopants, losses as low as 0.15 dB/km (at 1550 nm) and approach the theoretical limit of 0.14 dB/km, they still have some limits [6].

Silica offers its lowest loss at 1500 nm and lowest dispersion at 1310 nm and that is why most applications were made near this range, the near-IR (1300 - 1700 nm), exploring new technologies or designs to improve them.

The growing interest in other fields aside telecommunication such medical, biological and environmental for imaging and sensing made interesting new ranges of wavelength such the mid-IR ($> 2 \mu\text{m}$) [9].

New materials with broader transmission ranges are promising candidates for these fibers.

In Tab. 1.1 the differences between glasses can be observed.

Tab. 1.1 Comparison of different glasses for optical purposes [10].

	Silica	Tellurite	Fluoride	Chalcogenide
Refractive index n at $1.55 \mu\text{m}$	1.46	2–2.2	~1.5	2.3–3
Nonlinear refractive index n_2 ($\times 10^{-20} \text{ m}^2/\text{W}$)	2.5	20–50	2–3	100–1000
Raman gain coefficient g_R at $1.064 \mu\text{m}$ ($\times 10^{-11} \text{ cm}/\text{W}$)	0.93	32	1.1 ± 0.3	280–720
Raman shift (cm^{-1})	440	650–750	550	250–350
λ_0 , zero-dispersion wavelength of material (μm)	~1.3	~2	~1.7	>5
IR longwave transmission limit	Up to $3 \mu\text{m}$	$6\text{--}7 \mu\text{m}$	$7\text{--}8 \mu\text{m}$	$12\text{--}16 \mu\text{m}$
Reported lowest loss dB/m (wavelength)	0.15×10^{-3} ($1.55 \mu\text{m}$)	0.0204 ($1.56 \mu\text{m}$)	0.45×10^{-3} ($2.35 \mu\text{m}$)	0.023 ($2.3 \mu\text{m}$)
Thermal stability for fiber drawing	Excellent	Good	Poor	Good
Viscosity around fiber- drawing temperature	Flat	Steep	Steep	Flat
Durability in environment	Excellent	Good	Poor, hygroscopic	Good
Toxicity	Safe	Safe	Relatively high	Relatively high

Tellurite glasses can transmit up to 7 μm , fluoride glasses up to 8 μm , and chalcogenide glasses up to 16 μm ; these wavelengths are way longer than the silica transmission limit of 3 μm .

Tellurite glasses might be the best compromise for applications in the mid-infrared having a broad transmission window, low intrinsic loss, little photosensitivity, high optical damage threshold and high refractive index. Tellurites are also very stable chemically, thermally and mechanically being a simple oxides-based glass. They are also easy to modify with dopants [9].

Aside from the different glasses, also new designs are studied for imaging like disordered fibers. It has been demonstrated high-quality image transport through a meter-long glass-air disordered optical fiber [11]. Here, the fiber was made from fused silica, showing great potential having better imaging performance than some of the commercial multicore fibers but having still the limitation of the transmission range of silica. Other research about all-solid tellurite optical glass [12] shows promising opportunities for tellurite glasses.

In this thesis work we attempt to design, fabricate and characterize a tellurite-air disordered optical fiber with a clad of commercial silica glass for imaging in the mid-IR region. The research has been performed at CREOL, The College of Optics and Photonics at the University of Central Florida, in collaboration with the Politecnico di Torino where the tellurite glass, used for the core of the disordered fiber, was fabricated.

1.5 Structure of the thesis

Chapter 1 presents the history of fiber optics, the basic structure and functioning and the possible applications, in particular the applications for the topic of this work.

Chapter 2 is focused on tellurite glasses, their properties and applications with a special attention to the properties of the specific composition used in this study.

Chapter 3 is a review of the characteristics of photonic crystal fibers and the physics behind them; in particular, the mechanism of Anderson's localization used by disordered fibers and its state of the art are discussed.

Chapter 4 describes the common techniques for fiber drawing and the one chosen; the problems and advantages of each steps are described.

Chapter 5 shows the different properties of the glass and the fiber and the methods of characterization.

Chapter 6 draws the conclusions from the results emerged in the previous chapters.

2 Tellurite glasses

2.1 Introduction to tellurite glasses

A glass is not defined by its chemical composition but by a disordered spatial arrangement. It lacks the periodic and repeated structure of long-range order as the crystal; the glass is called “amorphous”. This structure is the consequence of failing to crystallize due to the fast cooling time which is faster than the crystallization time.

There are many substances that have a glassy state, in Tab. 2.1 there are some examples.

Tab. 2.1 *Examples of substances that achieve a glassy state [1].*

Substance	Glass temperature (K)
Natural rubber	200
PVC	347
Water	140
Glucose	305
Selenium	303
Beryllium fluoride	570
Germanium dioxide	800
Silicon dioxide	1350

Glasses exhibit unique characteristics that make them interesting.

They show many isotropic properties, thermodynamic metastability, a viscosity dependent from temperature and a glass transition range instead of exact melting temperature.

The metastability is given by the rapid cooling that froze in an amorphous state even if the state at the lowest energy would be the crystal structure. Faster the cooling more far away are the atoms and it's further away from the thermal stability.

Glasses are preferred in optics because crystalline materials are brittle and can't be made without defects and dislocations that will act as scatterers of light making losses higher.

Glasses do not have specific composition preferred in nature thus the flexibility in tuning the properties adding dopants is great, but only a limited selection of glasses are useful in the optic industry [1].

Optical glasses need a set of properties well defined, measurable with accuracy and reproducible:

- high light transmission, measured by internal transmittance;
- index of refraction and its dependence on wavelength;
- uniformity in light deflection in all its volume;
- high material homogeneity (content of bubbles, inclusions and other defects).

To manufacture a glass there are three ingredients:

- glass former is the main ingredient of the glass and it builds the network as silica (SiO_2), germanium dioxide (GeO_2) or boron trioxide (B_2O_3);
- glass modifiers are oxides that can't vitrify as the glass formers and can't therefore build the network but they can form weaker bonds with the glass former and make it easier to vitrify and change other features. Examples are calcium oxide (CaO), sodium oxide (Na_2O) or potassium oxide (K_2O);
- intermediates are oxides like alumina (Al_2O_3) or titanium dioxide (TiO_2) that can substitute in small measure the glass former or act as a modifier.

Discovered in 1952 by J.E. Stanworth [22,30], TeO_2 has remained unstudied for many years.

Tellurite glasses were thought to be intermediate glasses until 1984 [14], when it was produced the first pure TeO_2 , and never received much attention. Since the theoretical difficulties with amorphous solids were solved the interest in tellurite glass has grown, as can be seen from the augment of articles about tellurite glasses passing from the 4 articles of 1984 to the 175 of 2016 found using research engine "Scopus". Different books have been published about it [15-19] and five video seminars for international educational purposes have been performed [20].

In Fig. 2.1 it is possible to see how tellurites and chalcogenides have become the most interesting glasses in the recent years.

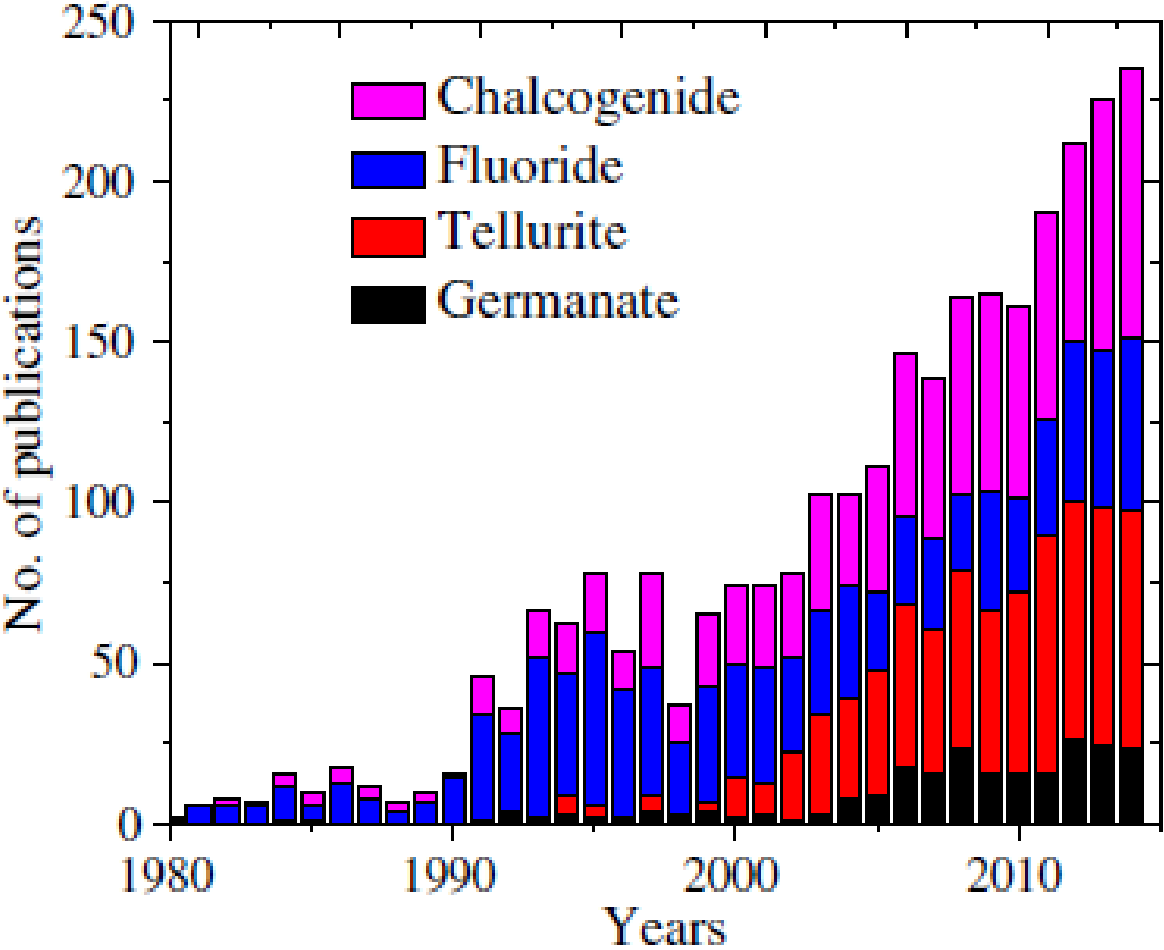


Fig 2.1 Number of publications between 1980 and 2014 reported in Web of Science. [30]

The main research on tellurite glasses up to now has been done on the tuning of characteristics of the glass modifying it with transition metal ions and rare-earth oxides [18].

2.2 Physical properties

Tellurium oxide don't form glass when quenched from the liquid or vapor state without very fast cooling [24], but with small concentrations of solute, less than 2 mol%, it drastically increases the tendency to form glass. In crystal form TeO_2 is formed only by TeO_4 trigonal bipyramidal units (tbp) [23].

When modifiers are added they enter the network and make the strong covalent bond Te-O weaker.

In Fig. 2.2 the trigonal bipyramid unit and the trigonal pyramid unit (tp) that appear in the glass form are shown. According to [21] in the bipyramid the equatorial triangle Te-O bonds (1) are shorter (0.185-0.195 nm) than the axial (2) bonds that vary between 0.205-0.215 nm depending upon the cationic charge.

Tellurium oxide-based glasses have three structural units, on the contrary (pyramid, distorted pyramid and bipyramid) each of them carries a lone pair of electrons which contribute to unusual physical properties.

The distorted pyramid ($\text{TeO}_{3+\delta}$) or intermediate polyhedron is due to excess of oxygens and can be formed thanks to the mutually interchange with four bridging oxygen sites and the lone pair electrons [21].

This is a unique feature of tellurite glasses which may provide a range of chemical environments for cations providing a means to dissolve larger concentrations of rare-earth oxides than in silicates, phosphates and fluorides [19-21].

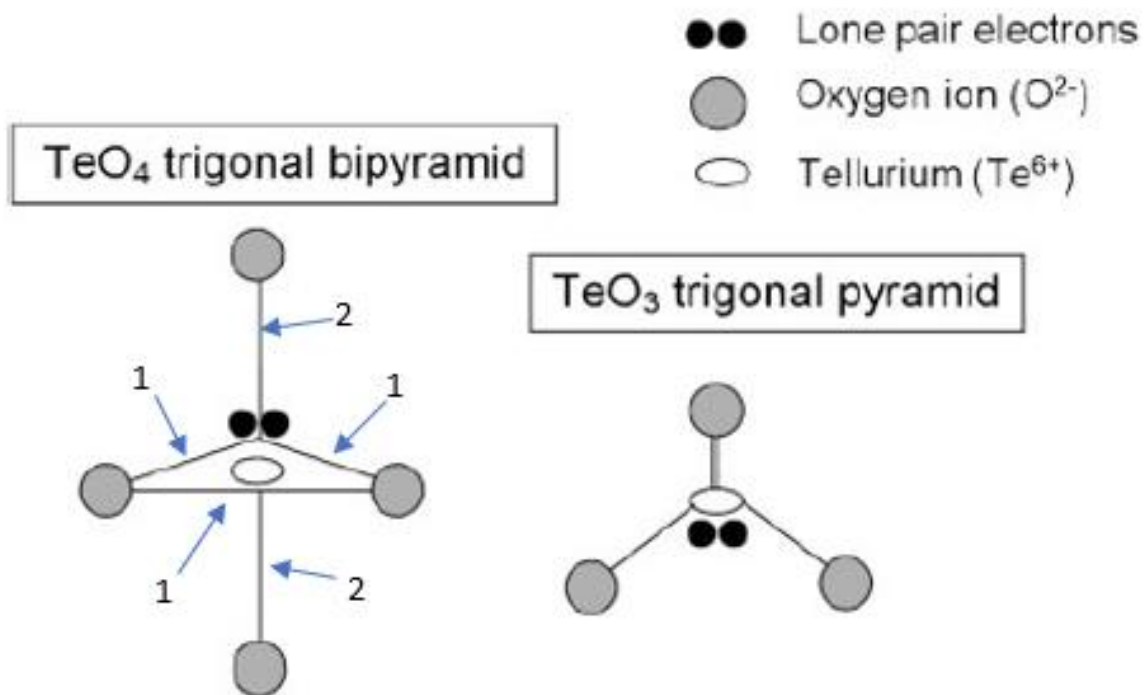


Fig. 2.2 *TeO₄ trigonal bipyramidal unit (left) and the TeO₃ trigonal pyramid unit (right) bonds. Labeled as 1 are equatorial triangle bonds, labeled as 2 are axial bonds.*

There are many interesting physical properties:

- high solubility of rare-earth elements given by the lone pair electrons that participate as structural units [21,25,26];
- low phonon energy (640-790 cm⁻¹ vibration bands) makes them interesting for near-IR and mid-IR lasers and amplifiers and sensor engineering [21];
- high refractive index in a range of 1.932-2.304 [10,21]. It is one of the highest in oxide glasses for visible as well as for near IR regions and is strongly dependent on the polarization of the constituent ions [19,21].
- broad transparency window of 0.4-7 μm better than both germanium oxide (GeO₂), 0.38-5 μm, and silicate (SiO₂), 0.2-3 μm, as shown in Tab 1.1 and in [21]. This range of

transmission is promising for mid-IR applications other than visible;

- low melting temperature normally under 700 °C [19] helps to make the energy needed for their production low;
- high thermal (resistance against devitrification) and chemical stability given by its tellurium-oxygen bond, which are better than fluoride and comparable to GeO_2 [21,30];
- low hygroscopy as opposed to phosphates or fluorides. This means they tend not to absorb water molecules and improves their resistance to environmental degradation [18,19].

The most common techniques to produce a tellurite glass are Chemical Vapor Deposition (CVD), melt quench method and the sol gel method and the first used was the melt quench method [19,27,28,29].

2.3 TNGPZ glasses

Many glass compositions exist thanks to the high solubility of rare-earth ions but not all of them are suitable for the production of fibers due to thermal stability [19]. The most common are made with 70-80 mol% of TeO_2 and 20-30 mol% of glass modifiers and intermediates like ZnO , WO_3 , Li_2O , Na_2O and most of them are from the ternary or quaternary systems. In particular, it's possible to identify two main families:

- $\text{TeO}_2 - \text{WO}_3 - \text{R}_2\text{O}$;
- $\text{TeO}_2 - \text{ZnO} - \text{R}_2\text{O}$

with R that can be Li, K or Na [19].

The most common glass is called TZN and it is composed by tellurium oxide (T), zinc oxide (Z) and sodium oxide (N) with a standard composition of 75 TeO_2 -20 ZnO - 5 Na_2O .

Our glass is composed of TeO_2 , Nb_2O_5 , GeO_2 , PbO and ZnF_2 , where the exact molar composition was not given by Politecnico di Torino for protection purpose.

Sodium oxide (Na_2O) is substituted because it is known to decrease glass durability [19], while the use of ZnF_2 instead of ZnO allows removing contaminating hydroxyl groups and increasing the thermal stability [31,32].

2.4 Existing tellurite glass applications

Applications for tellurite glass have grown, in the last few years, in an outstanding manner with great interest in photonic applications. Some of the most interesting have been:

- application on the back of amorphous silicon solar cells with a 0.45% increase in efficiency [33] and of 7% with tellurite glass doped with 1% of Tb^{3+} [35];
- tellurite thin films for optical waveguides and memory device produced by radio frequency (RF) sputtering [41];
- fabrication of a laser with maximum output power of 34 mW at 2040 nm in a 9 cm-long Ho^{3+} -doped tellurite glass-based fiber [34];
- extended bandwidth fiber amplifier of more than 80 nm for positive gain in 0.9-2.4 m long fiber [36,37];
- low loss tellurite fiber (< 50 dB km^{-1}) for Raman gain of 15-20 dB in a photonic crystal fiber; [38];
- photonic crystal fiber for supercontinuum generation in the 2-5 μm range; [39,40];
- all-solid disordered optical fiber for NIR optical image transport and hollow core for supercontinuum generation [12,42].

3 Disordered fibers

3.1 Introduction to photonic crystals

Photonic crystals (PhCs) are periodic optical nanostructures that can be found also in nature as in butterflies wings and some semi-precious stones [43]. They have a periodic modulation of the refractive index which gives peculiar properties [44].

The first study about control of light propagation through periodic structures was made in 1887 [45] but only in 1987, with Yablonovitch and John, intensive studies started [46, 47].

Photonic crystals are divided in three categories by their structures:

- one-dimensional (1D);
- two-dimensional (2D);
- three-dimensional (3D);

In Fig. 3.1 examples of the different structures are shown.

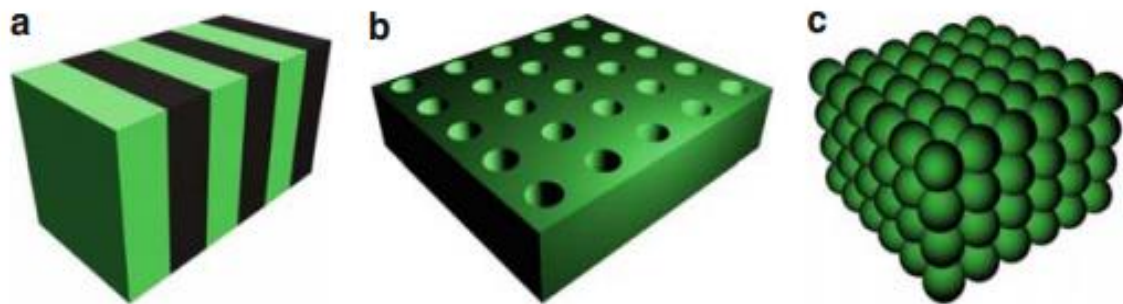


Fig. 3.1 *Examples of photonic crystals with 1D (a), 2D (b) and 3D (c) structures.*

Some examples are:

- Bragg Gratings for 1D used for many applications like antireflecting coatings to improve optical components like lenses or prisms and distributed reflector in vertical cavity surface emitting lasers. 1D PhCs can vary only refractive index, layer thickness and the number of layered structures [44];
- there are human made periodically arranged systems of dielectric rods in air, porous silicon with periodic pores but also the butterfly's wing found in nature, the two most commons are square and hexagonal [44];

- in nature the most common 3D configuration is the stone opal with its iridescence and there are many more artificially made because of the permittivity modulation along 3 dimensions [44].

Thanks to the similarities between photonic crystals and solid-state physics some properties and computation method of the latter can be applied. In particular, the periodic modulation of the refractive index can be compared to the behavior of electron-hole in atomic lattice and the both of them provide band gap. Determination of the eigenfunctions in a PhC is similar to the calculation of the particle-wave functions in the solid state.

This similarity is used to obtain the photonic band structure [44].

The photonic band gap (PBG) is the most important property of PhCs and refers to the energy where the light propagation is prohibited inside the PhC.

This means that these radiations are completely reflected when incident in the structure but if we introduce a defect it acts like a defect in a semiconductor creating a new eigen-state with energy equal to the eigen-frequency of the defect. A radiation that happens to be within the defect frequency will now propagate inside the structure or be guided like in waveguide if multiple defects are present.

PhCs possess frequency ranges allowed or forbidden and these information are given by the band structure; an example is reported in Fig. 3.2.

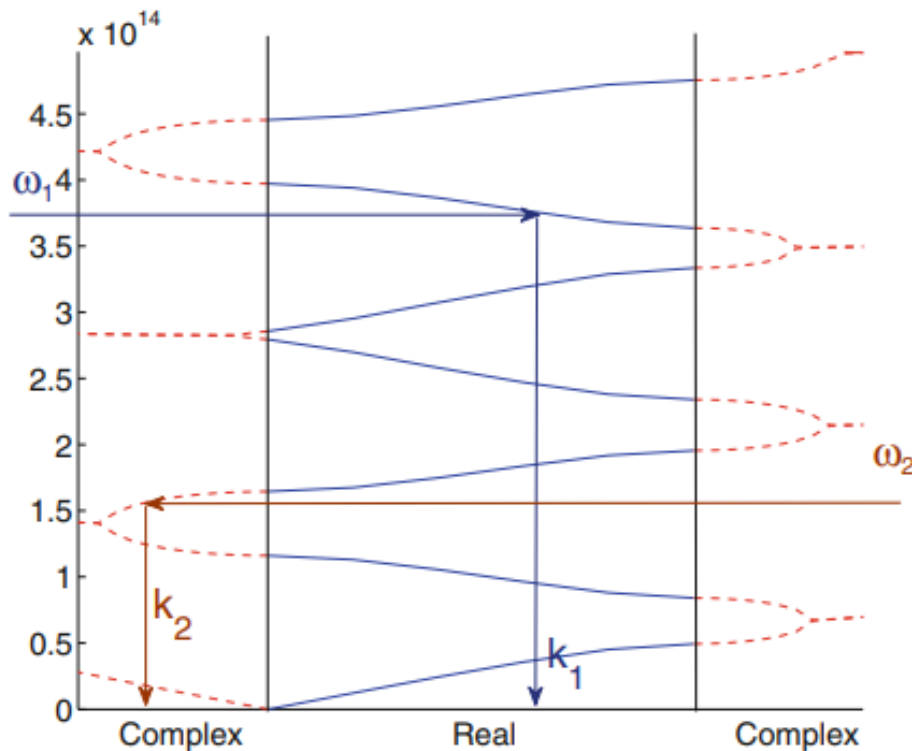


Fig. 3.2 Example of a band structure of 1D PhC [44].

The band structure represents the connection between the properties of the optical medium (PhC) and the properties of the radiation. The vertical axis shows the frequencies allowed to propagate (called “resonant frequencies” or “eigen-frequencies”) and the horizontal axis corresponds to the wave-vector of the radiation.

For each frequency there is a wave-vector that can be real or complex, for example for ω_l its wave-vector is k_l . If the vector is real, the wavelength simply propagates in the medium, if it is complex there is radiation attenuation or gain. The forbidden frequency ranges are called “photonic band gaps” [44].

3.2 Anderson localization

Anderson localization made its first appearance in the 1958 in the paper “Absence of Diffusion in Certain Random Lattices” in the context of electron motion [48]. This phenomenon, also called *strong localization* (to distinguish it from *weak localization* which is a precursor of Anderson localization when disorder is not strong enough) [49], is the absence of diffusive wave transport in highly disordered scattering media [50].

It can be observed from the wave-function of an electron to Bose-Einstein condensates and even in classical wave phenomena as acoustics and elastics [50]. In this thesis, its application in optics [51] with a disordered optic fiber is studied.

Anderson was trying to see if an increase of lattice disorder would lead to a decrease of the electrons mean free path therefore to lower conductivity, as the classical Drude theory suggested [52]. Anderson discovered that, beyond a critical amount of impurity scattering, the electrons would come to a complete halt making the electron trapped; a metal-insulator transition.

Before this critical amount, the diminished conductance between 2 points (weak localization) is given by the increased probability that electrons return at their starting point [52].

Anderson used a tight-binding model of an electron in a disordered lattice to explain localization, as in Fig. 3.3.

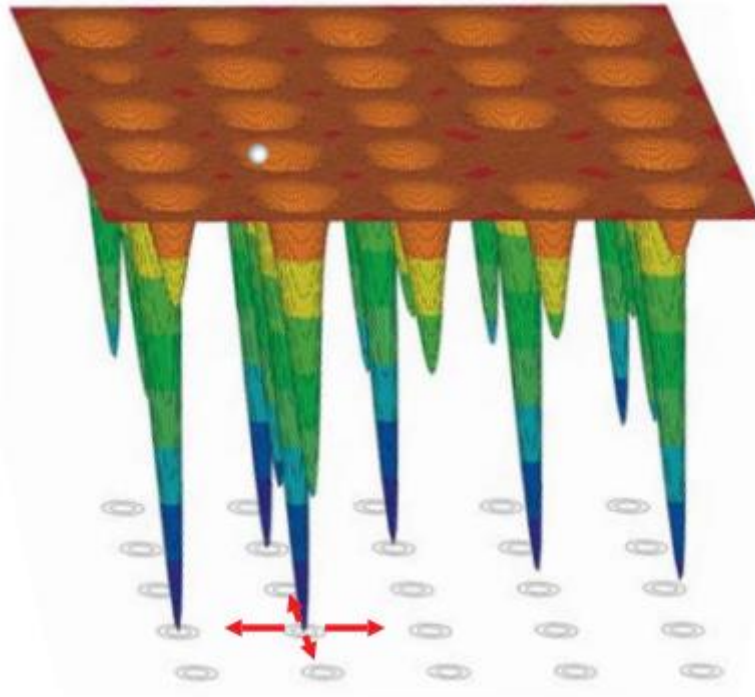


Fig. 3.3 *Tight-binding model [52] proposed by Anderson.*

In a disordered two-dimensional lattice, as the one shown, an electron cannot tunnel from one well to another randomly as in an ordered lattice because the depth of each well is different. Beyond a critical amount of randomness of these depths, the electron is localized in a certain region, even if on a scale greater than the lattice constant. The idea of “mobility edge” was introduced later by Mott. Electrons with energies near the band edge are localized, since they do not have enough energy to move around the lattice [52].

Anderson proposed that, if the disorder is strong enough, there will be localization independently of the dimension of the system [53]. Shortly after (M.E. Gertsenshtein, V.B. Vasil’ev 1959), it was established that in one-dimensional disordered systems (e.g. thin wires) all quantum states are localized [52]. It is important to remember that having all states localized in thin wires does not mean that conduction is always small, a “necklace state” can form with two or more localized modes [52].

In higher dimensions it was much harder to solve localization because there are more paths that electron can take making interference less effective [49], but in more than 50 years there have been many interesting results (e.g. Fröhlich and Spencer 1983, Simon and Wolff 1986, Aizenman and Molchanov 1993) [54] in this topic.

For dimension $d = 2$ it was solved approximately with Renormalization Group analysis, showing that even here there is always localization for any grade of disorder [55]. Therefore “true” metals do not exist with dimension of 1 or 2 and the MIT, Metal-Insulator Transition, shows up only with $d \geq 3$ with the mobility edge.

The mobility edge is the energy such that states below it are localized and above it are extended [58]. As shown in Fig. 3.4, when disorder increases the mobility edge moves toward the centre until the two edges meet in the centre and all the states are

Mobility edge

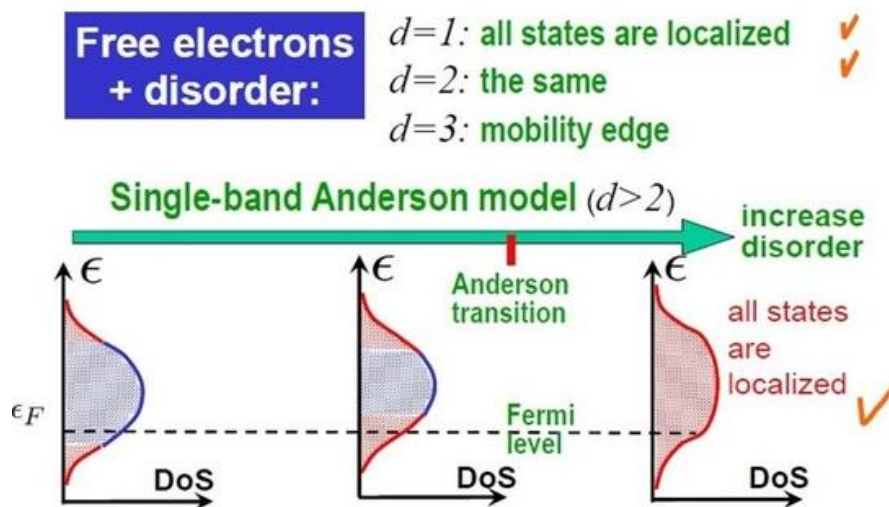


Fig. 3.4 Relationship between disorder and localization [57].

localized.

When the mobility edge, also called E_c , lies below E_f (Fermi level) the conductivity tends to a finite value as $T \rightarrow 0$, while it tends to zero if E_c lies above E_f .

The scaling theory of localization [55] predicts that the conductivity of a material depends on its size when it's close to the mobility edge [52], as in Fig 3.5.

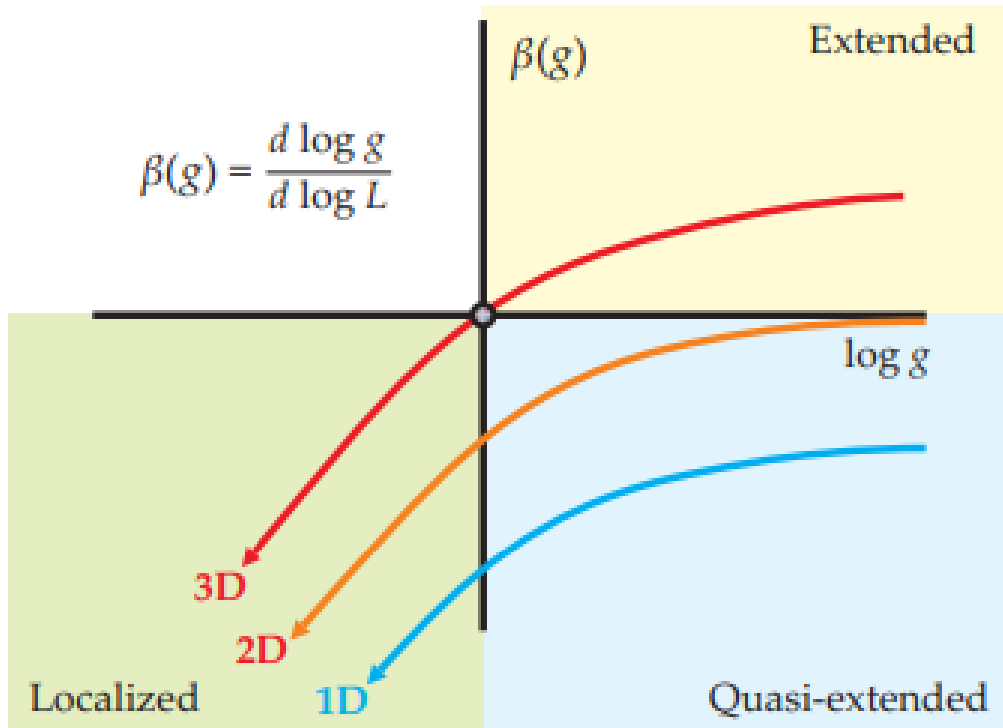


Fig. 3.5 Relationship between scaling function $\beta(g)$ and the average conductance g for different dimensions D . L is the system size for large g $\beta(g) \approx D-2$ [52].

The dimensionless scale parameter g governs the size dependence and it is a measure of conductance. It was defined by Edwards and Thouless [56] as the ratio between the Heisenberg time and the Thouless time. The Thouless time quantifies the time interval a conducting electron takes to arrive to the boundary through a zigzag motion from the inside of the sample, while the Heisenberg time is the longest time that an electron wavepacket can travel inside a finite size sample without visiting the same region twice [52].

When the Thouless time is greater than Heisenberg time a wavepacket can't reach the boundaries, thus the states are localized when $g < 1$, this criterion is universally valid having only the dimensionless conductance g as the only parameters [52].

In Fig. 3.5 it is shown that only for 3D the function $\beta(g)$ vanishes, for lower dimensions there is not a genuine phase transition MIT.

After localization of electrons, different wave-functions have been studied with interesting results but, among all classical wave systems, optical waves stand out thanks to the many possibilities to construct disordered background potential [50,59].

Each translucent medium scatters the light diffusively, but normally the scattering strength is far from the one required for 3D Anderson localization. To observe Anderson localization of light, many systems, like powders or solids with pores etched into them, have been synthesized. Some examples are reported in Fig 3.6.

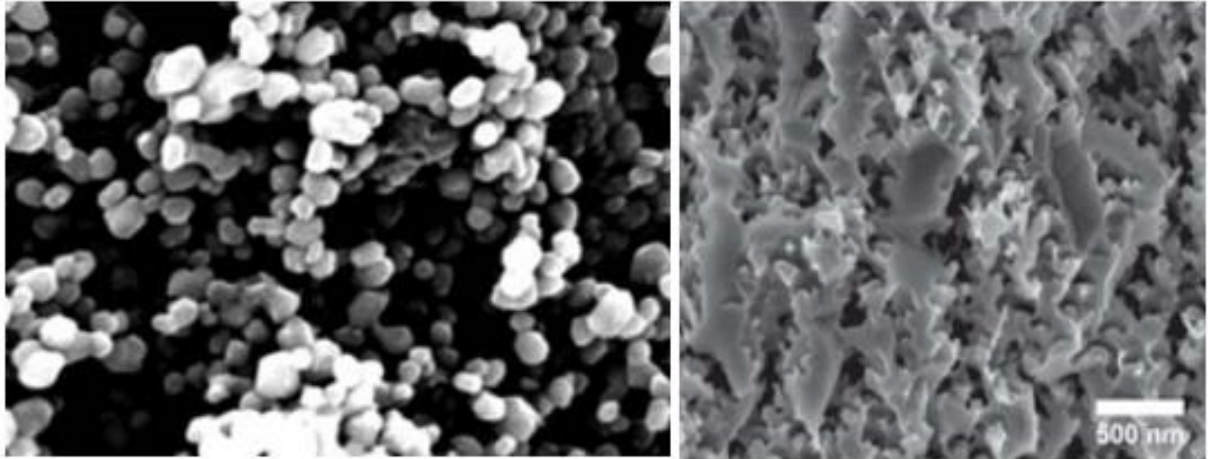


Fig. 3.6 *Left image reports titanium dioxide particles, 250 nm in diameter. Right image shows gallium arsenide powder with average particle size of 1 μm [52].*

They show high refractive index and submicron size mean free paths of the order of a wavelength. Moreover, they are designed to maximize the scattering without introducing absorption, which generally is present with the large refractive index wanted [50,52].

One way to observe localization avoiding absorption is to use light with a frequency below the electronic bandgap of a semiconductor, therefore not incurring in absorption.

3.2.1 Transverse Anderson localization

Transverse Anderson localization was suggested in 1980 by Abdullaev et al. [60] and in 1989 by De Raedt et al. [61] but only confirmed experimentally in the 2007 by Schwartz et al. [62] in a photorefractive crystal.

De Raedt et al. analyzed an optical waveguide with dielectric medium transversely random but longitudinally invariant, as shown in Fig. 3.7.

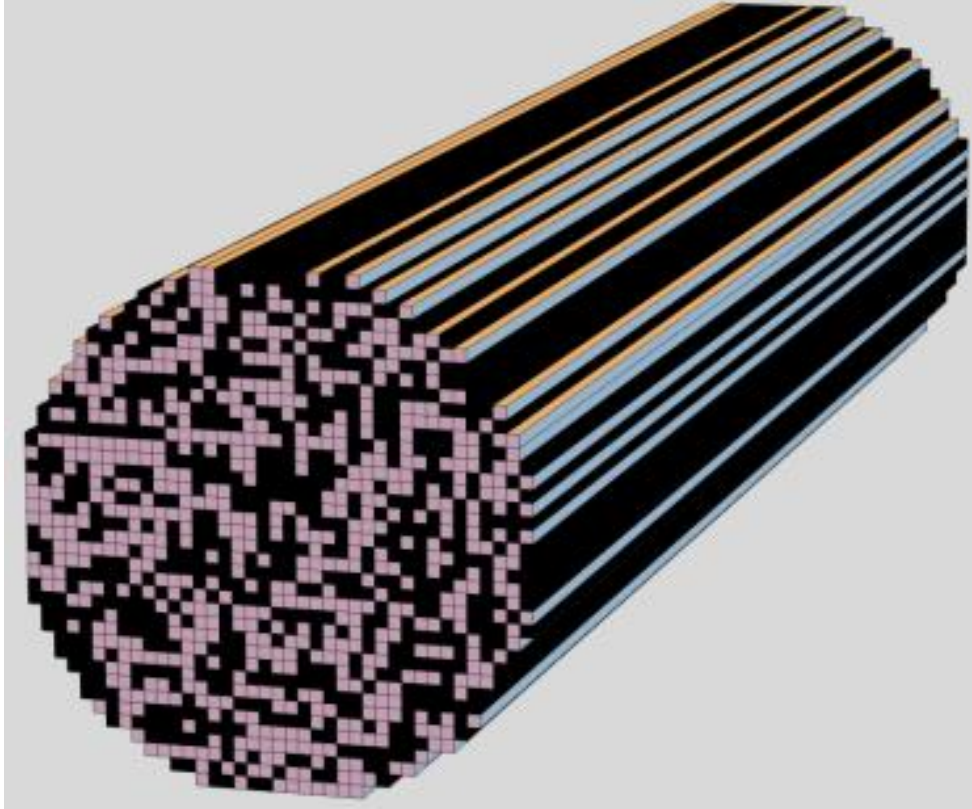


Fig. 3.7 Conceptual sketch proposed by De Raedt et al. for transverse Anderson localization in a quasi-two-dimensional system. The different color of the pixels represents the different refractive index. Two colors mean two different n [50].

The dimension of each pixel in this system is of the order of the wavelength of the light localized. An optical field launched in the longitudinal direction will remain localized in the transverse plane thanks to the transverse scattering. While it propagates longitudinally, the amplitude of the field decays exponentially in the transverse direction and the localization radius can be improved (decreased in size) with a greater refractive index contrast:

$$\Delta n = |n_2 - n_1|$$

Localization was observed even with $\Delta n \approx 0.10$ with a 50-50 polystyrene (PS) and polymethyl methacrylate (PMMA) optical fiber [63].

3.3 Applications of disordered fibers

In 2012 Karbasi et al. [63-65] observed for the first-time transverse Anderson localization in a disordered optical fiber for image transport that is normally based on multicore optical fibers.

Multicore fibers have been thoroughly studied in the years for their employment to transport optical images [66-70] and many limitations have been discovered.

The quality of the image is limited by the pixelation effect and the inter-core coupling results in low contrast images [71], that's why disordered fibers are of growing interest in this field. The polymeric fiber of Karbasi et al. had quality better or comparable with those obtained using commercial multicore image fiber but without any need of pre- and post- processing of the signal to obtain the image.

These fibers are of particular interest for the study of biological systems [71], as shown by the large number of publications and patents in the medical and biological fields [72-75].

3.4 State of the art of disordered optical fibers

In the last years, different disordered fibers have been produced with different materials and designs for some noteworthy achievements.

In Fig. 3.8 the polymeric fiber of Karbasi et al. is shown [63].

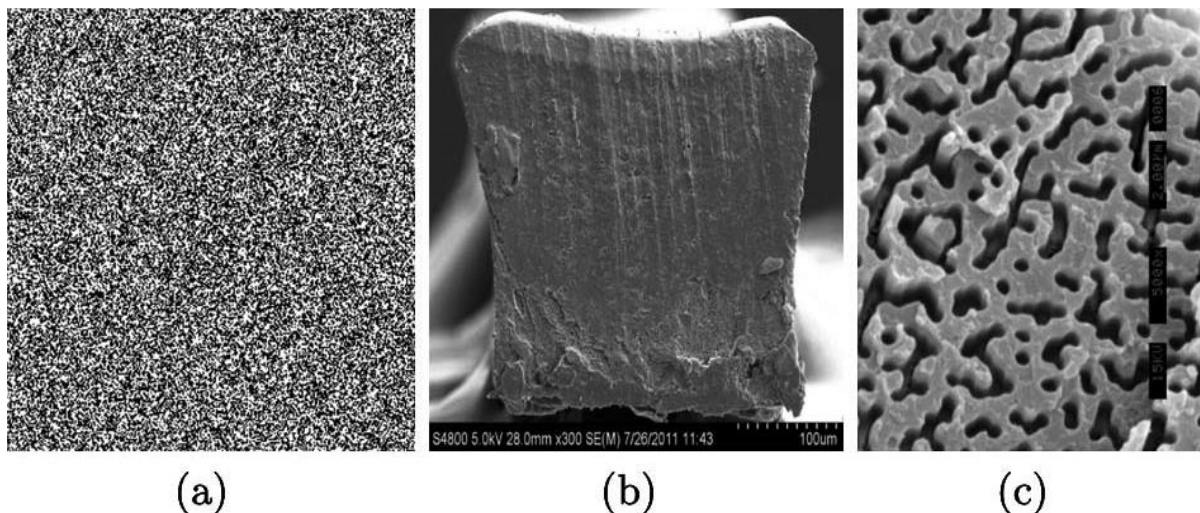


Fig. 3.8 (a) Sample refractive index profile used for simulations showing the two regions with different refractive index. (b) SEM image of the fiber's tip. (c) SEM image of the same tip but exposed to a selective solvent [63].

This fiber not only showed comparable image quality to the best commercial multicore imaging fibers, but it was made with PMMA and PS (Polystyrene) for an all-solid fiber. This means cheap materials and productions (lower temperature needed) and easy-to-achieve control of ratio between different refractive indexes but with high optical attenuation.

In 2019 Tuan et al. [76] successfully fabricated an all-solid tellurite glass optical fiber with transversely disordered refractive index profile. They demonstrated experimentally for the first time the transport of near-infrared (NIR) optical images through a 10 cm-long piece of this fiber with high contrast, high brightness and high matching ratio of different wavelength. It was produced with a 50-50 blend of $70\text{TeO}_2\text{-}8\text{Li}_2\text{O-}17\text{WO}_3\text{-}3\text{MoO}_3\text{-}2\text{Nb}_2\text{O}_5$ (TLWMN) and $75\text{TeO}_2\text{-}15\text{ZnO-}5\text{Na}_2\text{O-}5\text{La}_2\text{O}_3$ (TZNL) glasses for the core and the Δn was 0.095 at $1.55\ \mu\text{m}$. The fiber section is shown in Fig. 3.9.

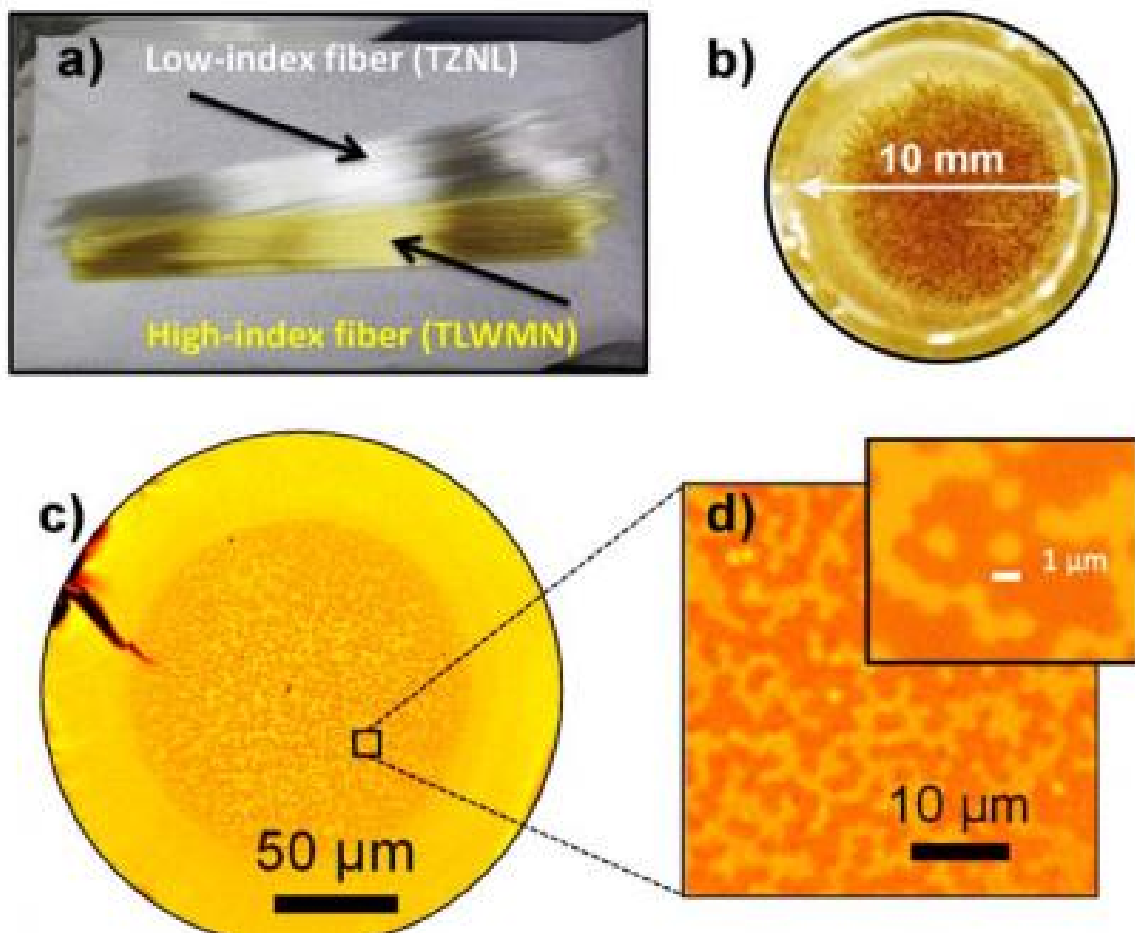


Fig. 3.9 a) the separated glass fibers used to fabricate the all-solid fiber. b) Dimensions of the preform with the randomly stacked fibers inside a cladding tube made of TZNL glass. c) Cross-section of the final fiber. d) Magnification of a random core part.

In order to improve localization with a greater Δn and lower optical attenuation, for the first time, in 2017, optical images have been transmitted through a random glass-air fiber structure [77] with attenuation of the order of 1 dB/m. The fiber is shown in Fig. 3.10.

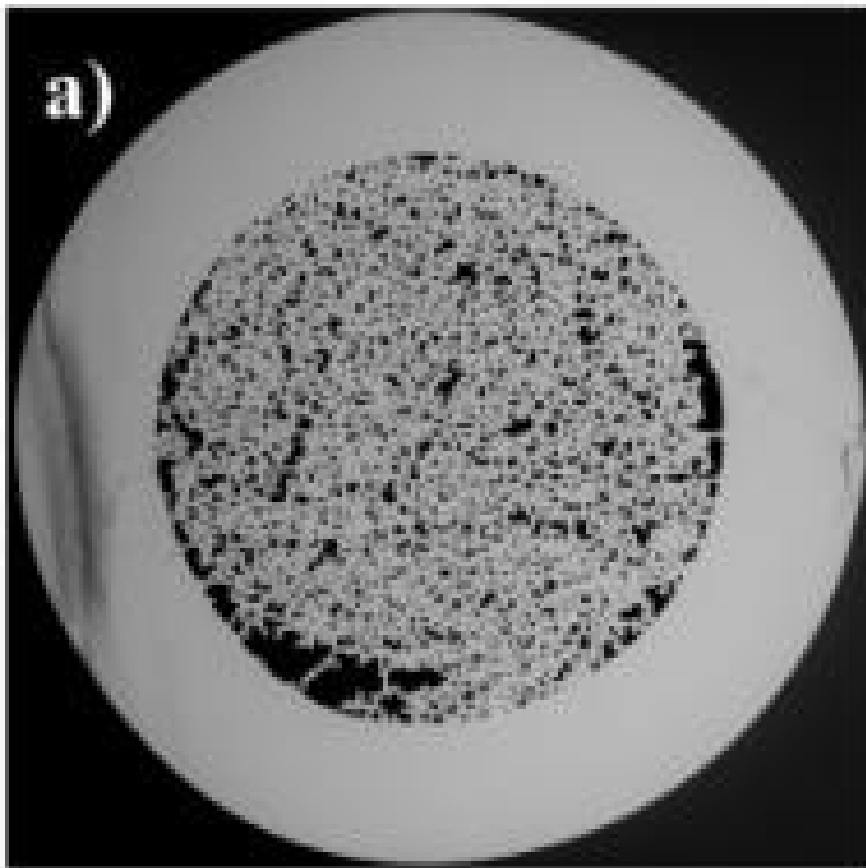


Fig. 3.10 *Cross section of the glass-air random fiber (GARF) [77].*

This fiber showed great performance combined with deep convolutional neural network (DCNN) [78], but there is still room for improvements, like a greater Δn with different glasses and improved air-fill ratio (this fiber had $\approx 26\%$ of air fraction when the desired ratio would be 50%).

4 Optical fiber production

4.1 Common techniques

Two steps are essential for the manufacturing of an optical fiber:

- Realization of a *preform*, a rod of glass that replicates in larger scale the fiber structure. Typically, it is 1 m-long with a diameter of 10-50 mm. The preform highlights the same refractive index profile of the final fiber [1];
- The preform is softened by heating and stretched to the desired diameter of the final fiber.

There are several techniques to produce the preform, each with advantages and disadvantages, but they can be divided in two categories: chemical vapor deposition (CVD) and rod-in tube.

Conventional rod-in-tube technique is shown in Fig. 4.1, it is very simple and can be modified to obtain different design aside single- or multi-mode fibers, like hollow core optical fibers or disordered fibers.

The rod and tubes constituting the preform are conventionally fabricated through melt-quenching technique [81].

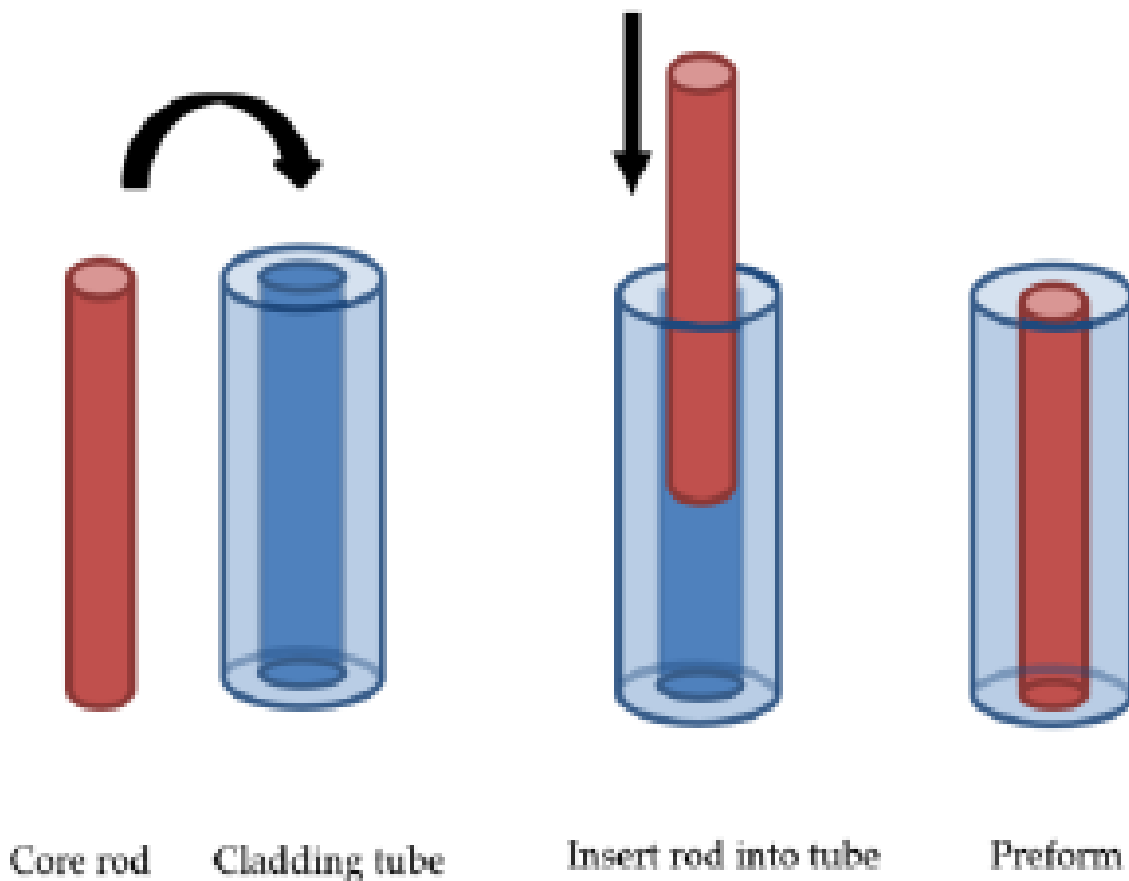


Fig. 4.1 *Illustration of the rod-in-tube preform fabrication steps [79].*

However, this technique produces core and cladding in two steps and the interface between them may be not perfectly air-free. Even if there are modified rod-in-tube techniques with better results [80], most of the preforms nowadays are created by CVD, that gives lower fiber losses (<0.5 dB/km) and is best suited for mass production.

Many different CVD fabrication processes have been developed for low-loss optical fibers including:

- Modified chemical vapor deposition (MCVD);
- outside vapor deposition (OVD);
- vapor-phase axial deposition (VAD).

These three methods are widely used in current industrial processes and all of them give very few impurities [82].

The most common is the MCVD, developed at Bell Laboratories in the 1974 [1]. As shown in Fig. 4.2, the gaseous reactants pass inside a glass tube, that will become part of the cladding.

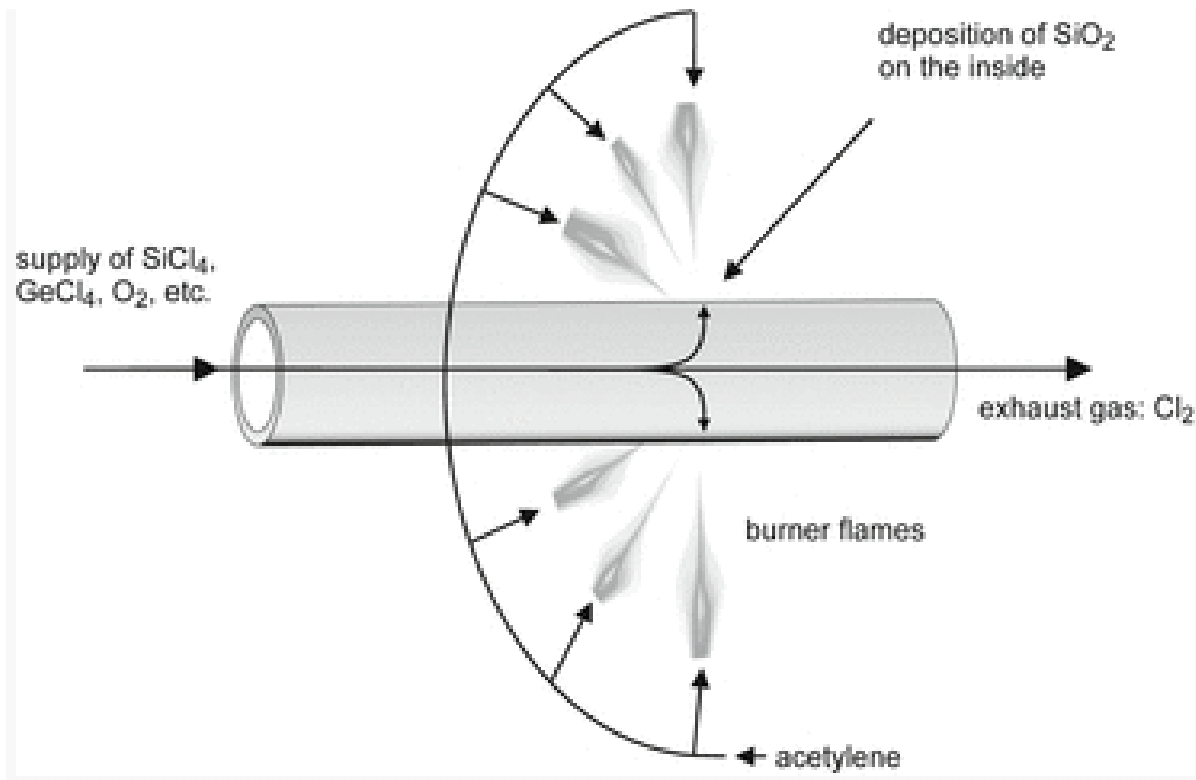


Fig. 4.2 Schematic illustration of modified chemical vapor deposition (MCVD) [1].

The burner around the rotating tube goes back and forth (so a uniform layer is formed) heating and causing the reaction (high temperature oxidation is the principal type of reaction) between chemical precursor and the glass. Many different gaseous reagents can be used such as SiCl₄, GeCl₄, BCl₃, PCl₃, POCl₃ and O₂ to provide the glass matrix and the dopants. The reaction produces submicroscopic glass particles which condense on the surface forming a porous layer (“soot”) which is then sintered. This step is repeated multiple times to get the desired amount of material and the composition can be changed every step with the gaseous reactants, therefore, controlling the refractive index along the radial direction. Finally, the hollow tube is heated and collapsed to a massive rod.

The main advantage here is that, thanks to the wall between the burner flame and the reaction zone, no residual gas and no water vapor is trapped, but the glass tube needs to have a very high purity and uniformity. Also, in the finished fiber, there is often a central dip in the refractive index caused by the leak of some of the dopant in the innermost layer.

Another technique is the outside vapor deposition (OVD), also known as soot process. This was the first process to achieve the reduction of losses to 20 dB/km in 1973 developed by Corning Glass Works. The main difference is that the glass is deposited outside on a massive glass mandrel of aluminum oxide, as shown in Fig. 4.3.

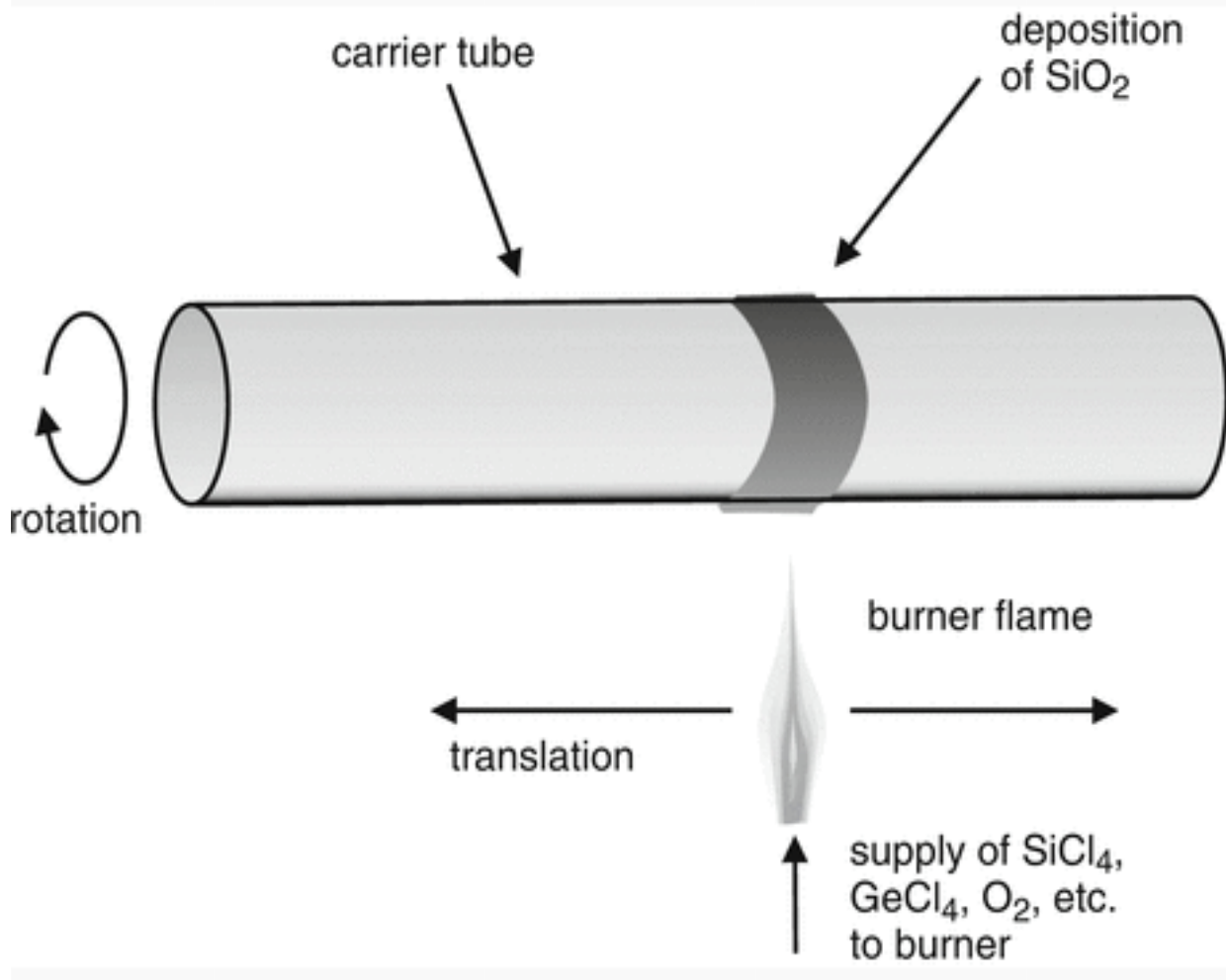


Fig. 4.3 Schematic illustration of the outside vapor deposition [1].

The rod is translated and rotated, while the burner condenses the glass particles on the rod from the gaseous reactants. The first layer will be the core, followed afterwards by the cladding while adjusting the concentrations of dopants in the refractive index profile. To allow the trapped gases and humidity to escape it is heated. Then, when they fully evaporated, the temperature is increased to the sintering temperature to remove the porosity. The cylindrical rod is then taken away and the hollow tube with porous layers collapsed while a drying gas is injected to decrease the hydroxyl content. The main disadvantage is the additional step to release trapped gases and humidity that can lower the quality of the preform [1,85].

Another variant of MCVD, developed in 1975 by Philips Research Laboratories, is the plasma chemical vapor deposition whose only difference is that it uses a microwave generator (3 GHz, several hundreds of watts), as shown in Fig. 4.4, instead of a burner, for heating.

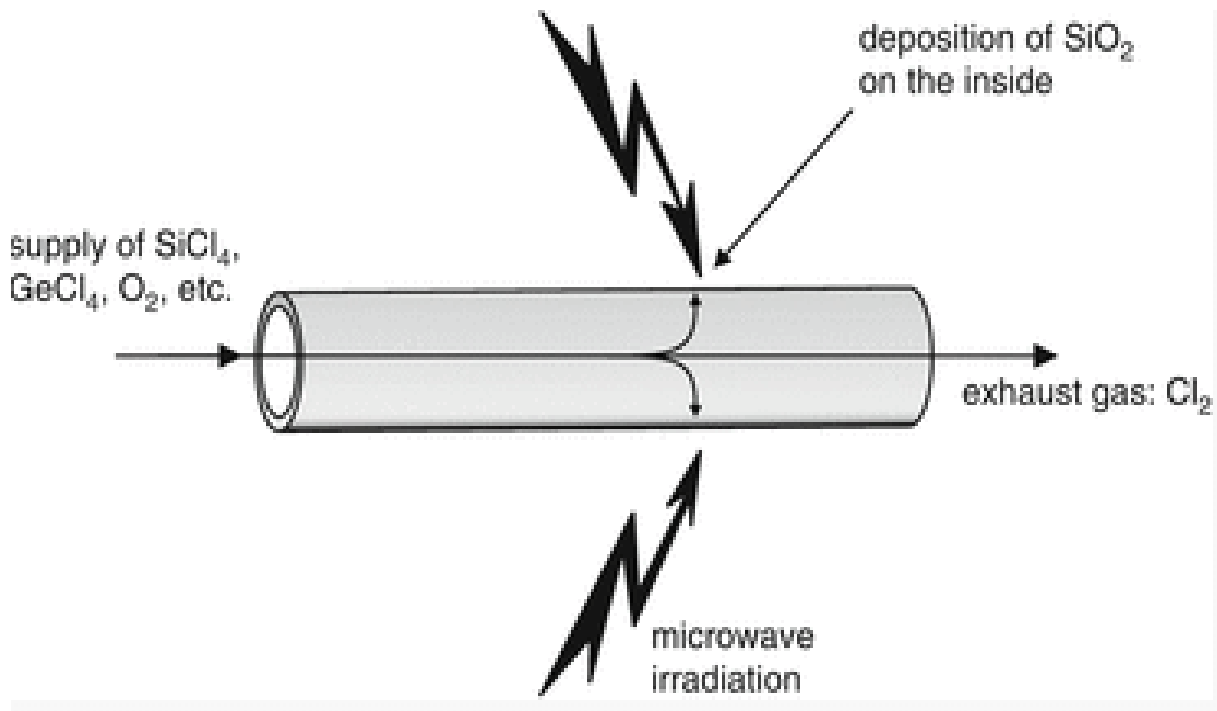


Fig. 4.4 Schematic illustration of the plasma chemical vapor deposition [1].

The temperature is kept at 1000 °C in order to minimize mechanical tensions between the glass tube and the multiple layers deposited inside. The plasma is more uniform than the burner, so no rotation is required and no sintering, because the layers are already free of pores. The main advantages are that this process is faster thanks to the reduced thermal cycling and it is very accurate in controlling the refractive index profile. This accuracy is given by multiple layers deposited; it is common to deposit 2000 layers. Unfortunately, it suffers as MCVD of the central index dip [1, 86].

Vapor phase axial deposition (VAD), developed in 1977 in Japan, is different from the previous ones. Here the layer grows on the end of a seed rod, so the fiber grows longitudinally. The rod, as shown in Fig. 4.5, is pulled along the axial direction, while the burners deposit the different layers with various mixtures. To secure the homogeneity of the fiber, it is constantly rotated. As for MCVD and OVD processes,

sintering is a necessary step, but no collapsing is required, and it is advantageous for the production of very long fiber preforms.

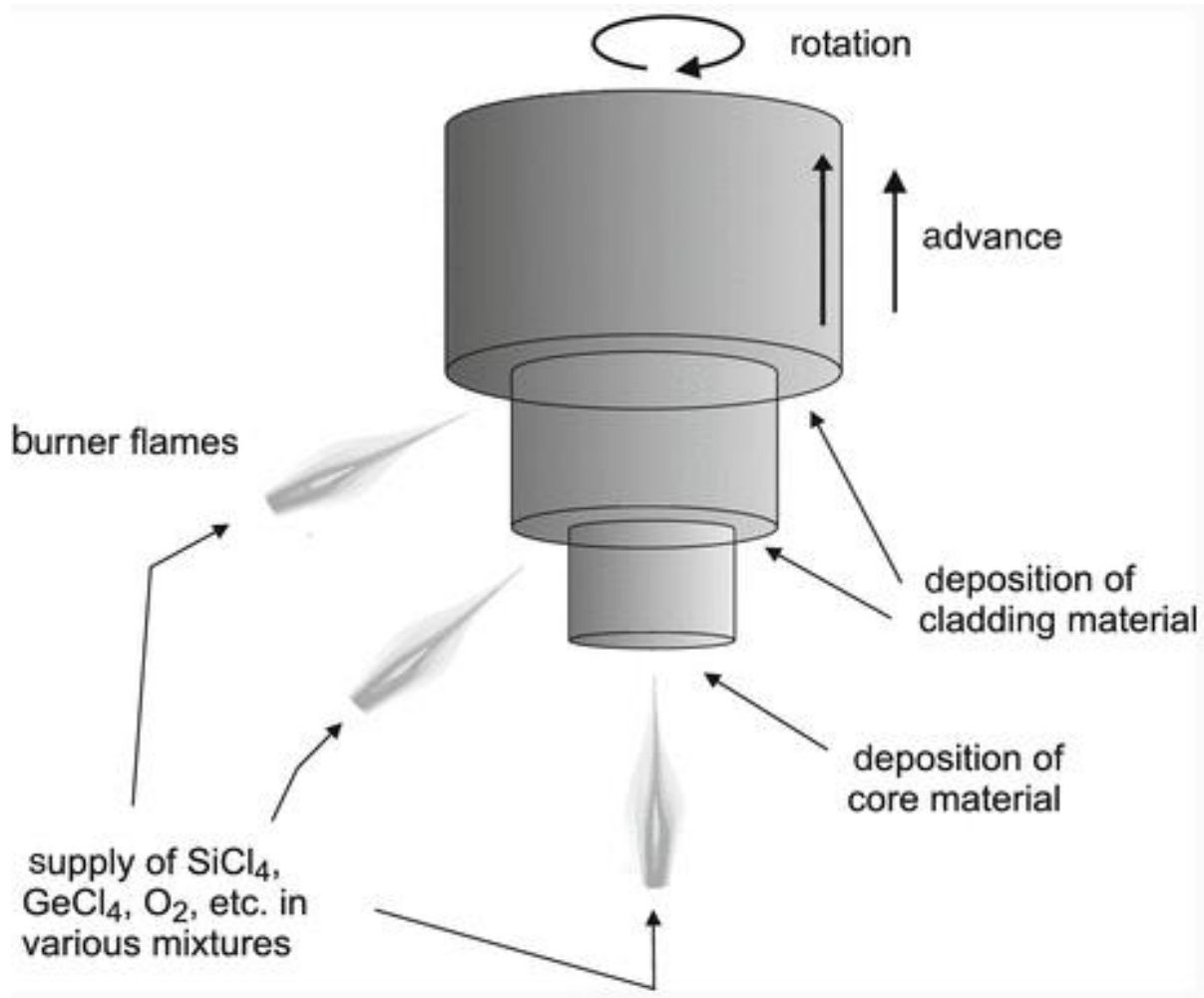


Fig. 4.5 Schematic illustration of vapor phase axial deposition (VAD) [1].

There are many other techniques, but these are the most common.

The preform (typically 1 m long and with a diameter of 10-50 mm) obtained is positioned in a drawing tower whose many steps, shown in Fig. 4.6, include:

- a feed mechanism that holds firm in place the preform;
- a furnace that heats the preform to the required viscosity above T_g ;
- a measurement of fiber diameter with a laser micrometer;
- an extruder that coats the fiber with UV-cure polymer coating;
- a measurement of coating diameter;

- a measurement of fiber tension with a dynamometer;
- coiling the fiber around a winding drum.

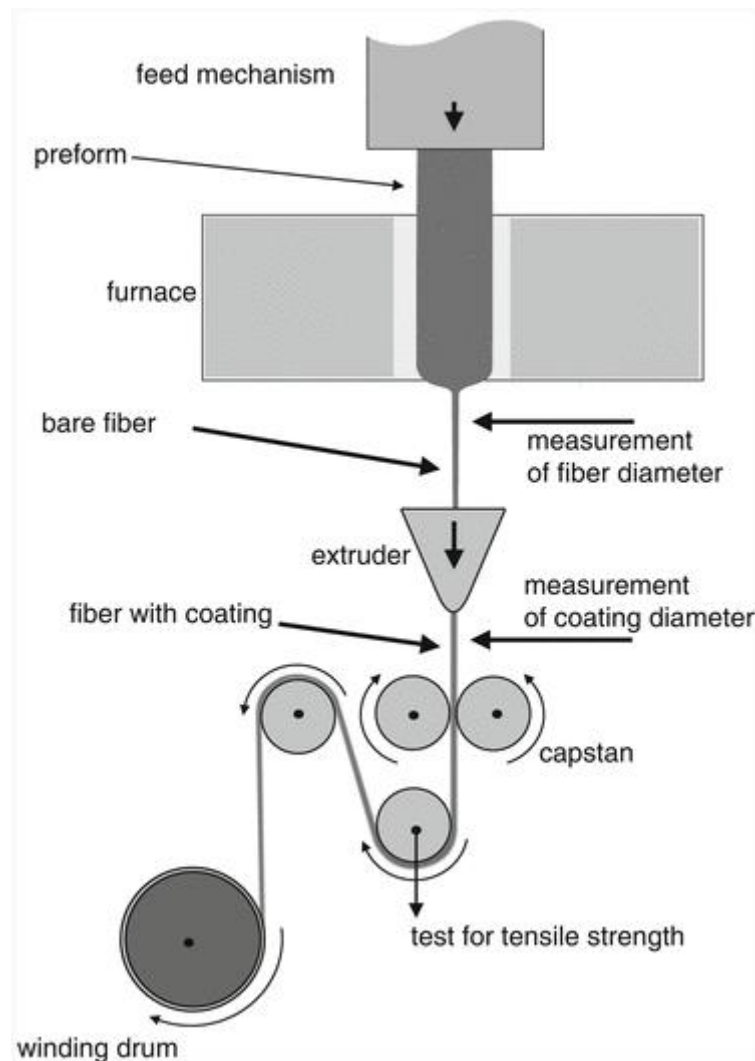


Fig. 4.6 Schematic illustration of a drawing tower [1].

A typical fiber drawn has a diameter of $125\ \mu\text{m}$, therefore from 1 m-long preform tens of km are obtained with a speed that depends on the viscosity of the fiber and the desired diameter, but never fast.

The drawing parameters have really strict tolerance demands, even slight variations affect the quality of the fiber. Furnace temperature and advance speed (divided in preform feeding speed and pulling speed) change the fiber feature, especially diameter and internal stress distribution. Closed-loop control of parameter is used to adjust these features. To avoid damage from abrasive contact and chemical influences by water, a plastic coating is applied immediately after cooling; there are

numerous kinds of coating for different applications, the most commons are epoxides and polyimides.

A technique to produce a fiber without making the preform is the double crucible method, where the melting and extrusion of the core and the cladding are made at the same time and co-extruded.

The fibers obtained using this method exhibit higher attenuations caused by impurities and normally are used for short-range applications. Typical outer diameters of these fibers range from 250 and 400 μm .

When drawing microstructured fibers with air holes, it is necessary to add a further step. Between the preform and the fiber there is an intermediate product, called cane, where the bundle made piling up capillaries and/or rods creates the desired geometry. This cane is stuck into the void of a wider tube (jacket) and fused again.

This helps to arrange the core geometry. With stack-and-draw it is important to avoid the collapsing of the holes, that's why slower speed and lower temperature are used alongside pressurizing the holes with inert gas. It is also important to avoid recrystallization of the glass in the second drawing.

There are other techniques to achieve microstructured fibers based on more ductile materials, like polymers, but they are not possible for tellurite glasses.

4.2 Chosen technique

The disordered tellurite-air fraction fiber is microstructured and the stack-and-draw technique has been chosen based on the previous studies by Tuan et al. [12,42,76], on the disordered fiber produced at the University of Central Florida (UCF) [11,77,78,87] and the work made by Matteo Facciano, a previous thesis student of the research group.

The glass chosen was fabricated at the Department of Applied Science and Technology (DISAT) of Politecnico di Torino, Italy, using the traditional melt-quenching technique. The chemicals were weighed and mixed within a dry box and they were subsequently melted at a temperature of 800 $^{\circ}\text{C}$ for 90 min in a chamber furnace under controlled atmosphere to minimize the hydroxyl ions (OH^-) content in the glass.

The melt was cast into a preheated brass mold, then annealed at a temperature around the transition temperature, T_g , for 3 h to relieve glass internal stresses, and finally cooled down slowly to room temperature.

This method was preferred to CVD because gaseous compounds of TeO_2 are difficult to obtain [80].

All these steps were followed to minimize the presence of impurities such dust and other elements in the initial raw materials. OH^- content is especially important because it gives a large spectral dip between 3 and 5.5 μm that causes the transmittance to diminish sensibly as shown in Fig 4.7.

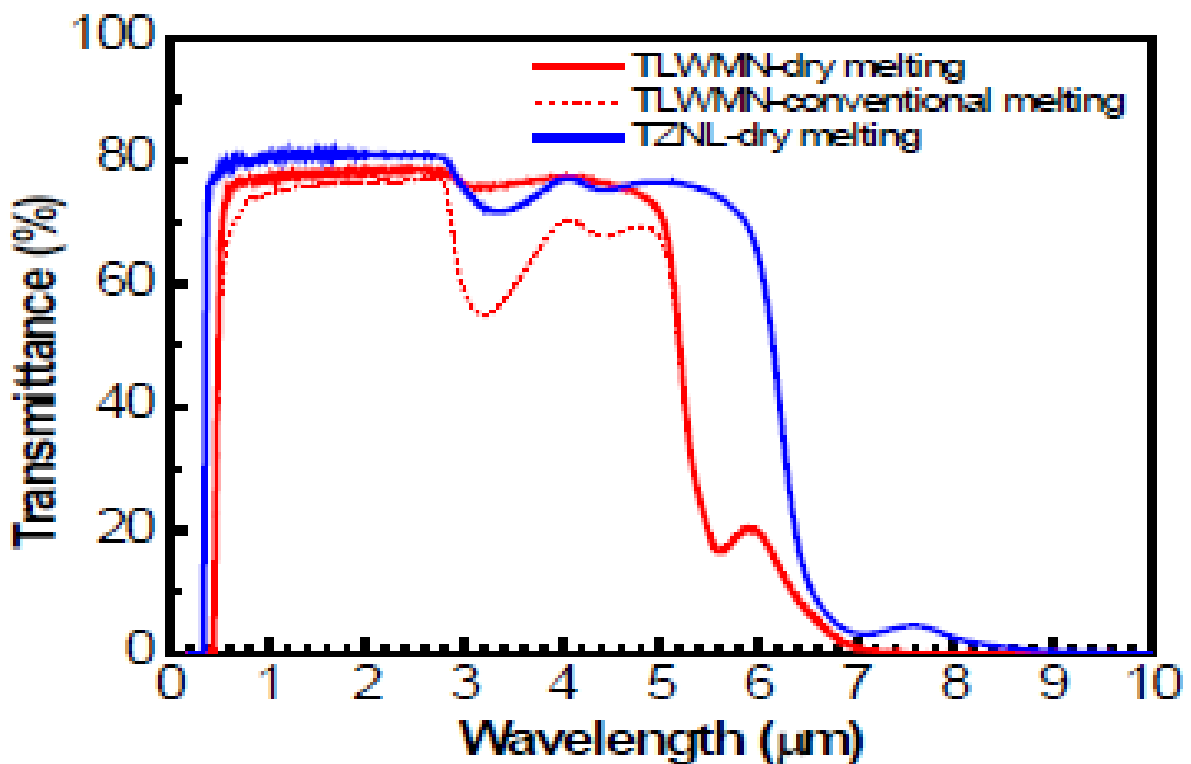


Fig. 4.7 Transmission spectra of different tellurite glasses with or without dry-melting [71].

For these reasons, all the processes were carried in an ultra-clean environment monitoring time and temperature to avoid any micro-bubble formation.

The glass composition was chosen to improve the performances compared to the glass used in the previous work, a classic TZN glass with 75% TeO_2 , 15% ZnO , 10% Na_2O in molar ratio.

This TNGPZ glass shows improved mechanical characteristics and, thanks to the use of ZnF_2 instead of ZnO , less hydroxyl impurities.

Fig. 4.8 shows the glass preform produced at Politecnico di Torino.



Fig. 4.8 *Tellurite glass preform produced at Politecnico di Torino.*

4.3 Choice of the glass tube

In this work the aim was to fabricate a glass-air random fiber (GARF) with high air-hole fill fraction and lower attenuation dB compared to a standard tellurite fiber. Tellurite fibers with losses less than 1 dB/m have been demonstrated [88].

Given that the tellurite preform is naturally more brittle than silica, and that it was available in small quantities only, a different core-clad material solution was proposed. A stronger glass without the optical properties of the tellurite glass will be used for the clad.

The most important properties for the clad material are T_g and coefficient of thermal expansion (α) to identify thermal compatibility, between clad and core glasses, and avoid the generation of high internal stresses. O'Donnell et al [89] made a comprehensive study about stresses and consequences for dissimilar core-clad tellurite fibers.

The internal stresses are more difficult to calculate in this case and they need to take into account the hydrostatic tension of liquid core surrounded by a solid cladding as shown by the equation of Khron (Eq. 4.1):

$$\sigma = \frac{(\alpha_1 - \alpha_2)(T - T_{g1})E}{(R^2/r^2)(1 - \mu)} + \frac{(\alpha_1^* - \alpha_2)(T_{g2} - T_{g1})}{((1 - R^2/r^2)/3K_1^*) - (1/(3K_2))}$$

Eq. 4.1 Equation by Khron to evaluate the fiber stress [89].

Where:

- 1 and 2 refers to core and clad, respectively;
- E is Young's modulus;
- μ is Poisson's ratio;
- R/r are clad radius/core radius;
- T is room temperature;
- T_g is in fact the strain point but it's assumed that the strain point is equivalent to the glass transition temperature;
- a may be different, ideally with the cladding having a lower a to ensure that the core is in compression to produce a physically strong fiber;
- $*$ refers to values just above T_g ;
- K^* is the bulk modulus above T_g which is typically 0.5 times bulk modulus below T_g .

Different tellurite fibers with dissimilar core-cladding have been reported with good results [89,90] and the internal stresses always played an important part.

The internal stresses can affect mechanical strength (also positively) and if too high cause the failure of the fiber but primarily they can affect the fiber refractive index, thus the waveguiding characteristics [91].

Generally, the clad of a single-mode fiber is under tension while the core is under compression due to the direct effect of the drawing, but with a multi-mode fiber with a larger core diameter and a different thermal expansion this can be completely changed if the parameters are wrong. For the clad material, a thermal expansion lower than the core is desired so that the fiber will be more robust.

Different combinations of materials have been studied to improve mechanical and corrosion resistance of innovative glasses [89,90], some examples for tellurite glass are shown in Table 4.1.

Tab. 4.1 Parameters and internal stress for similar and dissimilar core-cladding materials with TZN core [89].

Parameter	Core T2 Clad T1	Core T1 Clad Pyrex	Core T1 Clad silica
α_1 ($\times 10^{-6} \text{ }^\circ\text{C}^{-1}$)	22.2	21.9	21.9
α_1^* ($\times 10^{-6} \text{ }^\circ\text{C}^{-1}$)	—	77.4	77.4
α_2 ($\times 10^{-6} \text{ }^\circ\text{C}^{-1}$)	21.9	3.25	0.45
T ($^\circ\text{C}$)	21	21	21
T_{g1} ($^\circ\text{C}$)	275	278	278
T_{g2} ($^\circ\text{C}$)	—	560	1175
E (GPa)	54.5	54.5	54.5
R (μm)	125	125	125
R (μm)	8	19	21
μ	0.253	0.253	0.253
K_1^* (GPa)	—	18.3	18.3
K_2 (GPa)	—	42.1	54.5
σ	−24 kPa	−35 MPa	−115 MPa

The great difference in T_g and α augments dramatically the stresses but can also deplete the core of the tellurite glass if the temperature reached to draw the clad is too high due to the low boiling point of TeO_2 (1245 °C) [89].

The coefficient of thermal expansion of the TNGPZ glass has been evaluated to be $13 \cdot 10^{-6} \text{ }^\circ\text{C}^{-1}$ between 200 and 400 °C, more details will be reported in Chapter 5.2.

The T_g was calculated with differential thermal analysis (DTA) performed at Politecnico di Torino (see Fig. 4.9).

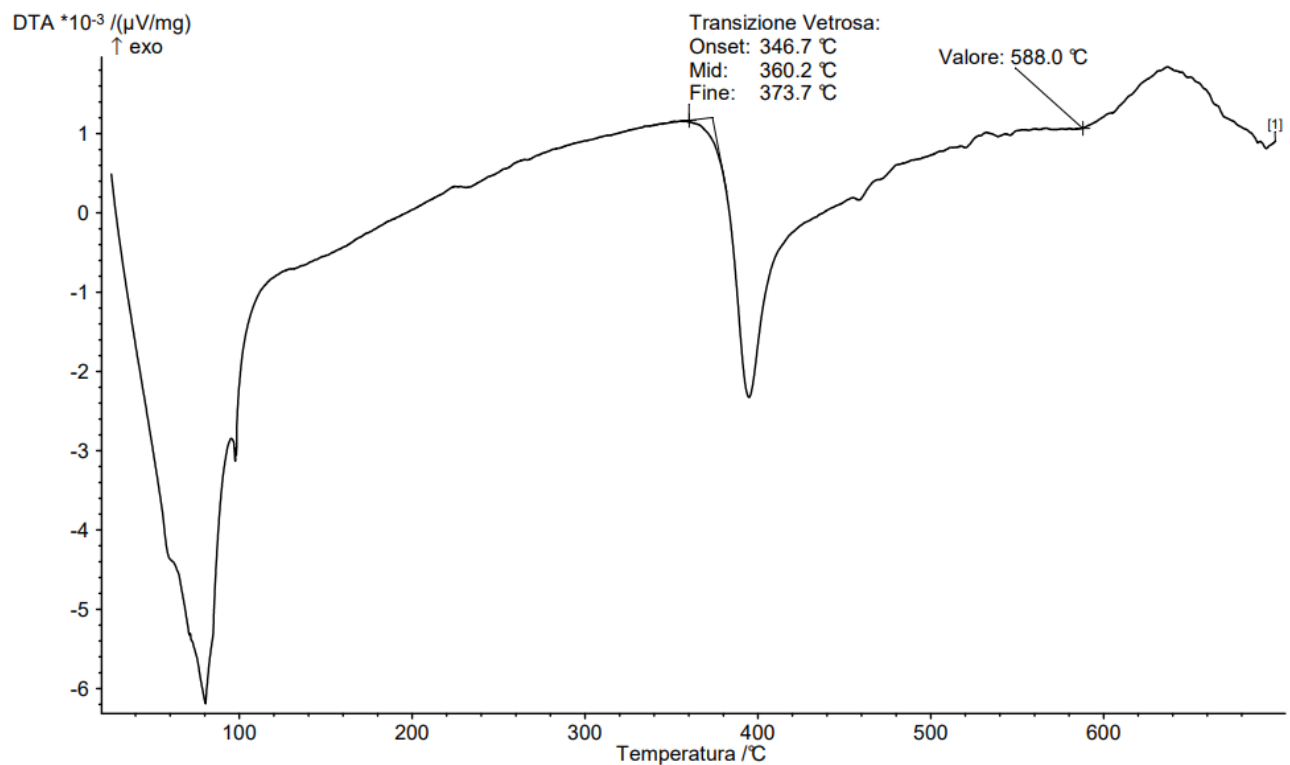


Fig. 4.9 DTA analysis with T_g and T_x underlined.

The T_g is 360.2 °C, while the T_x (onset crystallization temperature) is 588 °C.

For their highest thermo-compatibility, core and cladding glasses must show similar T_g and α . Moreover, the α of the clad should be lower to have compression stress on the core and its variability can be larger since the core diameter can be adjusted to decrease the stress. Compared to the previous TZN glass used in the thesis work of Matteo Facciano, showing $\alpha(20\text{-}250 \text{ }^\circ\text{C}) = 18.8 \cdot 10^{-6} \text{ }^\circ\text{C}^{-1}$ and $T_g = 283^\circ\text{C}$, the

TNGPZ exhibited lower α and higher T_g , respectively $\alpha(200-400\text{ }^\circ\text{C}) = 13 \times 10^{-6}\text{ }^\circ\text{C}^{-1}$ and $T_g = 360.2\text{ }^\circ\text{C}$.

To have a good thermal stability we need to operate at least $100\text{ }^\circ\text{C}$ under the onset crystallization temperature, under $150\text{ }^\circ\text{C}$ would be even better, that's why the clad glass to be chosen needs to show a T_g of at least $488\text{ }^\circ\text{C}$.

The aim of this fiber is to be able to show high quality imaging in the mid-IR region, this means a fiber with a larger diameter like the one fabricated at CREOL [77].

This GARF, shown in Fig. 3.9, has a core diameter of $270\text{ }\mu\text{m}$, $405\text{ }\mu\text{m}$ outer diameter, and stress calculation has been performed with this design for different glasses in theory finding some good candidate shown in Table 4.2.

Tab. 4.2 *Internal stress for some of the best choices found.*

Material	Tension	Characteristics
C5000 from Hoya	32.595 MPa	Low stress, similar T_g , not compressive
LF5 from Schott	- 56.452 MPa	Higher stress, higher T_g , compressive

The choice of the clad glass has been done between commercial available glasses; unfortunately, it wasn't possible to find a producer of the glass for the desired geometry, thus the choice fell upon the SCHOTT 8095, a lead-glass (28% PbO) with the following properties:

Mean coefficient of linear thermal expansion $a(20-300\text{ }^{\circ}\text{C})$	$9.1 * 10^{-6} \text{ }^{\circ}\text{C}^{-1}$
Glass transition temperature T_g	430 $^{\circ}\text{C}$
Glass temperature at viscosity η in dPa*s	10^{13} (annealing point) \rightarrow 435 $^{\circ}\text{C}$ $10^{7.6}$ (softening point) \rightarrow 630 $^{\circ}\text{C}$ 10^4 (working point) \rightarrow 982 $^{\circ}\text{C}$
Young's modulus E	$60 * 10^3 \text{ N} * \text{mm}^{-2}$
Poisson's ratio μ	0.22

This glass is not optimal, therefore fiber design parameters had to be reworked to keep internal stress low, thus a thicker wall is needed. The best dimensions for the clad tube are estimated to be 34 mm of outer diameter (OD) and 7.4 of inner diameter (ID). The producer could not make a new tube with the desired parameters; thus, it was decided for a tube with outer diameter of 33.5 and thickness of the wall of 5.460 mm (ID of 22.58 mm). The OD dimensions are sufficiently similar but to obtain the wall thickness desired a procedure has been developed and described in 4.4.

4.4 Fiber preparation

The tube will be collapsed in multiple steps decreasing the outer diameter of a factor of 1.5. After each step, the collapsed tube will be put inside the original tube, repeating the step till final dimensions as shown in Fig. 4.10.



Fig. 4.10 *Dimensions after each step of collapsing.*

With these dimensions the internal stresses should be less than 30 MPa (between -21.6 and -24.17 MPa). In this way, any critical stress should occur at the core/clad interface, however this approach is time consuming and the stresses inside the clad could be critical. This is the reason why annealing need to be performed but temperature and time of annealing must be carefully chosen to avoid devitrification or OH⁻ absorption. [92]

Stresses between core and clad should be lowered again by the tendency of the random air-glass fiber, where the voids tend to aggregate at the core-clad interface, as shown in CREOL's fiber in Fig. 3.9, where the air fraction was 26% but only 22.4% excluding the boundary areas [77]. The final fiber will have an outer diameter of 500 μm and an inner diameter of 150 μm , this means a smaller core but with less internal stresses.

Completed the production of the tube for the clad, the next step is the production of the final fiber with the following steps:

1. Production of 607 15-long tellurite capillaries near $150\ \mu\text{m}$ in diameter (calculation based on total volume of tellurite preform available);
2. stacking of the tellurite pieces, mixed together inside the cladding tube for the sake of randomness;
3. prefusing the tellurite disordered core with a cylinder of Schott 8095 to avoid any movement while drawing;
4. drawing of the preform to produce the fiber with an outer diameter of about $500\ \mu\text{m}$;
5. volume of the core is $12257\ \text{mm}^3$ and 50% of air filling is desired, this means $6128.5\ \text{mm}^3$ of tellurite;
6. total length of the fiber will be of 673 m.

When drawing the capillaries, a variation of their diameter is preferred to achieve a greater randomness. These capillaries are cut in pieces of 15 cm and then put together and mixed before being put inside of the clad tube. The randomness is wanted radially but along the fiber the design need to be maintained to have light transmittance; for an all-solid disordered fiber this is not a problem but with a GARF this is a critical point, especially if a 50% air fraction is wanted. That is why the following design, reported in Fig. 4.11, has been proposed.

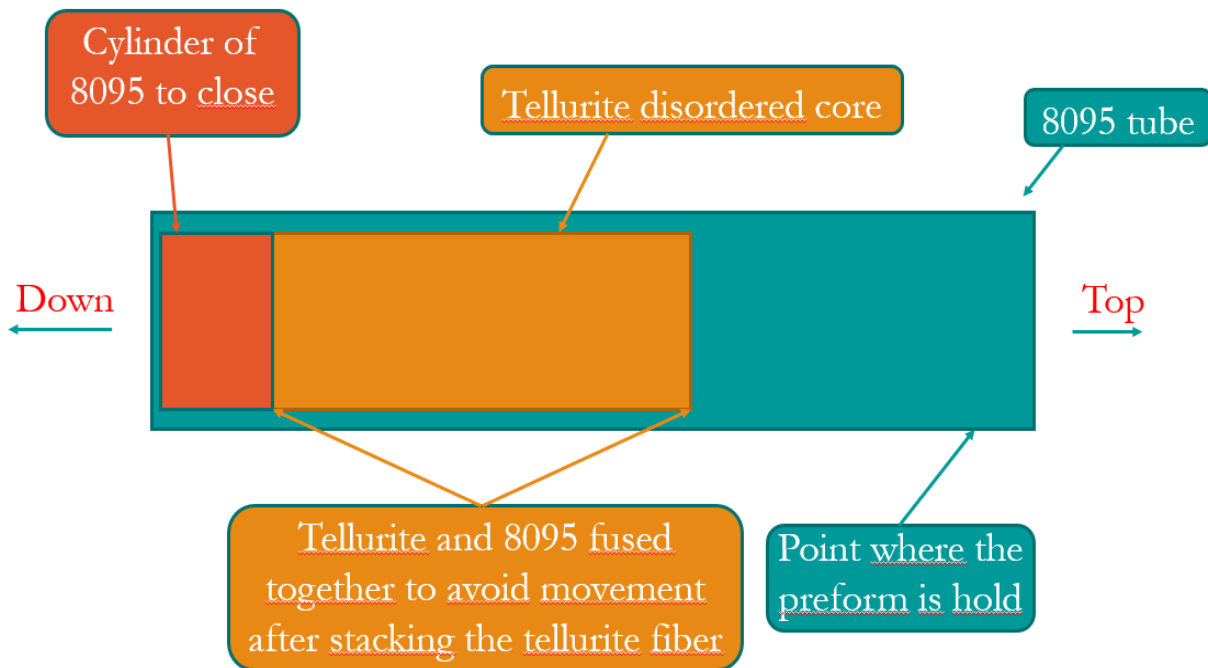


Fig. 4.11 Schematic illustration of the cane design.

A cylinder of SCHOTT 8095 is fused to close the last part of the tube, then the capillaries are put inside and fused to the tube and to the cylinder to avoid any movement in the top part, where there isn't a cylinder. Void is applied from the tower in the top part. The clad tube is longer because the first part will be lost in the holder.

To fuse these parts, it is critical that the instrument used won't damage the tellurite glass, which is very sensible. The classic method of the hydrogen flame can't be used because the temperature is too high, that's why a thermo scientific Lindberg/Blue M tube furnace (Fig. 4.12), where the glass will be heated above its T_g and periodically rotated to attain a homogeneous softening, will be used.



Fig. 4.12 *Thermo scientific Lindberg/Blue M tube furnace.*

Another critical point is the holder of the preform, which was the cause of the fatal failure in the last fiber.

Strategies as the use of brass fittings to hold the preform is not possible for such a brittle glass, it would surely cause cracks forming. Even the traditional method of a 3-screw aluminum tube would be dangerous, that's why a Teflon tape was proposed, thanks to the low temperature of the drawing, and it will hold the preform inside an aluminum alloy 6061 tube, which has a $\alpha(20-100^{\circ}\text{C}) = 23.6 \cdot 10^{-6} \text{ }^{\circ}\text{C}^{-1}$ and a diameter larger than 11.4 mm, for a length of 1 cm.

For the fiber drawing the value of viscosity needs to be between 10^4 – 10^7 Poise [93], the difference of T_g between the clad and tellurite glass means that the core will be less viscous and this could be a problem while drawing. This composition was studied to improve the performances of the glass compared to the TZN.

A classic TZN shows a T_g value of ≈ 280 °C, whereas our tellurite glass features a value of 360 °C. The temperature window for drawing is really small compared to silica fibers and even small temperature variations can considerably change the viscosity while drawing, as shown in Fig. 4.13, thus causing great fluctuations of fiber diameter.

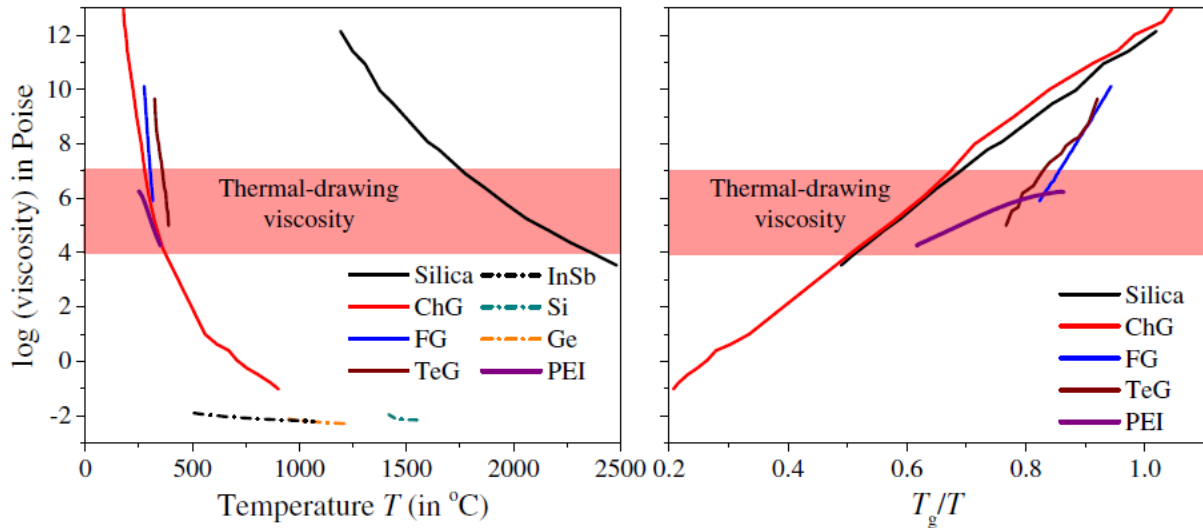


Fig. 4.13 Viscosity curves of different glasses [93].

4.5 Results

Unfortunately, the fiber drawing couldn't be performed due to the late arrival of the glass for the clad, some problems with the drawing tower, which needed repair, and the outbreak of COVID-19, which caused the university, in Florida as well in Turin, to close temporarily.

Despite it was not possible to manufacture the fiber, the most suitable conditions have been identified. A careful planning of each step suggests good chances of success when it will be possible to actually draw the fiber.

The main issues to address for a disordered glass-air fraction tellurite fiber are the following:

- The quality of the preform. Tellurite glass shows considerably lower transmittance than silica and the quality of the initial powders and the presence of hydroxyl group can dramatically alter the performance;
- the choice of the clad glass and its thermo-compatibility with the core are key for the internal stresses and the drawing of the fiber. The tellurite core

viscosity varies in a small range of temperatures, compared to silica; more information about viscosity is reported in Section 5.3;

- the design of the fiber and the drawing of capillaries to achieve a 50% of air fraction are not yet consolidated and the step of fusing together the clad and the core with the furnace need more study.

5 Characterization

Thorough characterization of the TNGPZ glass was performed to improve the success rate of drawing a good fiber. While analysis of the fiber was not possible, since the fiber was not drawn yet, the glass important properties and the techniques used to study them are proposed.

5.1 Glass thermo-mechanical properties

5.1.1 DTA

The DTA, or differential thermal analysis, is one of the best tools to investigate thermo-mechanical properties of a glass. The DTA consists of two holders, one for the sample and one for the reference, inside a chamber where the temperature increases or decreases while the temperature difference between the two of them is recorded; this happens because, even if the thermal cycle is the same, the temperature changes due to phase changes or other thermal processes.

The apparatus of a DTA is shown in Fig. 5.1.

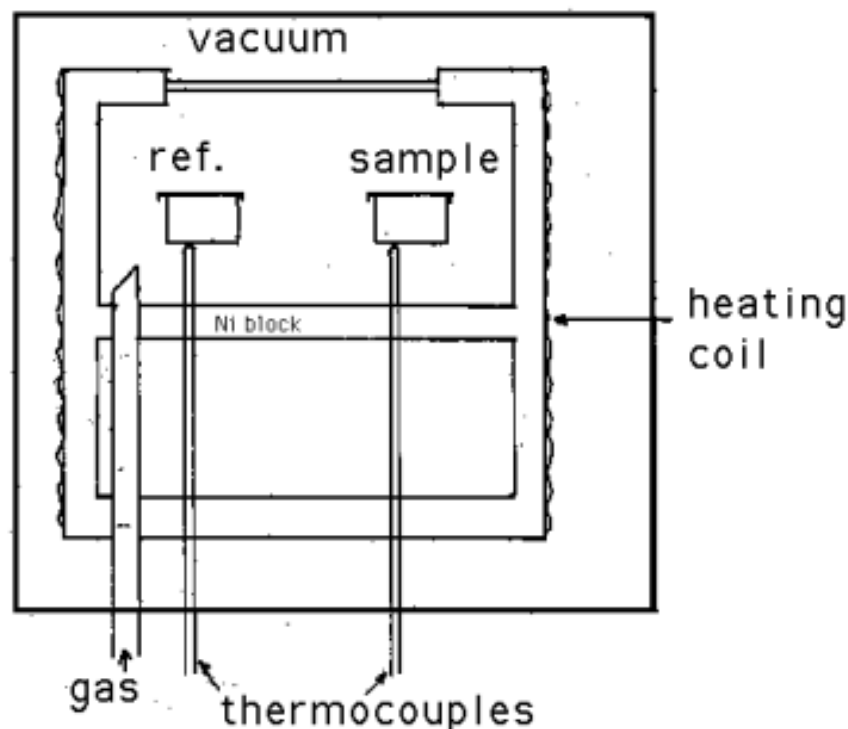


Fig. 5.1 *Schematic illustration of a DTA [94].*

Each DTA consists of:

- two sample holders, one used as a reference, of inert material like Al_2O_3 , Pyrex or platinum, depending on the desired heat cycle;
- two thermocouples connected to a voltmeter;
- a furnace with a swift response from the temperature programmer;
- a temperature programmer;
- a recording system with low inertia for an accurate measurement of variations.

The temperature is monitored by thermocouples, temperature sensors that use hot and cold junctions; the hot junction measures the temperature of the sample and compares this with the reference of cold junction (which is not the reference of the DTA but one inside the thermocouple), the voltmeter measures the voltage which is temperature dependent. The electrical voltage between the sample crucible and reference crucible, then, is plotted against temperature (as in Fig. 4.9) or time.

When the sample undergo a change, like glass transition, crystallization, melting point or chemical reactions, a peak or a valley are shown in the diagram, depending on whether the process is exothermic or endothermic. The area under these represents the enthalpy change. The analysis was carried out at Politecnico di Torino on $\cong 100$ mg fragment of tellurite preform in a pan of platinum-rhodium.

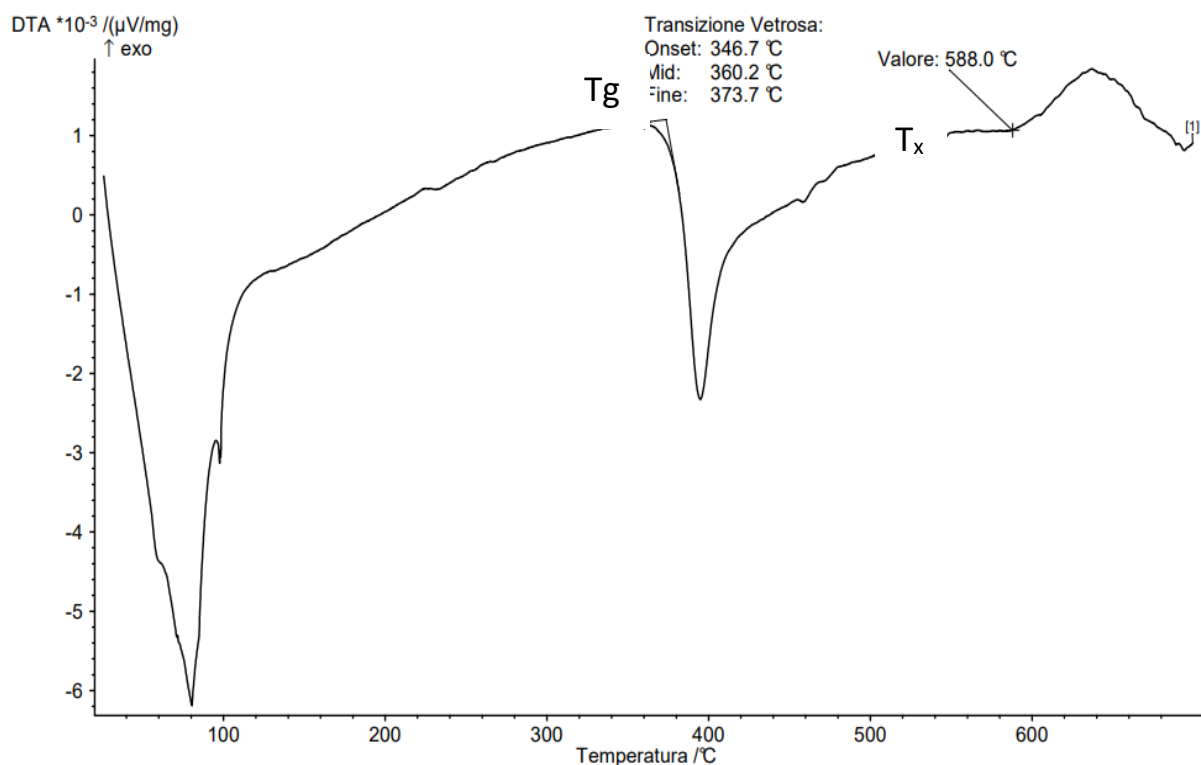


Fig. 5.2 DTA analysis with T_g and T_x underlined

There are two main changes between 20 and 700 °C, one endothermic (the first one) and one exothermic. The first one is the glass transition at 360.2 °C, whereas the second one is the crystallization, which begins at 588 °C. As said in Section 4.3, there is a common way to establish if a glass is suitable to produce an optic fiber, it's called thermal stability and it's calculated like this:

$$\Delta T = T_{x,onset} - T_g$$

A good temperature to draw the tellurite fiber is 150 °C under its T_x , which gives a range of 360-438 °C for drawing without any crystallization. However, it is acceptable to arrive till 488 °C if this temperature is acceptable for the clad glass. This glass has better stability against devitrification compared to a common TZN glass.

5.1.2 Dilatometry

The coefficient of thermal expansion, or CTE, is one of the most important factors for a multi-material optic fiber. In order to decide the clad glass, tellurite glass CTE is needed. The linear thermal expansion is a good first approximation of the general volumetric expansion and it follows this equation:

$$dL = \alpha L dT$$

where:

- dL is the change in length in mm;
- dT is the change in temperature in K;
- L is the length at room temperature in mm;
- α is the linear thermal expansion coefficient in K⁻¹.

α is defined as:

$$\alpha = \frac{1}{L} \frac{dL}{dT}$$

α is not constant but temperature dependent and its value is an average for a temperature range. In this approximation the material is considered isotropic and the pressure is ignored. It is possible to measure it with 2 different instruments; one put the sample vertical, it is the thermomechanical analyzer (TMA) instrument, whereas the other one put it horizontal, it is the dilatometer. In both cases the temperature is measured by a thermocouple, while a pushrod applies a constant force to the sample.

A linear variable differential transformer (LVDT) measures the movement of the pushrod caused by changes in dimensions when the temperature increases or decreases. The a is the slope of the curve of the graph temperature plotted against dimension change.

The sample dimensions for this analysis are not standard but depend on the specific instrument used. The measurement was performed at Politecnico di Torino, and a value of $13 * 10^{-6} \text{ } ^\circ\text{C}^{-1}$ between 200 and 400 $^\circ\text{C}$ was achieved. A common TZN shows a higher value of CTE, as shown in Table 4.1, thus this glass composition is more suitable for dissimilar core-clad optical fibers.

5.1.3 Viscosity

The viscosity measures the resistance of a fluid to deformation at a given rate and plays a crucial part for the optimization of fiber drawing. The speed of the process is dependent from the pulling speed and the viscosity, which is temperature dependent. The viscosity range suited to fiber drawing, as said before, is between 10^4 and 10^7 Poise. The Poise (P) is the unit of dynamic viscosity in the centimetre-gram-second (CGS) system and its analogous unit in the International System is the pascal-second ($\text{Pa} * \text{s}$), where:

$$1 \text{ Pa} * \text{s} = 10 \text{ P}$$

The most common technique used to study glass viscosity for fiber drawing is the parallel plate method (PPV), consisting of two horizontal flat plates where the upper one rotates while the lower one is stationary. A schematic illustration is shown in Fig. 5.3.

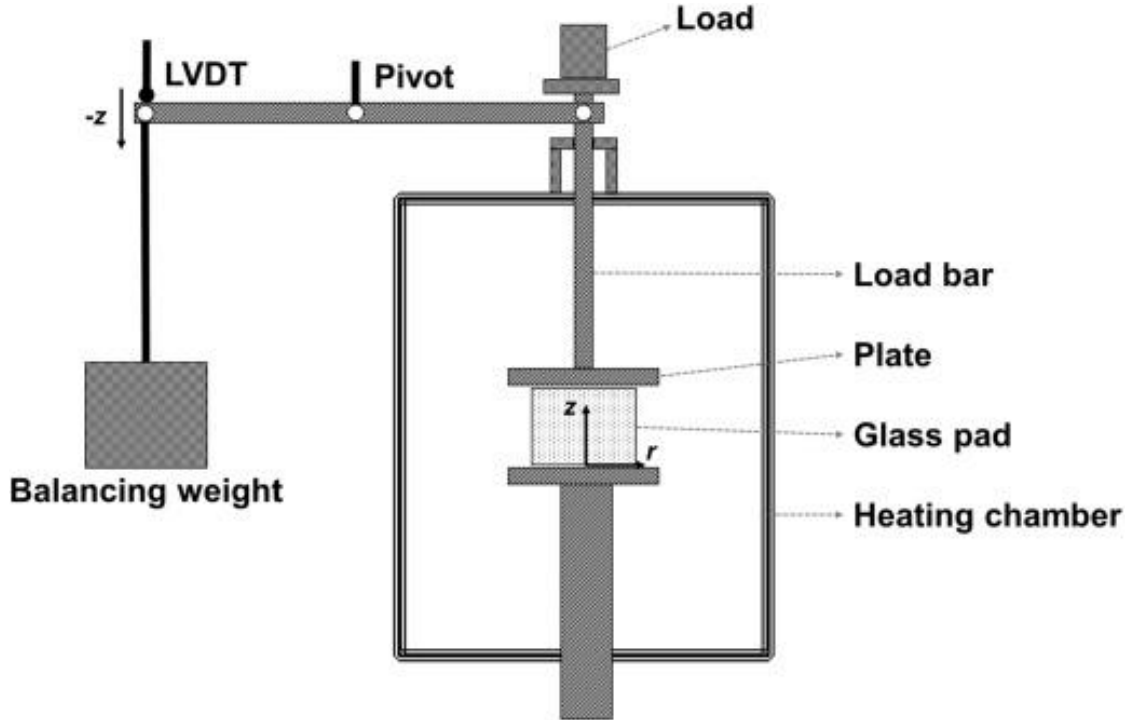


Fig. 5.3 Schematic illustration of a parallel disk viscometer [95].

The glass pad, typically 6 mm in diameter and 5 mm in length, is put between the two plates and pressed vertically, another LVDT collects the data of compression rate, which are used in the following equation to evaluate the viscosity [96]:

$$\eta = 2\pi \frac{Mgh^5}{30V\left(\frac{dh}{dt}\right)(2\pi h^5 + V)(1 + \alpha T)}$$

Where:

- η is the viscosity in Pa*s;
- M is the applied load in g;
- g is the gravitational acceleration in cm/s²;
- h is the height of the sample in cm;
- dh/dt is the compression rate in cm/s;
- a is the CTE of the glass in K⁻¹;
- T is the operating temperature in K

Unfortunately, it was not possible to perform the characterization and, not knowing the exact composition, it's not possible to retrieve exact data in literature but it is possible to identify a certain range. Our glass is a $\text{TeO}_2\text{-ZnF}_2\text{-PbO-Nb}_2\text{O}_5$ based fluorotellurite glass family, the presence of ZnF_2 decreases the viscosity [97]. Unfortunately, accurate studies about viscosity have not been made so far to the best of our knowledge.

As reported by Tincher et al. [98] in classic TZN glasses the overall η is largely driven by the role of ZnO as shown in Fig. 5.4.

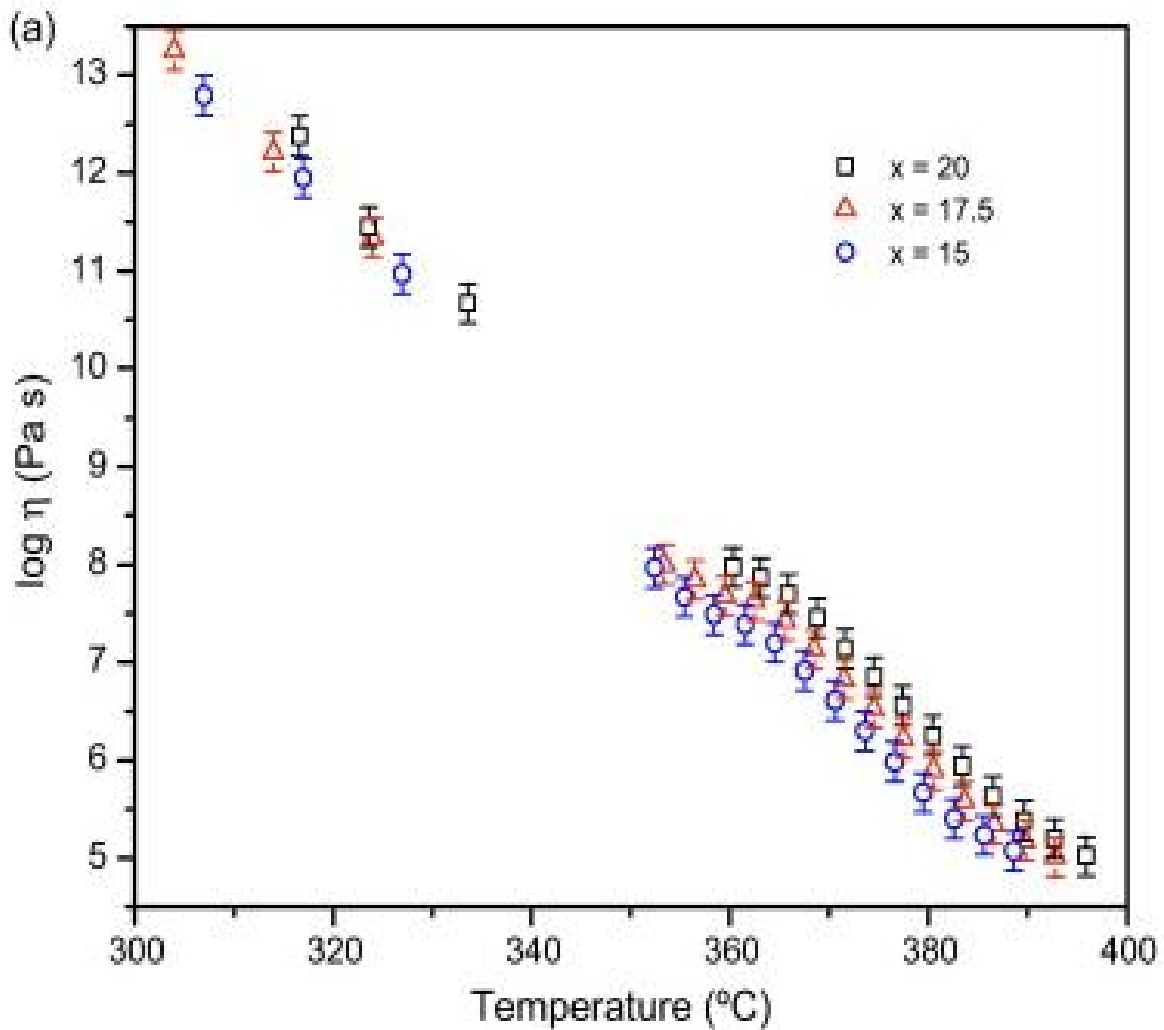


Fig. 5.4 *Log η as a function of temperature for a tellurite glass with the composition $(90-x)\text{TeO}_2 - 10\text{Bi}_2\text{O}_3 - x\text{ZnO}$ where x varies between 15 to 20 [98].*

The decrease is related to the augmented cross-linking caused by ZnO , but the change is relatively small compared to the very small drawing temperature window. For this composition, an optimal fiber drawing temperature of 370°C was reported

by Hill et al. [99]. The viscosity of our fluorotellurite glass should be higher but with a similar trend for the range between $\log\eta = 6$ and $\log\eta = 3$ that is the drawing range viscosity. Alas, the lack of data makes impossible to do accurate calculation, a characterization study should be done to optimize the drawing process.

5.1.4 Hardness

The hardness measures the resistance of the material surface to various kinds of permanent shape change when a force is applied. There are many different measurements of hardness but the most common is indentation hardness. There are various techniques based on the load and the geometry of the indenter. When the load applied is between 2 N and 30 kN it is a macro-indentation test, while for lower loads and penetrations greater than 0.2 μm it is called micro-indentation.

The indenter applies this load for a certain time provoking a plastic deformation, whose size and penetration depth are correlated to hardness according to the method used. No hardness measurements could be performed and there is not in literature mechanical characterization for hardness for this glass composition. Therefore, it is not possible to give a precise result but, in this chapter, the best technique to use and a reasonable range will be given.

In this case the best technique is the Vickers microhardness (HV), because tellurite glass is a brittle material. This nondestructive technique is normalized by ASTM E384 and ISO 6507 and calculates the size of the indentation left by a pyramid-shaped diamond indenter shown in Fig. 5.5.

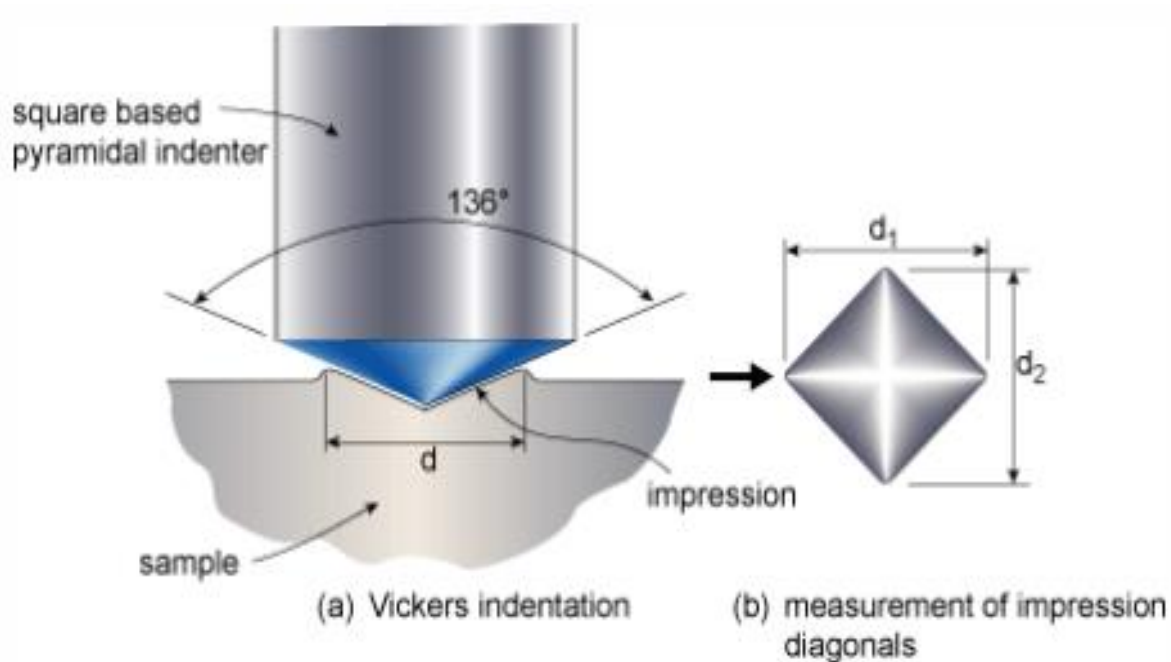


Fig. 5.5 Schematic illustration of Vickers indenters geometry and the resulting impression [100].

The HV value is calculated with the following equation:

$$HV = \frac{L}{A_c} = \frac{2L}{d^2} \sin \frac{136^\circ}{2} = 1,8544 \frac{L}{d^2}$$

where L is the load in kgf and d is the length of the diagonal measured from corner to corner on the residual impression in the specimen surface. The initial load is applied for 2-8 s and the test force is maintained for 10-15 s with loads under 1 kgf [101].

HV value is measured in kgf/mm² but can be expressed in MPa multiplying by 9.8065 its value.

It is important to use a sample with a polished layer as much regular as possible to have perpendicularity between the indenter and the sample. The test must be performed different times on different zones to obtain the average value.

From studies on other tellurite glass compositions, a reasonable range can be imagined for our TNGPZ glass. Values of HV between 3.01 GPa for zinc molybdenum tellurite and 4.52 GPa for zinc tellurite oxyfluoride have been reported

[102-104]. The hardness changes increasing the quantity of modifiers that break Te-O-Te network like AlF_3 or ZnF_2 [97,102,104] and it was supposed also to increase if the free volume in the alloy decreases as when Sb_2O_3 is added [103].

This value is pretty low compared to other glasses as silica (which has at least 750 HV) [105], but this was also one of the motives to use a different clad glass.

5.2 Glass optical properties

5.2.1 Refractive index

Thermo-mechanical characterization is important to optimize the drawing process, but for an optical fiber the optical properties are the most important. As explained in detail in Chapter 3, the refractive index (n) is a key characteristic for the performance of a disordered fiber and is strongly dependent on the composition because of the polarizability of the constituent ions. As reported by Jha et al. [21], refractive index of tellurite glass spans from 1.932 to 2.304, high compared to silica range between 1.45 and 1.52.

The measurement was performed at the premises of LINKS Foundation, Turin, and the results are reported in Fig. 5.6.

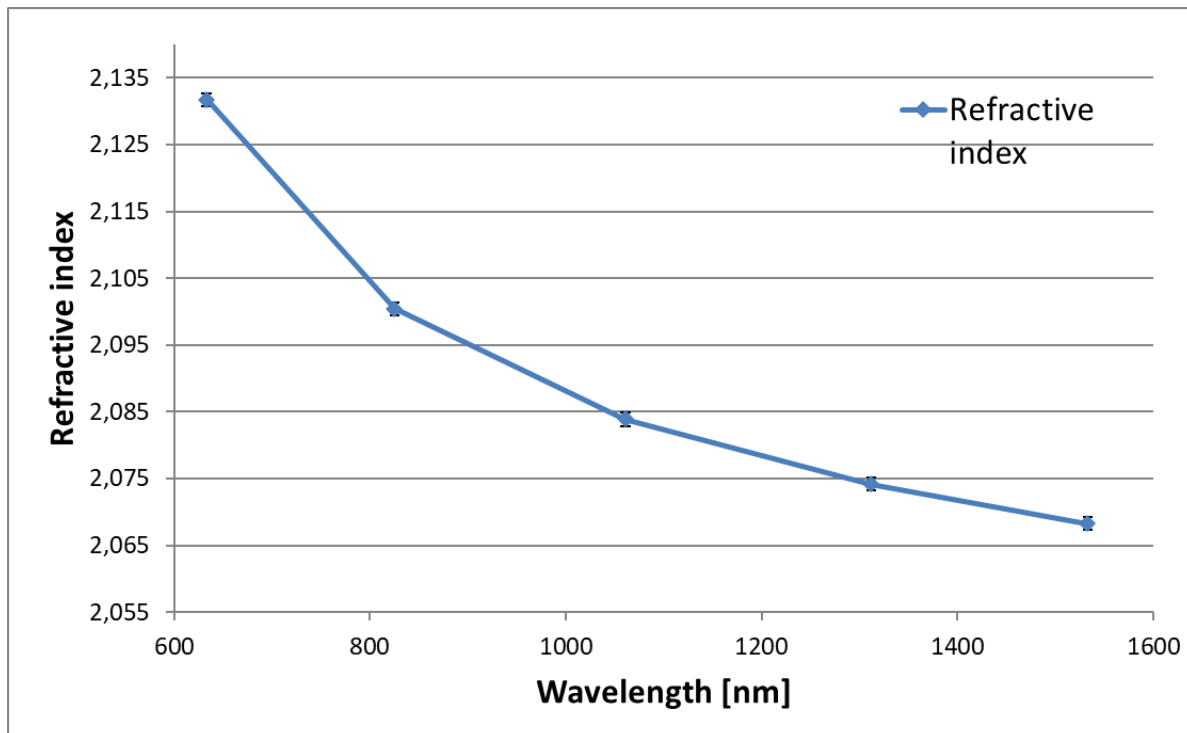


Fig. 5.6 Measurement of refractive index of the TNGPZ glass.

The large decrease of refractive index between 600 and 1200 nm is reported for other tellurite glasses such as TLWMN and TZNL (see Fig. 5.7).

Despite this decrease, the refractive index is still higher than 2 at 1600 nm, therefore the synthesized glass is an optimal candidate material for the producing of a disordered fiber. As shown in other fibers [11,12,63], good results have been obtained with differences between 0.095 to 0.5.

5.2.2 FTIR Spectroscopy

The Fourier Transform Infrared (FTIR) spectrometer was used to measure the absorption spectrum. This technique is one of the most used to characterize the absorption properties because it is able to simultaneously obtain the value for the entire range of wavelengths of interest. Classical spectroscopy instruments such as UV-Vis spectrometers, use monochromatic light and repeat the measurement for each wavelength desired. For Fourier-transform spectroscopy, the beam of light is composed of a combination of frequencies whose absorption is measured. Then, the procedure is repeated many times with a different combination of frequencies each time and, when all the data are obtained, they are processed by a computer to infer the absorption of each wavelength using a Fourier's transform. The advantages are an increased signal-to-noise ratio and a greater accuracy and precision.

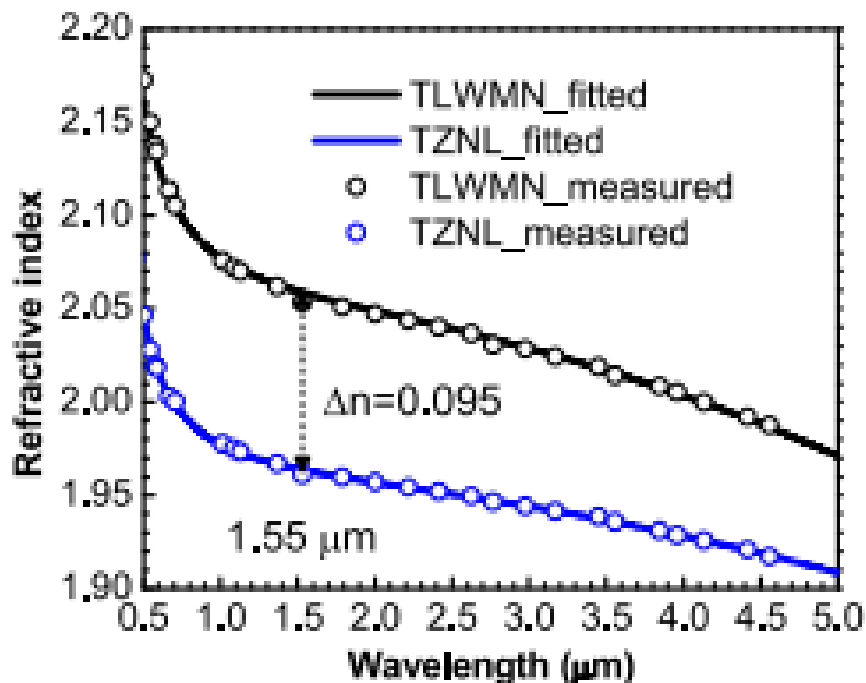


Fig 5.7 Refractive index dispersion of TLWMN and TZNL tellurite glasses [12].

Fig. 5.8 shows the absorption spectrum of the TNGPZ glass obtained in the range from 2.5 up to 5.5 μm .

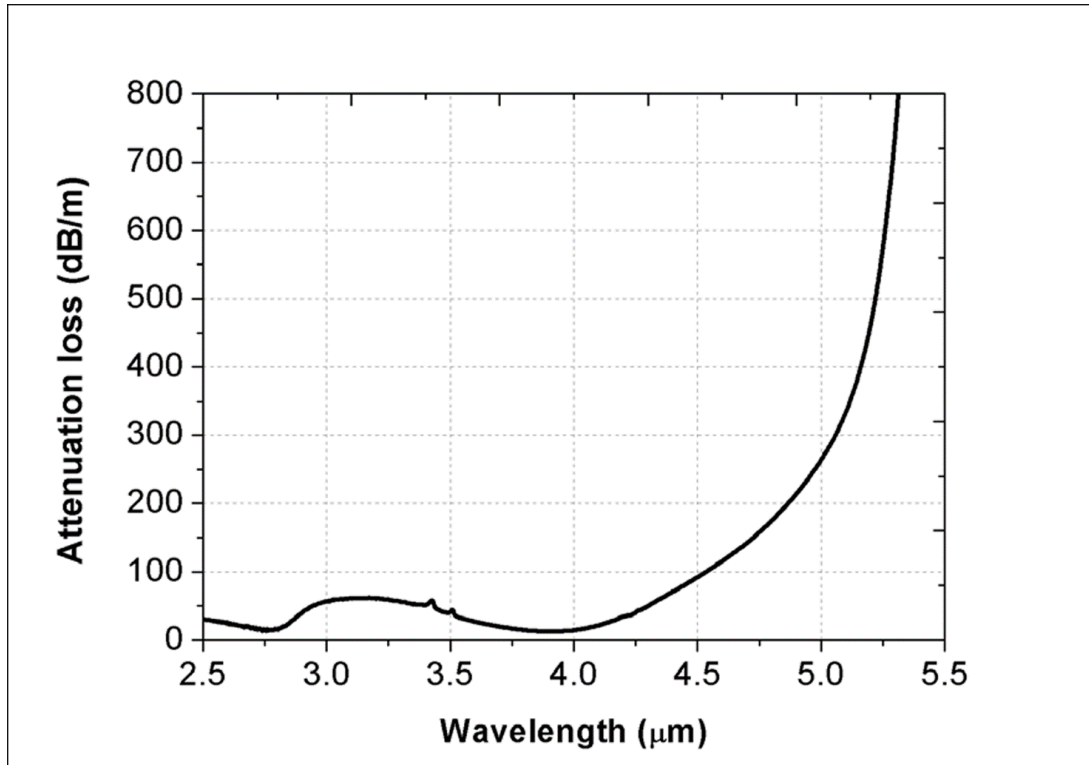


Fig. 5.8 IR absorption spectrum of TNGPZ glass.

This spectrum is in line with what reported in literature, with a peak of losses between 2.75 to 3.75 μm and the exponential growing of losses from 4.0 μm onward. This analysis is useful to study the best wavelength to work with lower losses, but it is particularly important to quantify the presence of OH^- or other contaminants.

This peak of losses is caused by the vibrations of OH^- , with the peak between 2.75 and 3.75 μm caused by a combination of weakly H-bonded OH^- and free OH^- [106].

This means that the hydroxyl groups were not completely removed using the dry atmosphere, but the improvement is still great, as it is shown by a comparison in Fig. 5.9 by Munasinghe et al. [107].

The use of dry atmosphere combined with fluoride raw materials in place of oxide decreased the losses. A multi-mode tellurite fiber produced by NP Photonics, Inc. has recently shown no measurable OH⁻ absorption at 3-4 μm and a minimum loss of 0.2 dB/m at 3.5 μm [108].

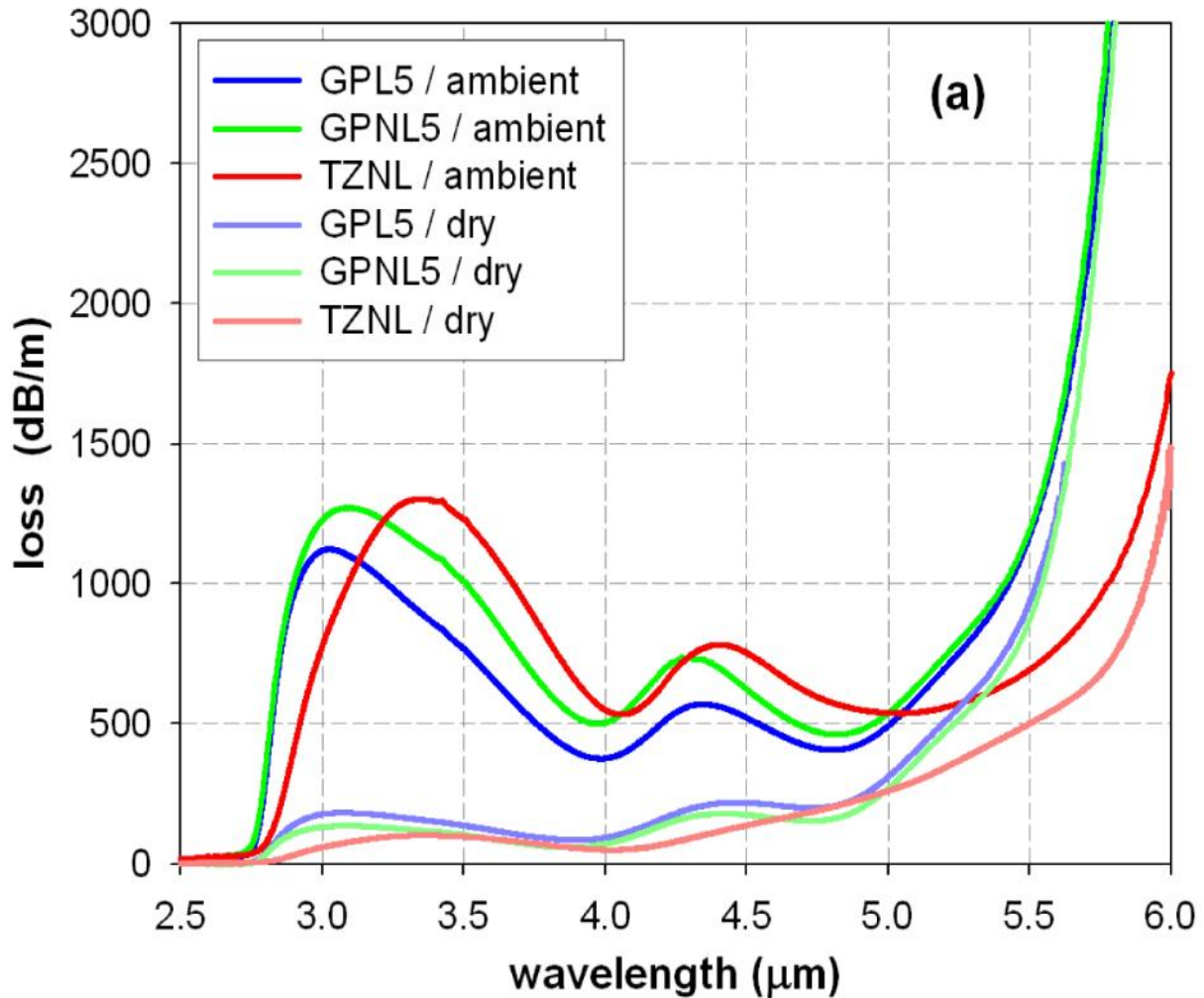


Fig. 5.9 IR absorption spectra of different bulk glasses melted in ambient and dry atmosphere [117].

5.3 Fiber properties

5.3.1 Cut-back method for total attenuation

The attenuation is the loss of optical power as a result of different mechanisms, such as absorption, scattering, bending and others. The total attenuation between two points of a fiber is measured by this equation:

$$A = 10 * \log_{10} \frac{P_X}{P_Y}$$

where:

- A is the total attenuation and is measured in dB;
- P_X is the power output in the first point (therefore closer to the optical source);
- P_Y is the power output in the second point.

The analysis will be made with a light source of white light (NKT), which will be connected to 2 m of commercial single-mode silica fiber to control if the quality of the splice is enough to see the light coming out of the single-mode fiber with a nice round shape. This single-mode fiber will be spliced to our tellurite fiber and will be spliced again to a 2 m single-mode fiber like the first that will go to a spectrometer to analyze the losses between 2500 and 6000 nm. The procedure is repeated 3 times to be sure the quality of the splice is good.

After collecting the losses, the procedure is repeated cutting the tellurite fiber shorter. In this way, losses for meter can be deducted from the difference of losses.

5.1 Results

Unfortunately, it was not possible to perform all the measurements on the tellurite glass. Where it has not been possible to have experimental data directly on our tellurite sample, a research in literature to infer the possible range of values expected has been done.

The DTA showed good stability against devitrification with a ΔT of 227.8 °C, with higher glass transition temperature compared to other TZN glasses.

The CTE measured is $13 * 10^{-6} \text{ } ^\circ\text{C}^{-1}$ between 200 and 400 °C, a lower value compared to common TZN glasses, this helps to find a compatible glass for the clad avoiding internal stresses.

For the viscosity, no accurate result was possible to acquire even from literature. Viscosity is not important for optical performances but to optimize the drawing process and obtain a good quality fiber; therefore, a direct measurement would be very useful and should be performed before attempting to fabricate it.

The hardness test is less critical, but it would be important to demonstrate how the different composition changed it. The hardness value of our TNGPZ glass should be higher than typical TZN glasses in any way.

The measured refractive index highlighted a $\Delta n \approx 1$ for the wavelength of 1.6 μm , thus showing promising results for Anderson localization.

The measured absorption spectrum shows low absorption for some wavelengths in mid-IR region and for wavelengths near 2500 nm, one of the regions well known as most efficient region to transmit light through biological tissues [109-110].

6 Conclusions

In this work an overview on tellurite glasses and disordered fibers with special focus on a TNGPZ glass made at the Politecnico di Torino has been presented.

The tellurite glasses have been previously reported in many studies as good candidates for infrared applications thanks to their broad transparency window, but in this study their application for disordered fibers for imaging in mid-IR have been the focus.

This glass shows a large refractive index and transmittance in near- and mid-IR regions, particularly useful for imaging in the biological field.

The absorption spectrum showed that further improvements in production techniques to decrease the OH⁻ content is needed, and a slight modification of composition could be helpful along the use of high-purity raw materials.

As shown by Tuan et al [12], even an all-solid tellurite disordered fiber with Δn of 0.095 transported high contrast, high brightness and high matching ratio images, thus a better result is expected.

Most of the work was dedicated on designing the fiber geometry and choosing the clad glass, unfortunately the unexpected problems precluded the drawing of the fiber and its characterization.

Nonetheless, the activity conducted at the University of Central Florida has been useful to plan a future drawing of the fiber, showing the promising features of such fiber.

7 List of symbols and abbreviations

TIR	Total Internal Reflection
n	Linear refractive index
SM	Single-mode fiber
MM	Multi-mode fiber
PMMA	Polymethylmethacrylate
OFS	Optical fiber sensor
USD	United States dollar
IR	Infrared
UCF	University of Central Florida
CREOL	The college of Optics and Photonics
DISAT	Department of Applied Science and Technology
tbp	Trigonal bipyramidal units
tp	Trigonal pyramid unit
CVD	Chemical Vapor Deposition
TZN	TeO ₂ - ZnO - Na ₂ O
TNGPZ	TeO ₂ -Nb ₂ O ₅ -GeO ₂ -PbO-ZnF ₂
NIR	Near Infrared
PhC	Photonic crystal
PBG	Photonic Band Gap
ω	Frequency
k	Wave-vector
MIT	Metal-insulator Transition
E_c	Mobility edge
E_f	Fermi level
PS	Polystyrene
TLWMN	TeO ₂ -Li ₂ O-WO ₃ -MoO ₃ -Nb ₂ O ₅

TZNL	TeO ₂ -ZnO-Na ₂ O-La ₂ O ₃
DCNN	Deep convolutional neural network
GARF	Glass-Air Random Fiber
MCVD	Modified Chemical Vapor Deposition
OVD	Outside Vapor Deposition
VAD	Vapor-phase axial deposition
T _g	Glass transition temperature
UV	Ultra-Violet
DISAT	Total Internal Reflection
α	Coefficient of thermal expansion
CTE	Coefficient of Thermal Expansion
E	Young's modulus
μ	Poisson's ratio
K	Bulk modulus
σ	Internal stress
T _x	Onset crystallization temperature
η	Viscosity
OD	Outer Diameter
ID	Internal Diameter
DTA	Differential Thermal Analysis
TMA	Thermomechanical Analyzer
LVDT	Linear Variable Differential Transformer
CGS	Centimetre-gram-second system
PPV	Parallel Plate Method
HV	Vickers microhardness
FTIR	Fourier Transform Infrared spectrometer
TIR	Total Internal Reflection
TIR	Total Internal Reflection

Bibliography

- [1] Mitschke F., 2016, *"Fiber Optics"*, Springer-Verlag Berlin Heidelberg. DOI 10.1007/978-3-662-52764-1_1
- [2] Crisp J., Elliott B. J., 2005 *"Introduction to Fiber Optics"*, Elsevier Science & Technology.
- [3] Fang Z., Chin, K. K., Qu, R., Cai, H., 2012, *"Fundamentals of Optical Fiber Sensors"*, John Wiley & Sons, Incorporated, ProQuest Ebook Central
- [4] Chu T. S., Hogg D. C., 1968, *"Effects of Precipitation on Propagation at 0.63, 3.5 and 1.6 Microns"*, Bell System Technical Journal 47, 723
- [5] Capps R.N., 1981, *"Optical fiber coatings. An overview with regard to opto-acoustic underwater detection systems"*, Industrial & Engineering Chemistry Product Research & Development.; 20:599-608. doi:10.1021/i300004a004.
- [6] Azadeh M., 2009, *"Fiber optics Engineering"*, Springer, Boston, MA, DOI 10.1007/978-1-4419-0304-4
- [7] Krohn D., 2006, *"Market opportunities and standards activities for optical fiber sensors"*, Optical Fiber Sensors Conference 2006, Hamden, CT, paper FB1
- [8] <https://www.mordorintelligence.com/industry-reports/optical-sensors-market>
- [9] Toulouse J., Lin A., Ryznyanskiy A., Belwalkar A., Guintrand C., Lafontaine C., Misiolek W., Biaggio I., 2011, *"Development of New Tellurite Fibers for mid-IR Applications"*, IEEE. [DOI: 10.1109/PHOTWMTM.2011.5730109]
- [10] Feng X., Horak P., Poletti F., 2017, *"Tellurite Glass Fibers for Mid-infrared Nonlinear Applications"*, Technological Advances in Tellurite Glasses, Springer Series in Materials Science, vol 254, Springer, Charm
- [11] Zhao J., Peysokhan M., Antonio-Lopez J.E., Sun Y., Abaie B., Mafi A., Correa R. A., Pang S, Schülzgen A., 2019, *"A path to high-quality imaging through disordered optical fibers: a review"* Appl. Opt. 58, D50-D60
- [12] Tong H. T., Kuroyanagi S., Nagasaka K., Suzuki T., Ohishi Y., 2018, *"Characterization of an all-solid disordered tellurite glass optical fiber and its near-infrared optical image transport"*, Jpn. J. Appl. Phys., Dec. 2018.
- [13] Hartmann P., 2014, *"Optical Glass"*, Spie
- [14] Lambson E.F., Saunders G.A., Bridge B., El-Mallawany R.A., 1984, *"The elastic behavior of TeO₂ glass under uniaxial and hydrostatic pressure"*, J. Non-Cryst. Solids 69, 117–133

- [15] El-Mallawany R.A., 2002, “*Tellurite Glasses Handbook: Physical Properties and Data*”, CRC Press, USA, 1st (2002), ISBN: 0849303680 9780849303685, (www.crcpress.com, engineering / Chemical, T)
- [16] El-Mallawany R.A., 2011, “*Tellurite Glasses Handbook: Physical Properties and Data*”, (CRC Press, USA) 2nd ed, (2011), ISBN: 9781439849835 1439849838 9781439849842 1439849846 <https://www.crcpress.com/Tellurite-Glasses-Handbook.../978143984>
- [17] El-Mallawany R.A., 2017, Introduction to Tellurite glasses, springer series in materials science, “*Technological Advances in Tellurite Glasses: Properties, Processing and Applications*”, Edit by V.A.G. Revera and D. Manzani, 1–13., <http://www.springer.com/gp/book/9783319530369>
- [18] El-Mallawany R.A., 2018, “*Tellurite Glass Smart Materials: Applications in Optics and Beyond*”, Springer International Publishing
- [19] Rivera V. A. G., Manzani D., 2017, “*Technological Advances in Tellurite Glasses*” Springer. [ISBN 978-3-319-53036-9]
- [20] El-Mallawany R.A., 2005, “*An introduction to Tellurite Glasses*”, 5 Video taped lectures provided as an educational resource for the entire international glass community available in video streaming format on IMI website; www.lehigh.edu/imi/resources.htm), http://www.lehigh.edu/~inimif/test_htm/
- [21] Jha A., Richards B.D.O., Jose G., Toney Fernandez T., Hill C.J., Lousteau J., Joshi P., 2012, “*Review on structural, thermal, optical and spectroscopic properties of tellurium oxide based glasses for fibre optic and waveguide applications*”, International Materials Reviews, 57:6, 357-382, DOI: 10.1179/1743280412Y.0000000005
- [22] Stanworth J. E., 1952, “*Tellurite glasses*”, Nature, 1952, 169, (4301), 581–582.
- [23] Wells A.F., 1984, “*Structural Inorganic Chemistry*”, Oxford, Clarendon Press, 5th Ed.
- [24] Sarjeant P. T., Roy R., 1967 “*New Glassy and Polymorphic Oxide Phases Using Rapid Quenching Techniques*”, J. Am. Ceram. Soc., 50, 500-03
- [25] Atanasova L.G., Baikusheva-Dimitrova G. N., 2012, “*Solubility of Tellurites of Rare Earth Elements*”, Journal of Chemical & Engineering Data 2012 57 (7), 1933-1938 DOI: 10.1021/je300079v
- [26] El-Mallawany R.A., 2002, “*Tellurite glasses handbook: physical properties and data*” CRC Press
- [27] Kokorina V., 1996, “*Glasses for Infrared Optics*”, CRC Press, Boca Raton, FL
- [28] Yamane M., Asahara Y., 2000, “*Glasses for Photonics*”, Cambridge University Press, Cambridge, ISBN 0521580536

- [29] El-Mallawany R.A., 2001, “*Tellurite Glasses Handbook—Physical Properties and Data*” CRC Press, London
- [30] Tao G., Ebendorff-Heidepriem H., Stolyarov A. M., Danto S. et al., 2015, “*Infrared Fibers. Advances in Optics and Photonics*”, 7, 379-458. [DOI: 10.1364/AOP.7.000379]
- [31] Massera J., Haldeman A., Jackson J., Rivero-Baleine C., Petit L., Richardson K., 2011 “*Processing of tellurite-based glass with low OH content*”, J. Am. Ceram. Soc. 4(1), pp.130–136.
- [32] Savelii I., De’sé’ve’davy F., Jules J. C., Gadret G., Fatome J., Kibler B., Kawashima H., Ohishi Y., Smektala F., 2013, “*Management of oh absorption in tellurite optical fibers and related supercontinuum generation*”, Opt. Mater. 35, 1595–1599
- [33] Yang F., Liu C., Wei D., Chen Y., Jingxiao L., Yang S.E., 2014, “*Er³⁺–Yb³⁺ co-doped TeO₂–PbF₂ oxyhalide tellurite glasses for amorphous silicon solar cells*”, Opt. Mater. 36, 1040–1043
- [34] Li D., Xu W., Kuan P., Li W., Lin Z., Wang X., Zhang L., Yu C., Li K., Lili H., 2016, “*Spectroscopica nd laser properties of Ho³⁺ doped lanthanum-tungsten-tellurite glass and fiber*”, Ceram. Int. 42, 10493–10497
- [35] Florencio L.d.A., Gomez-Malagon L.A., Lima B.C., Gomes A.S.L., Garcia J.A.M., Kassab L.R.P., 2016, “*Efficiency enhancement in solar cells using photon down-conversion in Tb/Yb-doped tellurite glass*”, Sol. Energy Mater. Sol. Cells 157, 468–475
- [36] Mori A., Ohishi Y., Sudo S., 1997, “*Erbium-doped tellurite glass fibre laser and amplifier*”, Electron. Lett., 33, (10), 863–864.
- [37] Mori A., Ohishi Y., Yamada M., Ono H., Nishida K., Oikawa K., Sudo S., 1997, “*Gain characteristics of tellurite-based erbium-doped fiber amplifiers for 1.5-microm broadband amplification*”, Dallas, TX, USA, IEEE, 251–252.
- [38] Kumar V., George A. K., Knight J. C., Russell P. S., 2003 “*Tellurite photonic crystal fiber*”, Opt. Express, 11, (20), 2641–2645.
- [39] Liao M., Chaudhari C., Qin G., Yan X., Suzuki T., Ohishi Y., 2009, “*Tellurite microstructure fibers with small hexagonal core for supercontinuum generation*”, Opt. Express, 17, (14), 12174–12182.
- [40] Liao M., Gao W., Duan Z., Yan X., Suzuki T., Ohishi Y., 2012, “*Supercontinuum generation in short tellurite microstructured fibers pumped by a quasi-cw laser*”, Optics Letters, 37(11), 2127-2129. [DOI: 10.1364/OL.37.002127]

- [41] Camilo M.E., Kassab L.R.P., Assumpção T.A.A., Cacho V.D.D., Alayo M.I., 2014, “*Fabrication and characterization of pedestal optical waveguides using TeO₂–WO₃–Bi₂O₃ thin film as core layer*”, *Thin Solid Films* 571, 225
- [42] Tong H. T., Nishiharaguchi N., Suzuki T., Ohishi Y., 2018, “*Fabrication of a Novel Tellurite Hollow Core Optical Fiber and Supercontinuum Light Propagation in Its Hollow Core*”, ICETE 2018, Vol. 1: DCNET, ICE-B, OPTICS, SIGMAP and WINSYS, 246-250
- [43] Laine, V.E., 2010, “*Photonic Crystals: Fabrication, Band Structure and Applications*”, Nova Science Publishers, Incorporated, 2010. ProQuest Ebook Central, <https://ebookcentral.proquest.com/lib/ucf/detail.action?docID=3018190>.
- [44] Sukhoivanov I.A., Guryev I.V., 2009, “*Photonic crystals , Physics and practical Modeling*”, Springer, Berlin, Heidelberg
- [45] Rayleigh L., 1887, “*On the maintenance of vibrations by forces of double frequency, and on the propagation of waves through a medium endowed with a periodic structure*”, *Philosophical Magazine* 24, 145–159
- [46] Yablonovitch E., 1987, “*Inhibited spontaneous emission in solid-state physics and electronics*”, *Phys. Rev. Lett.* 58, 2059–2062
- [47] John S., 1987, “*Strong localization of photons in certain disordered dielectric superlattices*”, *Phys. Rev. Lett.* 58, 2486–2489
- [48] Anderson P. W., 1958, “*Absence of diffusion in certain random lattices*”, *Phys. Rev.*, vol. 109, no. 5, pp. 1492–1505
- [49] Dossier Localisation d’Anderson in Images de la Physique 2009, <http://www.cnrs.fr/publications/imagesdelaphysique/2009.htm>
- [50] Mafi A., Ballato J., Koch K. W., Schülzgen A., 2019, “*Disordered Anderson Localization Optical Fibers for Image Transport—A Review*”, in *Journal of Lightwave Technology*, vol. 37, no. 22, pp. 5652-5659, 15 Nov.15, 2019
- [51] Segev, M., Silberberg, Y., Christodoulides, D. N., 2013, “*Anderson localization of light*”, *Nature Photonics*, 7(3), 197–204. <https://doi.org/10.1038/nphoton.2013.30>
- [52] Lagendijk A., van Tiggelen B., Wiersma D. S., 2009, “*Fifty years of Anderson Localization*”, *Physics Today* 62:8, 24-29 doi: 10.1063/1.3206091
- [53] Guan C., Guan X., 2019 “*A brief introduction to Anderson Localization*”, May 18, 2019, <http://web.mit.edu/8.334/www/grades/projects/projects19/GuanChenguang.pdf>
- [54] Hundertmark D., 2007, “*A short introduction to Anderson localization*”, <https://faculty.math.illinois.edu/~dirk/preprints/localization3.pdf>

- [55] Abrahams, E., Anderson, P., Licciardello, D. and Ramakrishnan, T., 1979, “*Scaling Theory of Localization: Absence of Quantum Diffusion in Two Dimensions*”, Physical Review Letters, 42(10), pp.673-676
- [56] Thouless, D. J., 1972, “*A relation between the density of states and range of localization for one dimensional random systems*”, Journal of Physics C: Solid State Physics, 5(1), 77–81. <https://doi.org/10.1088/0022-3719/5/1/010>
- [57] Celardo G.L., 2018, “*Localization of Light in subradiant Dicke states: a mobility edge in the imaginary axis.*”, International Workshop Disordered Systems, https://pcs.ibs.re.kr/PCS_Workshops/DisSLoTT_Talks_files/Giuseppe%20Luca%20Celardo.pdf
- [58] Mott N., 1978, “*Metal-insulator transitions*”, Physics Today 31, 11, 42, doi: 10.1063/1.2994815
- [59] Wiersma D. S., Bartolini P., Lagendijk A., Righini R., 1997, “*Localization of light in a disordered medium*”, Nature, vol. 390, no. 6661, p. 671
- [60] Abdullaev S. S., Abdullaev F. K., 1980, “*On propagation of light in fiber bundles with random parameters*”, Radiofizika, vol. 23, no. 6, pp. 766–767
- [61] De Raedt H., Lagendijk A., de Vries P., 1989 “*Transverse localization of light*”, Phys. Rev. Lett., vol. 62, no. 1, pp. 47–50
- [62] Schwartz T., Bartal G., Fishman S., Segev M., 2007, “*Transport and Anderson localization in disordered two-dimensional photonic lattices*”, Nature., 446(7131):52-55. doi:10.1038/nature05623
- [63] Karbasi S., Mirr C. R., Yarandi P. G., Frazier R. J., Koch K. W., Mafi A., 2012, “*Observation of transverse Anderson localization in an optical fiber*”, Opt. Lett. 37, 2304-2306
- [64] Karbasi S., Mirr C. R., Frazier R. J., Yarandi P. G., Koch K. W., Mafi A., 2012. “*Detailed investigation of the impact of the fiber design parameters on the transverse Anderson localization of light in disordered optical fibers*”, Opt Express. 2012;20(17):18692-18706. doi:10.1364/OE.20.018692
- [65] Karbasi S., Hawkins T., Ballato J., Koch K. W., Mafi A., 2012, “*Transverse Anderson localization in a disordered glass optical fiber*”, Opt. Mater. Express, vol. 2, no. 11, pp. 1496–1503, Nov. 2012
- [66] Han J. H., Lee J., Kang J. U., 2010, “*Pixelation effect removal from fiber bundle probe based optical coherence tomography imaging*”, Opt. Express 18(7), 7427–7439
- [67] Chen X., Reichenbach K. L., Xu C., 2008, “*Experimental and theoretical analysis of core-to-core coupling on fiber bundle imaging*”, Opt. Express 16(26), 21598–21607
- [68] Reichenbach K. L., Xu C., 2007, “*Numerical analysis of light propagation in image fibers or coherent fiber bundles*”, Opt. Express 15(5), 2151–2165

- [69] Pertsch T., Peschel U., Kobelke J., Schuster K., Bartelt H., Nolte S., Tunnermann A., Lederer F., 2004, “*Nonlinearity and disorder in fiber arrays*”, Phys. Rev. Lett. 93, 053901
- [70] Ford H. D., Tatam R. P., 2011, “*Characterization of optical fiber imaging bundles for swept-source optical coherence tomography*”, Appl. Opt. 50(5), 627–640
- [71] Tuan T.H., Kuroyanagi S., Nagasaka K., Suzuki T., Ohishi Y., 2018, “*Near-infrared optical image transport through an all-solid tellurite optical glass rod with transversely-disordered refractive index profile*”, Opt. Express, Vol. 25, No. 13 , 16054
- [72] Clark R. J. H., Hester R. E., 1996, “*Biomedical Applications of Spectroscopy*”, Wiley & Sons
- [73] Mantsch H. H., Chapman D., 1996, “*Infrared Spectroscopy of Biomolecules*”, Wiley & Sons
- [74] Lahiri B. B., Bagavathiappan S., Jayakumar T., Philip J., 2012, “*Medical applications of infrared thermography: A review*”, Infrared Phys. Technol. 55(4), 221–235
- [75] Mil'Shtein S., 2006, “*Infrared scanning for biomedical applications*”, Scanning 28(5), 274–277
- [76] Tong H. T., Kuroyanagi S., Nagasaka K., Suzuki T., Ohishi Y., 2019, “*Characterization of an all-solid disordered tellurite glass optical fiber and its NIR optical image transport*”, Japanese Journal of Applied Physics, Vol. 58, 032005
- [77] Zhao J., Antonio-Lopez J. E., Correa R. A., Mafi A., Windeck M., Schülzgen A., 2017, “*Image Transport Through Silica-Air Random Core Optical Fiber*”, in *Conference on Lasers and Electro-Optics*, OSA Technical Digest (online) (Optical Society of America, 2017), paper JTu5A.91.
- [78] Zhao J., Sun Y., Zhu H., Zhu Z., Antonio-Lopez J. E., Correa R. A., Pang S., Schülzgen A., 2019, “*Deep-learning cell imaging through Anderson localizing optical fiber*”, Adv. Photon. 1(6) 066001, <https://doi.org/10.1117/1.AP.1.6.066001>
- [79] Gieriej A., Filipkowski A., Pysz D., Buczyński R., Vagenende M., Van Vlierberghe S., Dubruel P., Thienpont H., Geernaert T., Berghmans F., 2020, “*Fabrication and characterization of step-index biocompatible and biodegradable polyesters based optical fiber*”, Proc. SPIE 11355, Micro-Structured and Specialty Optical Fibres VI, 113550L, doi: 10.1117/12.2556161

- [80] Chen Q., Wang H., Wang Q., Chen Q., Hao Y., 2015, “*Modified rod-in-tube for high-NA tellurite glass fiber fabrication: materials and technologies*”, *Applied Optics*, 54(4), 946-952. [DOI: 10.1364/AO.54.000946]
- [81] Paschotta R., 2008, “*Encyclopedia of Laser Physics and Technology*”, Wiley-VCH, Berlin, [ISBN 978-3-527-40828-3]
- [82] Yajima T., Yamamoto J., Kinoshita Y., Ishii F., Hirooka T., Yoshida M., Nakazawa M., 2014, “*OH-Free, Low Loss Single-Mode Fibre Fabricated by Slurry Casting/Rod-in-Tube Method*”, *2014 The European Conference on Optical Communication (ECOC)*, Cannes, pp. 1-3, doi:10.1109/ECOC.2014.6963829.
- [83] Nagel S. R., MacChesney J. B., Walker K. L., 1982, “*An Overview of the Modified Chemical Vapor Deposition (MCVD) Process and Performance*”, *IEEE Transactions on Microwave Theory and Techniques*, 30(4), 305-322. [DOI:10.1109/TMTT.1982.1131071]
- [84] Pierson H. O., 1999, *Handbook of Chemical Vapor Deposition (CVD)*. Noyes publications, Park Ridge, New Jersey. [ISBN 978-0-8155-1432-9]
- [85] Schultz P. C., 1980, “*Fabrication of Optical Waveguides by the Outside Vapor Deposition Process*”, *Proceedings of the IEEE*, 68(10), 1187-1190. [DOI:10.1109/PROC.1980.11828]
- [86] Geittner P., Küppers D., Lydtin H., 2008, “*Low-loss optical fibers prepared by plasmaactivated chemical vapor deposition (CVD)*”, *Applied Physics Letters*, 28, 645. [DOI:10.1063/1.88608]
- [87] Zhao J., Antonio-Lopez J. E., Zhu Z., Zheng D., Pang S., Correa R. A., Schülzgen A., 2018, “*Image transport through meter-long randomly disordered silica-air optical fiber*”, *Sci. Rep.* 8, 3065
- [88] Wang J.S. , Vogel E.M. , Snitzer E., 1994, “*Tellurite glass: a new candidate for fiber devices*”, *Opt. Mater.*, 3, pp. 187-203
- [89] O'Donnell M. D., Richardson K., Stolen R., Seddon A. B., Furniss D., Tikhomirov V. K., Rivero C., Ramme M., Stegeman R., Couzi M., Cardinal T., 2007, “*Tellurite and Fluorotellurite Glasses for Fiberoptic Raman Amplifiers: Glass Characterization, Optical Properties, Raman Gain, Preliminary Fiberization, and Fiber Characterization*”, *Journal of the American Ceramic Society*, Vol. 90, issue 5, 1448-1457
- [90] Furniss D., Shephard J. D., Seddon A. B., 1997, “*A novel approach for drawing optical fibers from disparate core/clad. Glasses*”, *Journal of non-crystalline Solids*, Vol. 213-214, 141-146

[91] Yablon A. D., 2004, “*Stresses and strains frozen into optical fibers*”, Optical Fiber Communication Conference, 2004. OFC 2004, Los Angeles, CA, USA, 2004, pp. 325-.

[92] Rose A. H., 2000, “*Annealing optical fiber: Applications and properties*”, American Ceramic Society Bulletin. 79. 40-43.

[93] Tao G., Ebendorff-Heidepriem H., Stolyarov A. M., Danto S., Badding J. V., Fink Y., Ballato J., Abouraddy A. F., 2015, “*Infrared fibers*”, Adv. Opt. Photon. 7, 379-458

[94] H. K. D. H. Bhadeshia, <https://www.phase-trans.msm.cam.ac.uk/2002/Thermal1.pdf>

[95] Song Y., Won, C., Kang S., Lee H. W., Park S., Park S., Yoon, J., 2018, “*Characterization of glass viscosity with parallel plate and rotational viscometry*”, Journal of Non-Crystalline Solids. 486. 27-35. 10.1016/j.jnoncrysol.2018.02.003.

[96] ASTM International, 2002, C 1351M-96. *Standard Test Method for Measurement of Viscosity of Glass Between 104 Pa·s and 108 Pa·s by Viscous Compression of a Solid Right Cylinder.*

[97] Liao G., Chen Q., Xing J., Milanese D., Fokine M., Ferraris M., 2008, “*Thermal and optical properties of new fluorotellurite glasses for photonics application*”, Proc. SPIE 6998, Solid State Lasers and Amplifiers III, 69981U (16 April 2008); <https://doi.org/10.1117/12.782637>

[98] Tincher B., Massera J., Petit L., Richardson K., 2010, “*Viscosity properties of tellurite-based glasses*”, Materials Research Bulletin, Volume 45, Issue 12, Pages 1861-1865, ISSN 0025-5408, <https://doi.org/10.1016/j.materresbull.2010.09.008>.

[99] Hill C.J., Jha A., 2007, “*Development of novel ternary tellurite glasses for high temperature fiber optic mid-IR chemical sensing*”, Journal of Non-Crystalline Solids, Volume 353, Issues 13–15, 2007, Pages 1372-1376, ISSN00223093, <https://doi.org/10.1016/j.jnoncrysol.2006.10.061>.

[100] <https://benjaminmousseaux.wordpress.com/2014/12/11/vickers-hardness-tests/>

[101] Linköpings Universitet, Institutionen För Fysik, Kemi Och Biologi, and Linköpings Universitet, Tekniska Fakulteten, 2017, “*Indentation Hardness Measurements at Macro-, Micro-, and Nanoscale: A Critical Overview*”, Tribology Letters 65.1: 1-18. Web.

- [102] Sidek, H.A.A.; Rosmawati, S.; Halimah, M.K.; Matori, K.A.; Talib, Z.A., 2012, “*Effect of AlF_3 on the Density and Elastic Properties of Zinc Tellurite Glass Systems*”, *Materials* vol. 5,8 1361–1372. 13 Aug. 2012, doi:10.3390/ma5081361
- [103] Dariush S., Torkashvand Z., 2017, “*Thermomechanical Properties of Sb_2O_3 - TeO_2 - V_2O_5 Glassy Systems: Thermal Stability, Glass Forming Tendency and Vickers Hardness*”, *Journal of Electronic Materials* 46.4: 2158-163. Web.
- [104] Linganna K., Jung-Hwan In, Park J., Ju H. C., 2018, “*Thermal and mechanical properties of tellurite glasses for mid-IR molded glass lens applications*”, *Proc. SPIE 10742, Optical Manufacturing and Testing XII*, 107421L (14 September 2018); <https://doi.org/10.1117/12.2320438>
- [105] Wilantewicz T. E., Varner J. R., 2008, “*Vickers indentation behavior of several commercial glasses at high temperatures*”, *Journal of Materials Science*, 43(1), 281-298. [DOI:10.1007/s10853-007-2174-9]
- [106] Savelii I., Desevedavy F., Jules J., Gadret G., Fatome J., Kibler B., Kawashima H., Ohishi Y., Smektala F., 2013, “*Management of OH absorption in tellurite optical fibers and related supercontinuum generation*”, *Optical Materials*, 35(8), 1595-1599. [DOI: 10.1016/j.optmat.2013.04.012]
- [107] Munasinghe H. T., Winterstein-Beckmann A., Schiele C., Manzani D., Wondraczek L., Afshar V. S., Monro T. M., Ebendorff-Heidepriem H., 2013, “*Lead-germanate glasses and fibers: a practical alternative to tellurite for nonlinear fiber applications*”, *Opt. Mater. Express* 3, 1488-1503
- [108] www.npphotonics.com, retrieved April 1, 2015.
- [109] Mil'shtein, S., 2006, “*Infrared scanning for biomedical applications*”, *Scanning* 28, 274
- [110] Smith A. M., Mancini M. C., Nie S. M., 2009, “*Second window for in vivo imaging*”, *Nat. Nanotechnol.* 4, 710.

Acknowledgements

This thesis had a very troubled genesis between supplier delays, broken furnaces and global pandemics; despite this, the international experience linked to this work has been vital for me and there are many people, in Italy and the USA, whom I would like to thank.

My thanks go to the Politecnico di Torino, my alma mater, and to its professors, Davide Janner, my supervisor who supported me from Italy not only for the thesis; and to Daniel Milanese, who started this whole project and has made me develop a passion for optical fibers. Thanks to Diego Pugliese, tireless researcher who followed me and helped me write this thesis.

Thanks to the university that welcomed me, the University of Central Florida, where I was able to carry out my research despite all the delays and problems, which taught me how to cope with the unexpected. Thanks to Prof. Axel Schülzgen, who has followed me throughout my stay in Florida and made me feel part of the group. Thanks to all the fantastic PhD students and researchers who helped me feel at home and with whom I shared this precious adventure: thanks Stefan, Steffen, Juan Carlos, Daniel and everyone else.

I had the support of many people getting this far, starting with my family: thanks to my mother Viviane, a tireless supporter who always listened and pushed me since I was a child; thanks to my sister Nicole who always helps me by putting myself in front of everything and everyone and on whom I can always count and thanks to my father Leopoldo always encouraging me to follow my dreams.

But this thesis, and this degree, would never have come with the same speed and ease had it not been for the support and love of Oriana, always ready to spur me on and tirelessly proofread, being the editor of everything I've written. In every difficult and sad moment, she was next to me, a companion on a journey to the borders of the solar system and beyond.

And finally, a thank you to all my friends who have helped me indirectly with their affection: To Fulvio, my brother of choice, thanks for the endless speeches on all human knowledge and this unbreakable friendship. Thanks to the nerds, Matteo, Simone, Tommaso and Alessandro for the beautiful evenings spent together in other worlds. And finally, thanks to all the others who have not found a place in these few lines but who are in my memories.

Ringraziamenti

Questo lavoro di tesi ha avuto un percorso molto travagliato tra ritardi di fornitori, fornaci rotte e pandemie globali; nonostante questo l'esperienza internazionale legata a questo lavoro è stata vitale e ci sono molte persone, in Italia e negli USA, che vorrei ringraziare.

Un grazie va al Politecnico di Torino, la mia *alma mater*, e ai suoi professori, Davide Janner, mio relatore che mi ha supportato dall'Italia non solo per la tesi, e a Daniel Milanese, che ha dato il via a tutto questo progetto e ha fatto crescere in me la passione per le fibre ottiche. Un grazie a Diego Pugliese, instancabile ricercatore che mi ha seguito e aiutato nella stesura di questa tesi.

Grazie all'università che mi ha ospitato, la University of Central Florida, dove ho potuto svolgere la mia ricerca nonostante tutti i ritardi e le problematiche che mi hanno insegnato ad affrontare con fantasia i problemi inaspettati. Grazie al Prof. Axel Schülzgen che mi ha seguito per tutta la mia permanenza in Florida e mi ha fatto sentire parte del gruppo. Un grazie a tutti i fantastici dottorandi e ricercatori che mi hanno aiutato a farmi sentire a casa e con cui ho condiviso questa preziosa avventura; Grazie a Stefan, Steffen, Juan Carlos, Daniel e a tutti gli altri.

Per riuscire ad arrivare fino a qui ho avuto il supporto di molte persone, a partire dalla mia famiglia: Grazie a mia madre Viviane, instancabile sostenitrice che ascolta sempre e mi spinge da quando son piccolo; grazie a mia sorella Nicole che mi aiuta sempre mettendomi davanti a tutto e tutti e sui cui posso sempre contare e grazie a mio padre Leopoldo per il suo incitarmi sempre a seguire i miei sogni.

Ma questa tesi, e questa laurea, non sarebbero mai arrivate con la stessa rapidità e facilità se non fosse stato per il sostegno e l'amore di Oriana, sempre pronta a spronarmi e a rileggere instancabilmente per trovare gli errori e fare da editor di ogni mio scritto. In ogni momento difficile e di tristezza è stata accanto a me per accompagnarmi in un viaggio ai confini del sistema solare e oltre.

E infine un grazie a tutti i miei amici che mi hanno aiutato indirettamente con il loro affetto: A Fulvio, mio fratello di scelta, grazie per gli infiniti discorsi su tutto lo scibile umano e a questa amicizia infrangibile. Grazie ai nerd, Matteo, Simone, Tommaso e Alessandro per le belle serate passate insieme in altri mondi. E grazie infine a tutti gli altri che non hanno trovato posto in queste poche righe ma che sono nei miei ricordi.